Missouri S&T Library and Learning Resources

Scholars' Mine

Masters Theses

Student Theses and Dissertations

Fall 2018

Application of seismic attributes for 3-D seismic visualization contributed in structural and stratigraphic interpretation of the Tangahoe and Farewell formations in the Kupe Field, Taranaki Basin, New Zealand

Housam Hussein Grabeel

Follow this and additional works at: https://scholarsmine.mst.edu/masters_theses

 Part of the Geology Commons, and the Geophysics and Seismology Commons

Department:

Recommended Citation

Grabeel, Housam Hussein, "Application of seismic attributes for 3-D seismic visualization contributed in structural and stratigraphic interpretation of the Tangahoe and Farewell formations in the Kupe Field, Taranaki Basin, New Zealand" (2018). *Masters Theses*. 7821.
https://scholarsmine.mst.edu/masters_theses/7821

This thesis is brought to you by Scholars' Mine, a service of the Missouri S&T Library and Learning Resources. This work is protected by U. S. Copyright Law. Unauthorized use including reproduction for redistribution requires the permission of the copyright holder. For more information, please contact scholarsmine@mst.edu.

APPLICATION OF SEISMIC ATTRIBUTES FOR 3-D SEISMIC VISUALIZATION CONTRIBUTED IN STRUCTURAL AND STRATIGRAPHIC INTERPRETATION OF THE TANGAHOE AND FAREWELL FORMATIONS IN THE KUPE FIELD, TARANAKI BASIN, NEW ZEALAND

By

HOUSAM HUSSEIN GRABEEL

A THESIS

Presented to the Faculty of the Graduate School of the

MISSOURI UNIVERSITY OF SCIENCE AND TECHNOLOGY

In Partial Fulfillment of the Requirements for the Degree

MASTER OF SCIENCE IN GEOLOGY AND GEOPHYSICS

2018

Approved by

Dr. Kelly Liu, Advisor
Dr. Stephen Gao
Dr. Neil Anderson

© 2018

Housam Hussein Grabeel

All Rights Reserved

ABSTRACT

Taranaki Basin is a mainly offshore basin covering an area of approximately 100,000 km^2, elongated across the western margin of New Zealand's north island. However, the modern limit of the basin is extended toward the deep water to cover about 330,000 km^2. The basin is divided by tectonic activities into northern and southern grabens. The southern region has become the most extensively researched district in recent years as its prime lithology and structural trap distributions provide numerous hydrocarbon fields. One such field is the Kupe Field (256 km^2), which lies on a northerly-plunging, reverse-faulted, and inversion structure of Manaia anticline. The Kupe_3D seismic data allow for detailed structural and stratigraphic interpretation of Farewell (reservoir) and Tangahoe formations. A number of attributes, i.e, amplitude gain control (AGC), frequency filtering, structural smoothing, variance, chaos, envelop, iso-frequency, and instantaneous phase were generated in this study. RGB (red, green, and blue) and CMY (cyan, magenta, and yellow) color blending techniques were applied utilizing Box Probe to reveal more edge continuity for fault and channel detections. In addition to top Tangahoe horizon, thirteen faults and channels associated with the Tangahoe interval were studied to better understand their initiation. Additionally, multiple faults and top Paleocene horizon (Farewell reservoir) were highlighted based on the visible displacement of reflected and continuous layers within each vertical and horizontal seismic section.

ACKNOWLEDGEMENTS

All thanks to Allah and then to all people who walk me through this work. I would like to express my sincere appreciation to my advisor, Dr. Kelly Liu, for her academic advising and assistance provided to complete this study and to obtain my master's degree. I would also like to thank Dr. Stephen Gao, and Dr. Neil Anderson for their advising and for being my committee members.

I am very grateful to my sponsors, the University of Zawia and the Libyan Ministry of Higher Education, for giving me this opportunity to pursue my graduate studies in the geology and geophysics program at Missouri University of Science and Technology.

Special thanks to Dr. Mohamed Rashed Embashi, Dr. Elnuri Fhiad, and Dr. Salem Sharata for their endless support. I would like to extend my thanks to Emily Seals, the technical editor at the Office of Graduate Studies

My deepest thanks to my mother, father, siblings, and to my gorgeous one for supporting me and believing in me in bad and good times. Without them, I would not have reached the end line. Last but not least, I am thankful to each person who has supported and motivated me even with a single word. Thank you all.

TABLE OF CONTENTS

Page

LIST OF ILLUSTRATIONS

Page

LIST OF TABLES

Page

1. INTRODUCTION

1.1. AREA OF STUDY

The Taranaki Basin is a mainly offshore basin that was considered to be extended to the continental edge and covers an area of approximately 100,000 km^2, elongated across the western margin of New Zealand's north island. However, seismic surveys acquired deeper beneath the recent bathymetric limit (Figure 1.1) of New Caledonia Basin show that the modern limit of the Taranaki Basin may extend toward the deep water to cover about 330,000 km^2 (King and Thrasher, 1996; NZP&M, 2014). The basin is currently considered to be the only productive basin in New Zealand, and Figure 1.1 illustrates some of the productive hydrocarbon fields within the basin. The Taranaki Basin is contiguous with the Reinga Basin and the West Coast basins to the north and the south, respectively (NZP&M, 2014). The basin was divided by tectonic activities into northern and southern grabens (Figure 1.1). The southern region, at which the area of interest is located, has become the most extensively researched district in recent years as its prime lithology and structural trap distributions suggest the potential existence of hydrocarbon accumulations (King and Thrasher, 1996; NZP&M, 2014).

The Kupe Field lies on a northern-plunging reverse-faulted inversion structure of Manaia anticline (Figure 1.2; Roncaglia et al., 2008). Within the field, intensive exploration was begun by the time the Kupe South-1 was drilled and initial gas accumulation was discovered in 1986 (Bierbrauer and Leitner, 2011). As a consequence, in 1989, the Kupe South 3D seismic survey was acquired over the southern portion of the

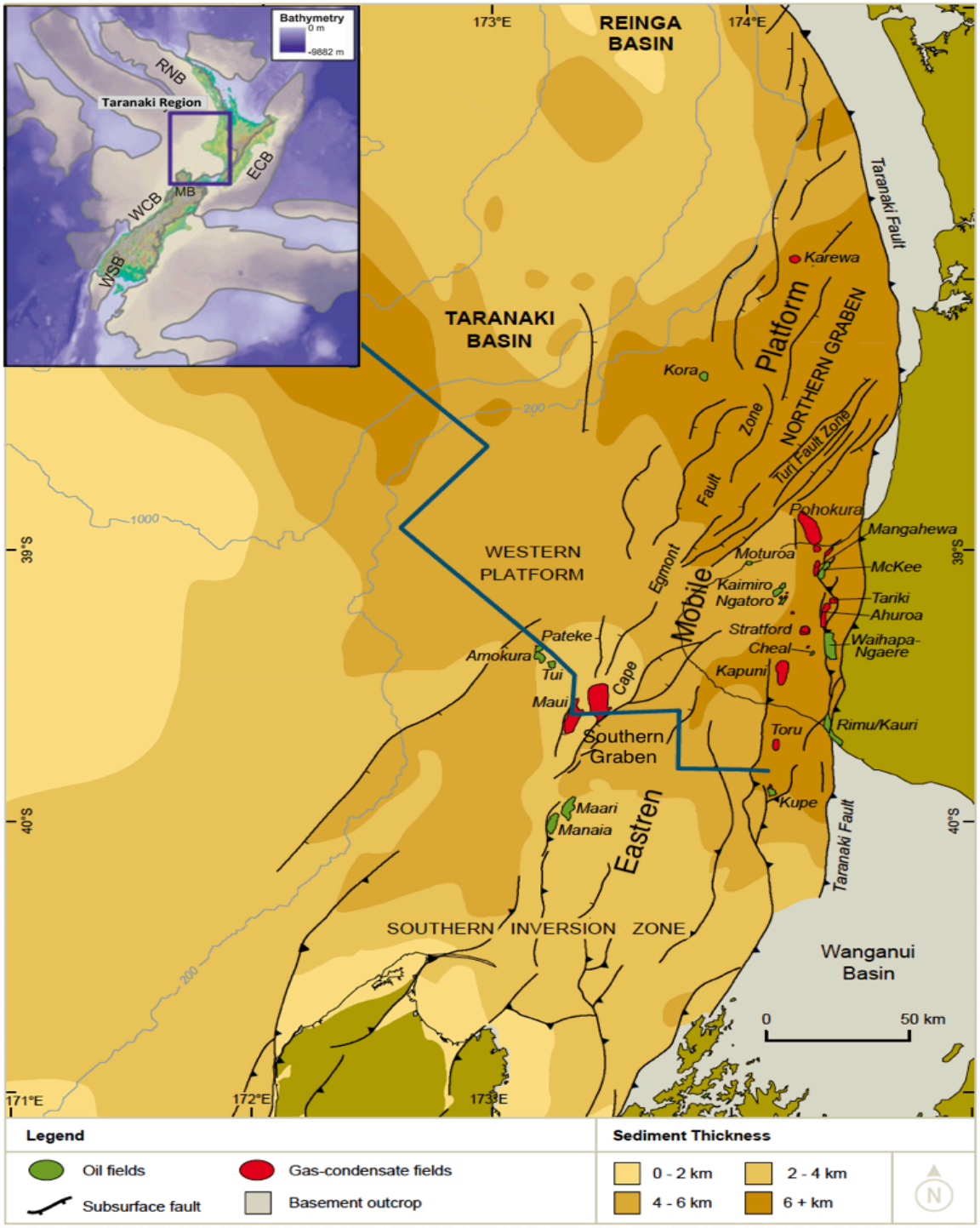

Figure 1.1. Map of the Taranaki Basin location.The map illustrating oil and gas fields, basin structures, and sediment thickness (Modified from NZP&M, 2014). The inset shows the location of the basin on a bathymetric map of Zealandia, with Taranaki adjacent basins. ECB, East Coast Basin; MB, Murchison Basin; RNB, Reinga–Northland Basin; WCB, West Coast basins; WSB, Western Southland basins.

Kupe condensate Gas field which located 35 km off southern Taranaki coastline on the crest of the Manaia Anticline (Figures 1.2 and 1.3).

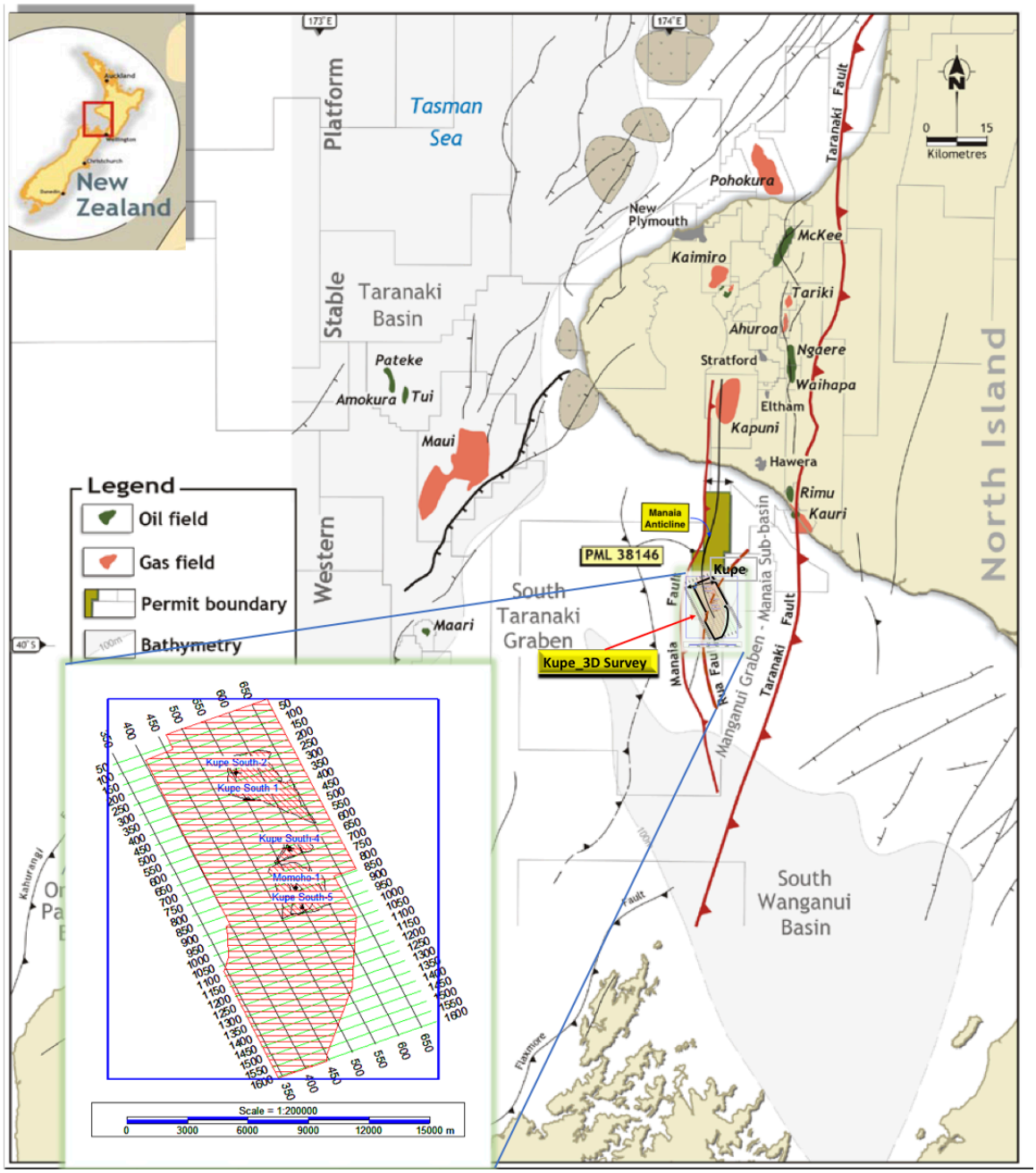

Figure 1.2. Detailed location map of the Kupe_3D seismic survey (Modified from Bierbrauer and Leitner, 2011).

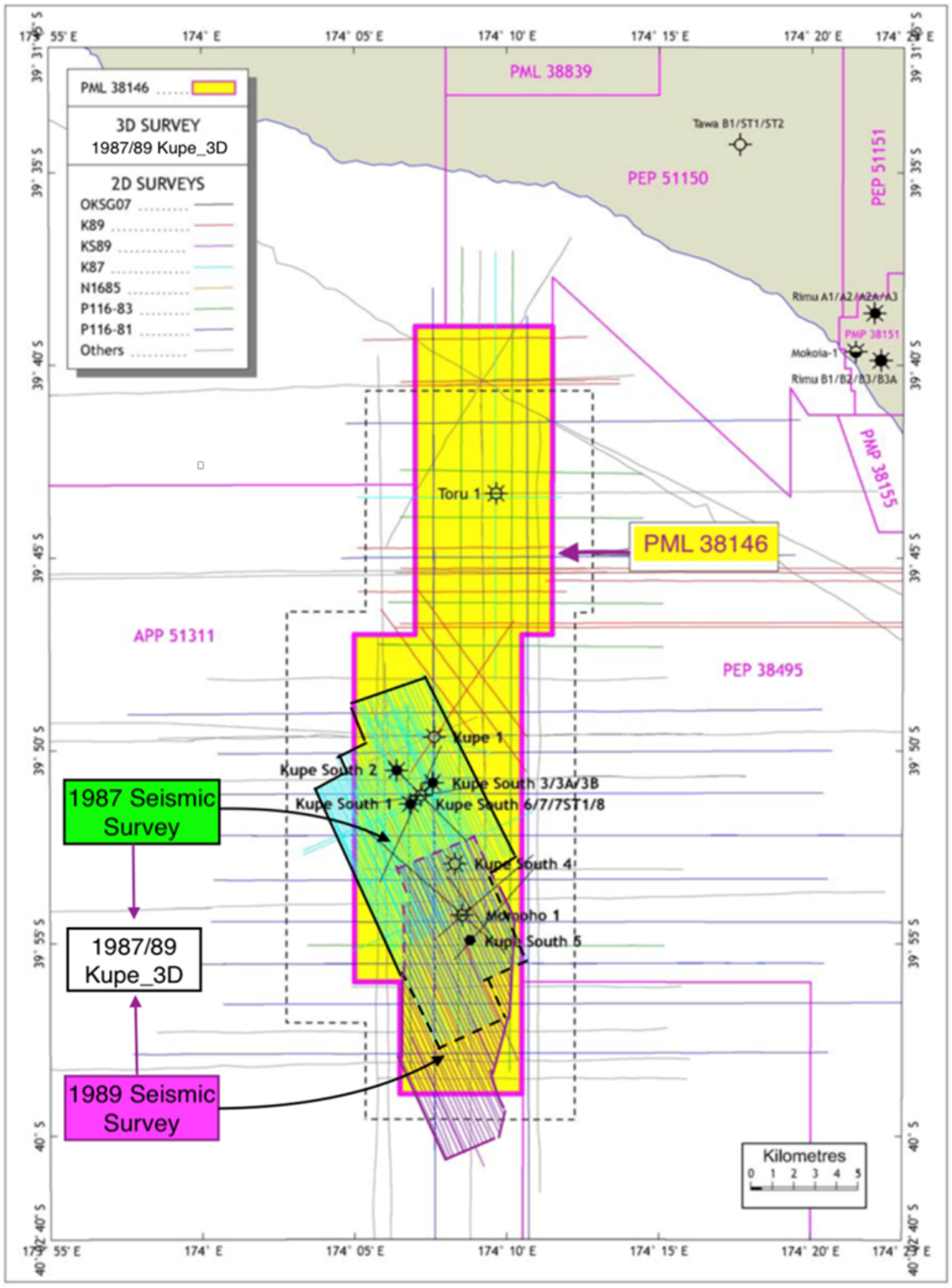

Figure 1.3. Detailed Kupe South 1987/89 3D seismic survey location map (Modified after Constantine, 2008).

The field is situated in the East Mobile Platform (Eastern Mobile Belt) of the Taranaki Basin and has an approximately aerial extent of 256 km^2. The Kupe 3D seismic data, which was acquired in1989, were merged with 1987 reconnaissance 3D data to cover the southern half of the PML 38146 (Figure 1.3), which is located in the center of the Kupe Area (CFA) in the offshore Taranaki Basin (Singh, 1989). Within the CFA including the study area, all the petroleum exploration and development wells are located on the crest of the Manaia Anticline. No wells have been drilled in adjacent synclines (Fohrmann et al., 2012). Geologically, the study area consists of ten formations deposited throughout the Late Cretaceous to Pleistocene age, i.e, North Cape, Puponga, Farewell, Otaraoa, Taimana, Lower and Upper Manganui, Kiore, Matemateaonga, Tangahoe, and Giant Foresets formations (Figure 2.4).

1.2. PREVIOUS STUDIES

The Taranaki Basin has received great attention and has been studied since the first hydrocarbon discoveries in the 1950 s. More than 400 wells were drilled, though none of which was drilled beyond the shelf edge. The structural evolution, tectonics, and geologic influence of the basin place it to have considerable potential for further discoveries (NZP&M, 2014).

In the Kupe South Field, several wells were drilled (Figures 1.3 and 1.4) following the 1975 oil show exploration well (Kupe-1) and the 1986 hydrocarbon discovery well (Kupe South-1). In 1986, the Kupe South-1 has penetrated the top of the reservoir at depths of 100 m more than the predicted one. Seismic study explained that the 100 m offset was caused by the 180 m throw of the Kupe South Fault. The well

encountered 63 m hydrocarbon colums subdivided to 43 m and 20 m of gas and oil column, respectively. Thereafter, in 1987 Kupe South-2 was drilled and showed 34 m of gas column on an oil leg in a separate pressure system. In the same year, the Kupe South-3 penetrated the same contacts of the previous well and provided more productivity for the reservoir with maximum flow rate of 4526 bopd and 9.66 mmcfgd (Schmidt, 1989). Subsequently, the following wells were drilled, i.e., the 1989 wet gas discovery (Kupe South-4), the 1990 oil discovery (Kupe South-5), and the 2008 gas discovery (Momoho-1). The rest of the wells within the study area were drilled in 2008 as development wells. These wells are Kupe South-6, Kupe South-7, Kupe South-7ST1, and Kupe South-8, all of which are oil and wet gas discovery (Constantine, 2008).

In terms of drilled formations, approximately 100 m of the Farewell Formation was expected to be penetrated by Momoho-1 before to reach the bottom of the Puponga Formation, but only 24.6 m might be intersected if the Farewell Formation is not absent altogether. If the Farewell Formation is absent, the top of the Puponga Formation must be placed too deep in the well. Within the area of interest, the hydrocarbon predominantly was found in the Paleocene Farewell Formation underneath the Base Marin Shale (BMS) of the Otaraoa Formation. Thus, the determination of the corresponding seismic reflector of this formation is vital to examine the reservoir (Bierbrauer and Leitner, 2011). The lowest 2 to 15 m of the marine shale was recorded to have an acoustic impedance of 15,000 g-m/cc/s, whereas the underlying reservoir more typically ranges from 8,000 to 9,000 g-m/cc/s. The base is quite sharp (Schmidt, 1989).

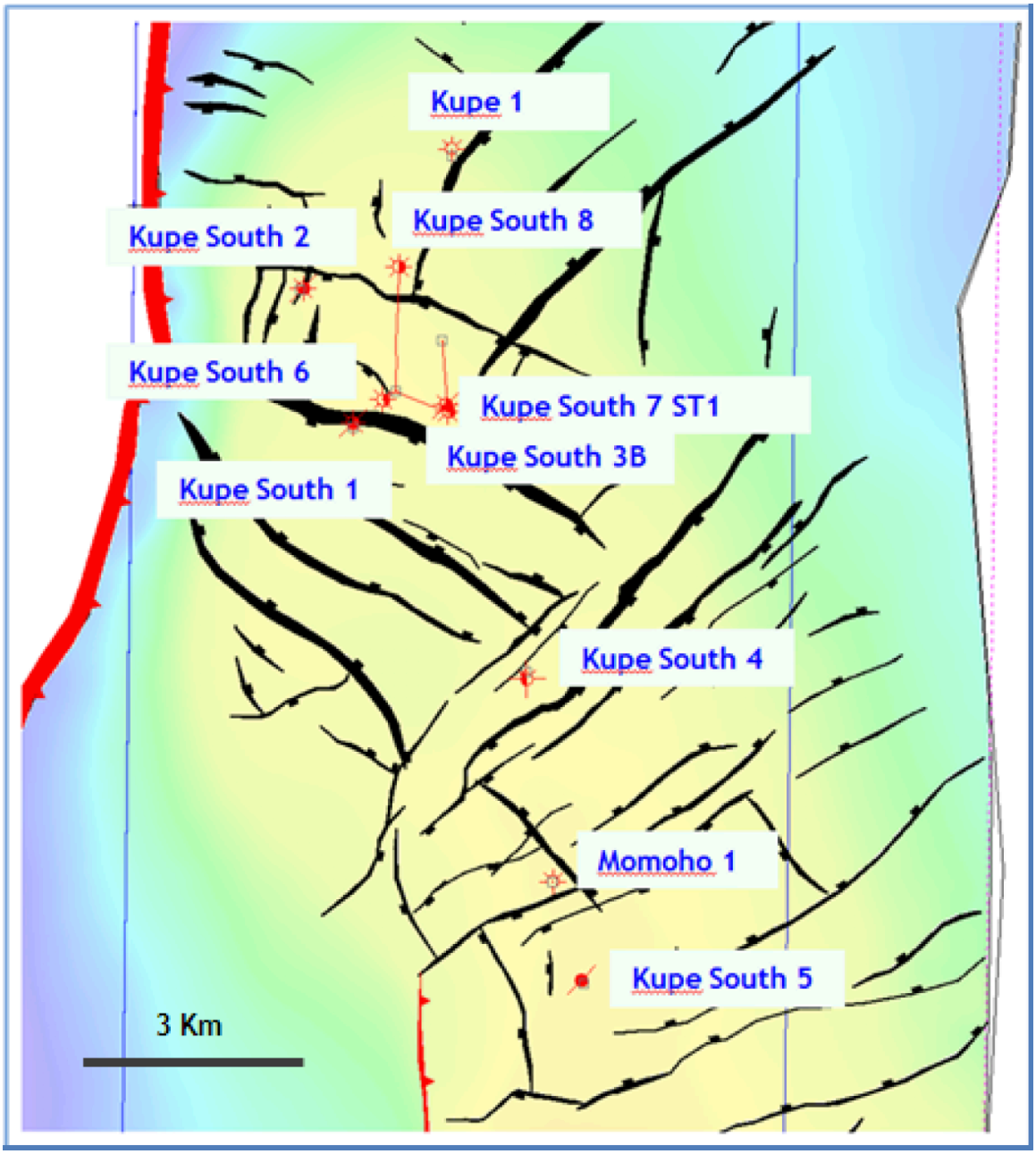

Figure 1.4. Kupe South well locations on schematic structure map (Bierbrauer and Leitner, 2011).

1.3. OBJECTIVES

The purpose of the study is to provide better understanding of the geological setting of the Kupe_3D Field using the available well logs, well data, and seismic data. Structure and stratigraphic features within the Tangahoe Formation and Farewell Formation are the aiming targets within the study area.

This study aims to identify and analyze the geometry of stratigraphic features noticed within the Kupe survey seismic data at the top of the Tangahoe Formation, as well as to detect and interpret various faults within the formation to better understand their initiation force. Moreover, the study examines the cause of after drilling depth offset found at the top of the Farewell Formation (Reservoir) in a production well that was drilled in the northern part of the study area. In addition to that, the study aims to reveal the overall distributions of the faults and fractures within the Farewell Formation.

2. REGIONAL GEOLOGY

2.1. GEOLOGICAL SETTING AND TECTONIC HISTORY

The Taranaki Basin is a basically extensional Cretaceous-Cenozoic sedimentary basin that was evolved as a marine basin under a convoluted geological history (Figure 2.1). As illustrated in Figure 1.2, the basin is situated on the western margin of the North Island of New Zealand that can be described as the subduction zone between the Pacific Plate and Australian Plate (Figure 2.2). The Taranaki Basin was initiated under rift-drift tectonic movements during the separation of the eastern Gondwana (New Zealand from Australia), generating the Tasman Sea (Higgs et al., 2012; King and Thrasher, 1996). The basin continued its development since the Late Cretaceous to the recent time (Figure 2.1) to be subdivided into two main platforms, i.e., the Passive Western Platform, which has been relatively tectonically stable, and the Eastern Mobile Platform that was subdivided into the northern graben and southern graben (Figures 1.1 and 2.2) as a result of Neogene convergent tectonism overprinting the older structure of the basin (King and Thrasher, 1996).

During the Late Cretaceous and in some locations extending in the Paleocene, rifting controlled by extensional movements has occurred with local hasty subsidence, and regional sedimentations within fault grabens and half grabens appear to have begun in the Northern Graben (Figure 2.1). Thereafter, the Taranaki paleo-coastline of the Paleogene period was oriented NE-SW, and the shoreline kept transgressed and regressed intermittently (Higgs et al., 2012). Throughout the Eocene to Early Oligocene, a passive

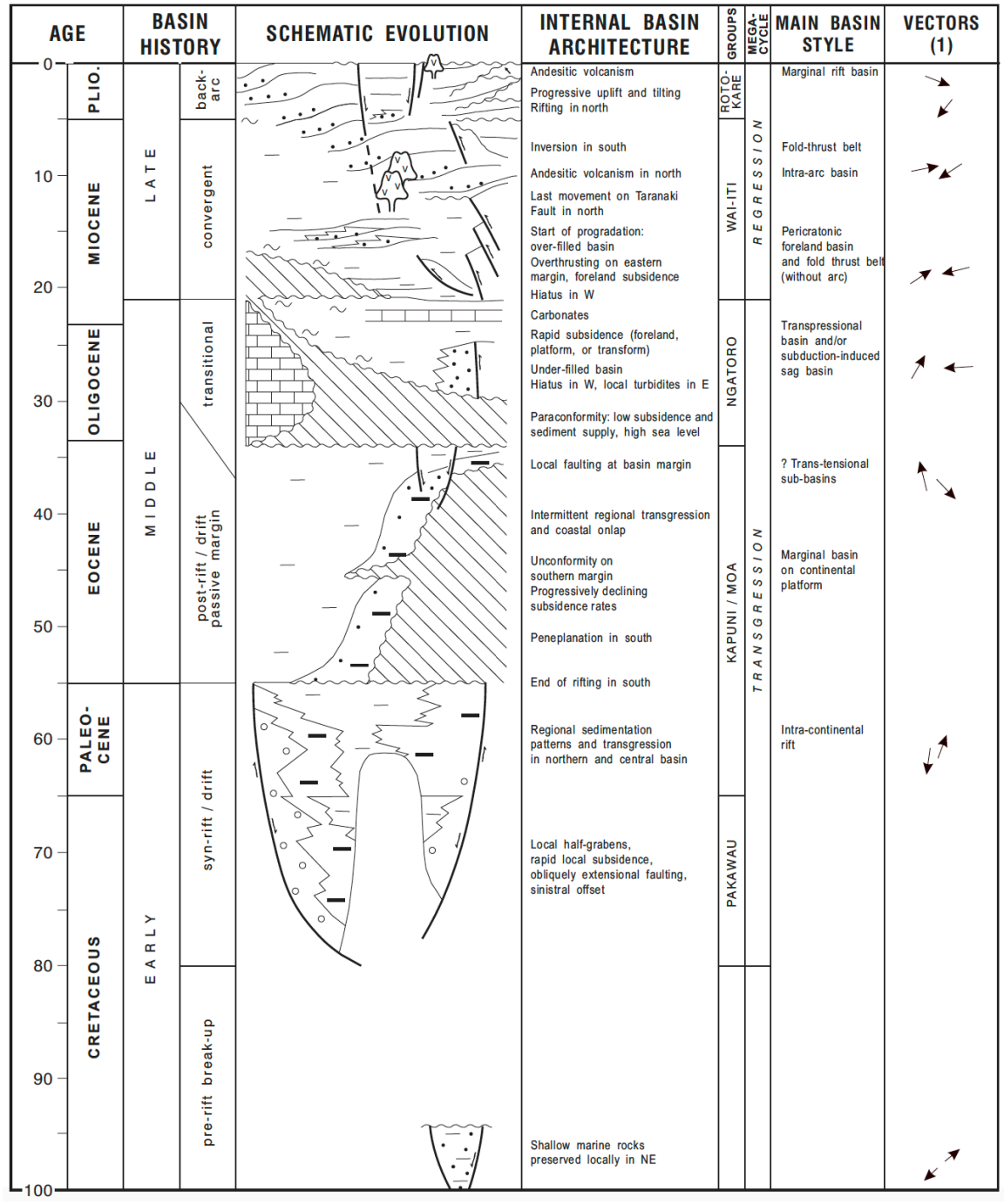

Figure 2.1. Schematic illustration of the Taranaki Basin evolution. Note: The arrows indicate general directions and style (divergence pre-c.30 Ma, convergence post-c.30 Ma) of relative motion across the Pacific-Australian plate boundary at the approximate latitudes of the Taranaki Basin (King and Thrasher, 1996).

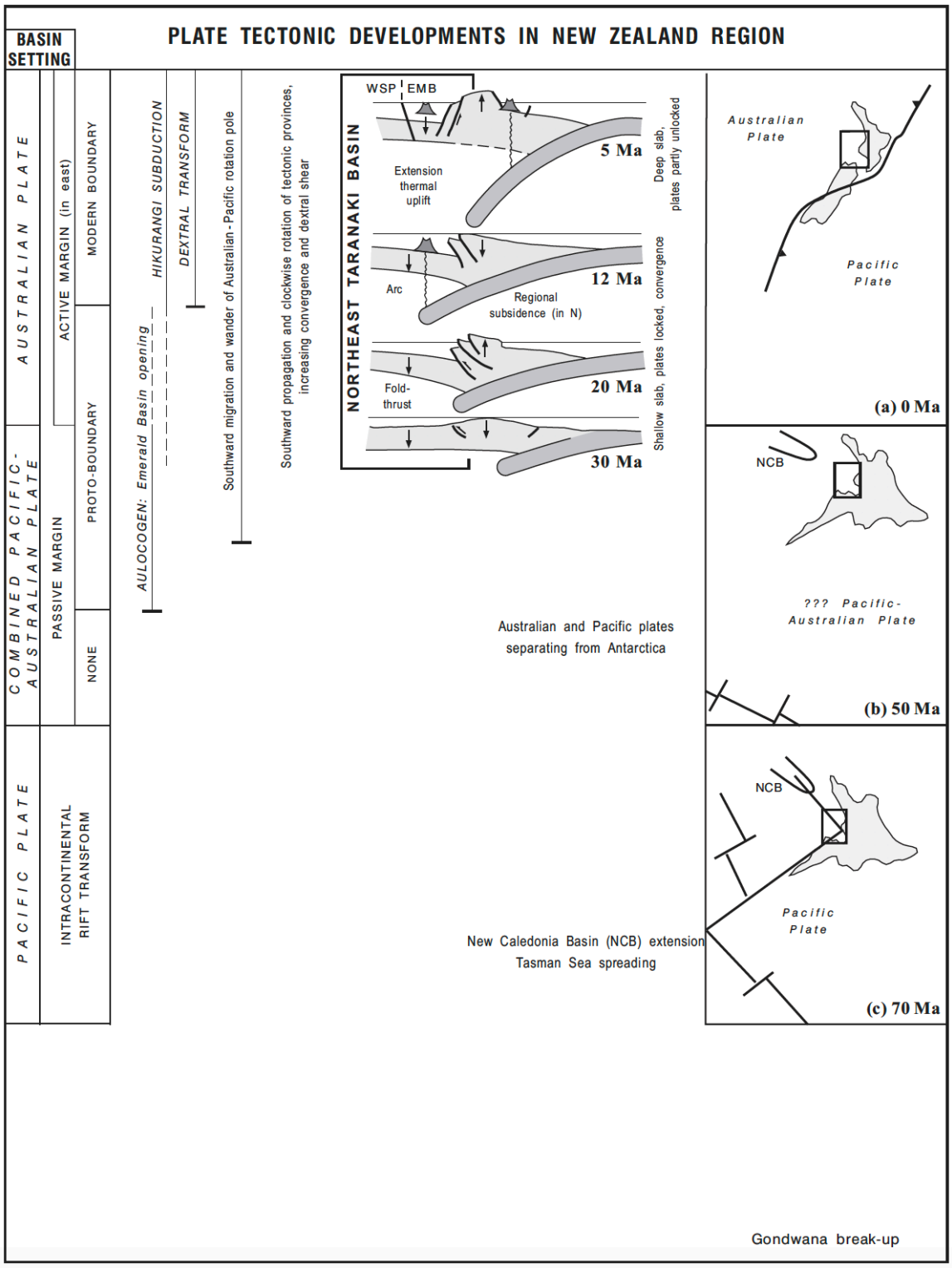

Figure 2.2. Timetable of events and tectonic controls. WSP = Western Stable Platform, EMB = Eastern Mobile Belt of the Taranaki Basin, and Gondwana break-up throughout 70 Ma (King and Thrasher, 1996).

margin was established adjacent to the subcontinent (Higgs et al., 2012; King and Thrasher, 1996). Early this time, decreasing in subsidence rate occurred in the Taranaki Basin followed by unconformity on the southern margin of the basin.

By the late Eocene and throughout the Oligocene epoch, the Taranaki Basin experienced intermittent regional transgression, and sediments were on-lapping over the coastal plain and the continental shelf. Thereafter, local faulting that might have resulted from transitional-tensional movement formed a sub-basin at the basin margin (Higgs et al., 2012; Schmidt, 1989). After that, a fast subsidence occurred in the eastern side with a major transgression in the shoreline, causing the northern graben of the Taranaki Basin paleo-water depth to reach the bathyal depth. Thus, the basin was under-filled. This came as consequences of the diagonal collision between the Pacific Plate and Australian Plate that caused a compression and uplift to the east of the basin (Higgs et al., 2012; Schmidt, 1989). As the strata of the Eocene time becomes thicker toward the eastern margin of the Taranaki Basin at which tectonic activities were associated with creating a new plate boundary, the Taranaki Fault was suggested to have been controlling the subsidence of the basin during the middle-upper Eocene (Higgs et al., 2012). Oligocene wrench fault offsets may give an estimation of the onsite of this compression in the Kupe area (Schmidt, 1989).

Eastern areas of inversions that had previously uplifted sometime during the Early Miocene (20 Ma) have latterly (12 Ma) partially subsided to exceed the deepening that was reached in the western platform (Figures 2.1 and 2.2). These zones have the thickest clastic sediment successions that were derived from eroded high locations (King and Thrasher, 1996). In the south, the extensional fault inversion that was interpreted in the

Kupe structure recorded that a compression and a truncation were continued during the Miocene (Schmidt, 1989). Thereafter, in the Pliocene, progressive uplift and tilting rifting in the north and back-Arc tectonic regimes affected the east of the Taranaki Basin, reconstructing the eastern mobile platform of the basin. Hence, the northern extensional graben and southern compressional graben of the Taranaki Basin were established as they were controlled by the Cape Egmont and Oakura Fault systems (Schmidt, 1989). The southern graben, where the Kupe Field is located, is characterized by thrusting faults and structural inversion, whereas the northern graben, where the extensional regime is dominant, is described as a graben of oblique and normal faulting (Knox, 1982; Schmidt, 1989). However, Pliocene to recent age exhibits normal faulting in the Kupe area that may be associated with compaction drape over the Manaia anticline (Knox, 1982).

Since the Taranaki basin is a rift basin, the coal deposited during the Late Cretaceous-Eocene was mostly accumulated as synrift and half graben sediments. It also provides source, reservoirs, and intra-formational cape rocks. The Oligocene marine shale (Otaraoa Formation), which was formed during the major transgression, makes a regional cape rock within the basin (Schmidt, 1989).

2.2. LOCAL SETTING

The Kupe Field was discovered within the Manganui Graben-Manaia Sub-Graben, which was evolved throughout the Late Cretaceous under the tectonism of the Manaia Fault (Figure 1.2). Since the Paleocene to the Eocene, subsidence sustained during the Eocene, and minor marine intrusions have occurred within fluvial sedimentation (Kapuni Group) (Schmidt, 1989; King and Thrasher, 1996). Because the

graben was initiated along the Manaia Fault, the depocenter of this time was elongated north-south adjacent to the fault (Schmidt, 1989). Thereafter, at the uppermost Eocene throughout the beginning of Early Oligocene, the Kupe area experienced tilting uplift that triggered erosion activity east of the Manaia Fault. As a consequence, the previously deposited strata of the Eocene and probably part of the Paleocene have eroded (Schmidt, 1989). The event of the tilting uplift at the southeastern part of the Taranaki Basin was locally interpreted as a result of early inversion of the Manaia Fault or regionally as tilting of the basin margin (Schmidt, 1989). This tilting uplift corresponds to the main structure within the Kupe Area (Manaia Anticline) (King and Thrasher, 1996).

The rapid subsidence that followed the Oligocene tectonic movement affected the Kupe area and caused a marine transgression to occur through to the Miocene (Schmidt, 1989). According to Constantine (2008), within this marine environment, the marl and mudstone deposition were dominated (Otaraoa, Taimana, and Manganui formations) (Figure 2.3). The compression stress under which the Kupe area was evolving during the Miocene induced truncation that pre-dated a shoreline regression in the Early Pliocene. After the regression occurred, the Kupe location became exposed to the terrestrial sedimentations to be accumulated; during this period, the lower Matemateaonga Formation (conglomerate, sandstone, and coal) was deposited (Schmidt, 1989). In the Late Pliocene, shoreline transgression induced by basin subsidence has occurred. As a consequence, marine sediments were accumulated in the Kupe area forming the Upper Matemateaonga and Tangahoe formations. Since the Late Pliocene to recent age, marine deposition continued forming the younger formation in the area (Whenuakura

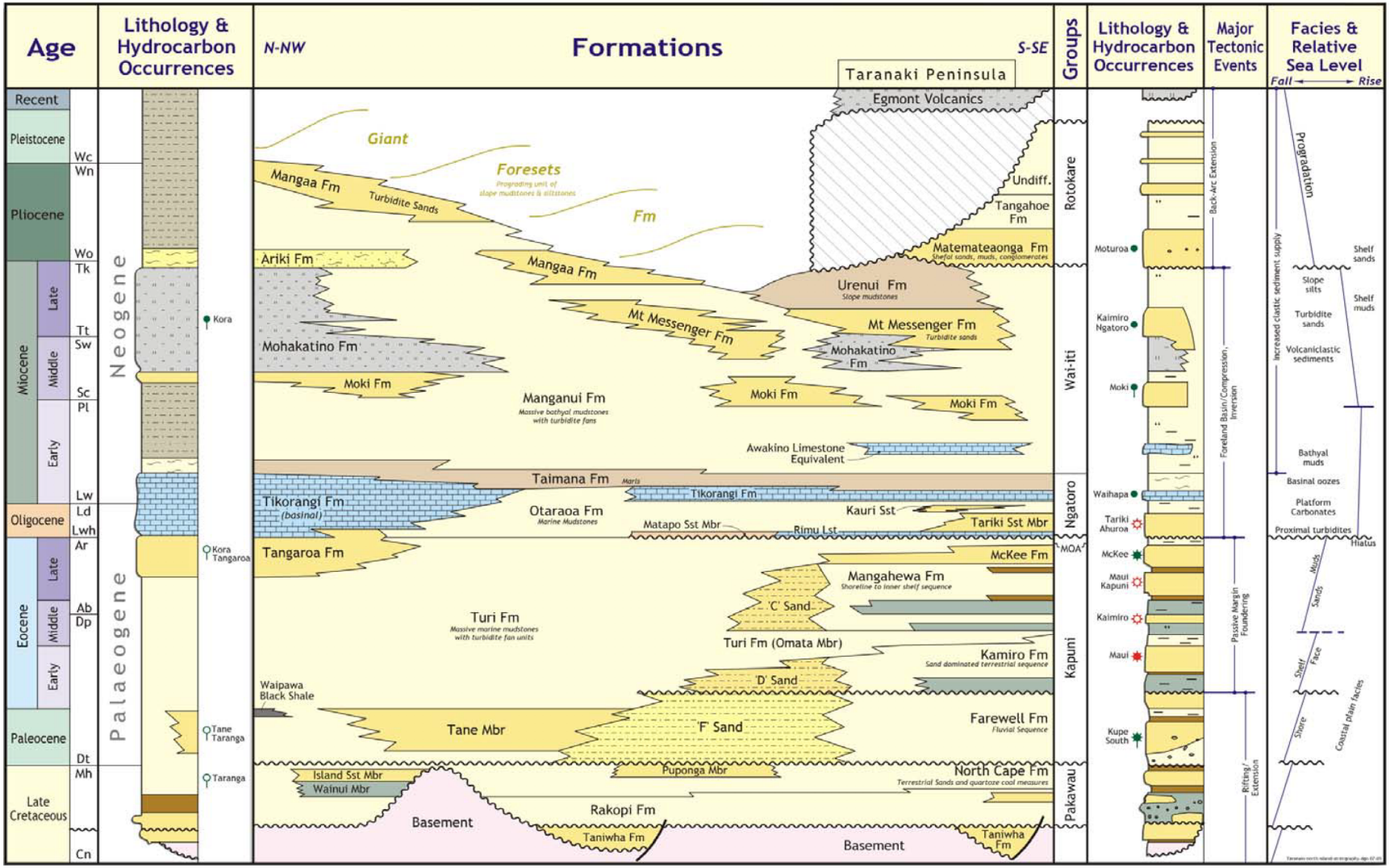

Figure 2.3. General stratigraphic layout of the greater Taranaki Basin (Constantine, 2008).

Formation) (Schmidt, 1989). The fluvial deposits of the Paleocene are the main composition of the reservoir within the Kupe South field (Farewell Formation).

2.3. STRATIGRAPHY

Overall the strata succession in the Taranaki Basin can be generally described as Cretaceous-Cenozoic cycles of deposition divided into the shoreline transgression period starting in the Late Cretaceous and ending by the Early Miocene (Figure 2.3). These strata followed by regression continue to the resent time (King and Thrasher, 1996). The area of study, as part of the Southern Inversion Zone, contains a recognized stratigraphic succession (Kapuni Group) that forms a great hydrocarbon system in addition to different active plays. The following sections briefly designate the geological column, the hydrocarbon system, and its depositional environments that were penetrated by Kupe south wells within the area of study (Figure 2.4 and 2.5).

2.3.1. North Cape Formation. The North Cape Formation represents the upper formation of the Pakawau Group (Rakopi and North Cape Formations). This group represents the source rock in many fields in the Taranaki Basin (Figure 2.6) and might be also in the locality of the Kupe South field (Schmidt, 1989). It can be described first as marginally marine sediments deposited in rift valleys during the uppermost Late Cretaceous (King and Thrasher, 1996; Roncaglia et al., 2008). The North Cape Formation is about 1800 m thick in the Manaia sub-basin (King et al., 2009; Thrasher et al., 1995). The North Cape Formation, which may have the potential to be top seal, overlies the Rakopi Formation in the Kupe South field, and it is mostly comprises of coastal sandstone, shallow marine siltstone, and some local conglomerate with coal joints (King

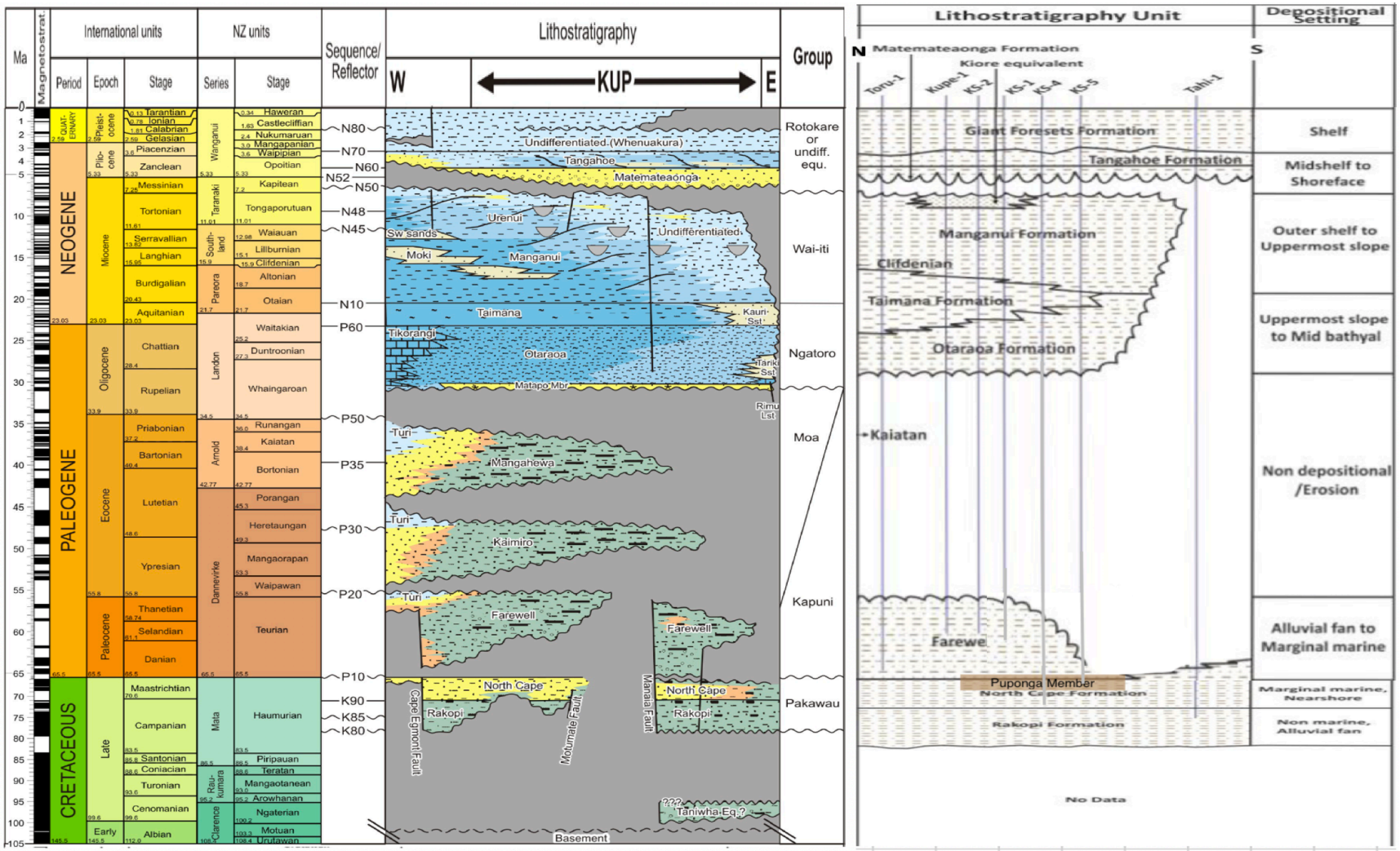

Figure 2.4. Simplified chronostratigraphic column north-south and east-west sections of the Kupe areasouthern Taranaki Basin (Modified from Fohrmann et al., 2012; Roncaglia et al., 2008).

et al., 2009). The North Cape Formation has been reached in the Kupe South field in the well Kupe South-4 (Bierbrauer and Leitner, 2011).

2.3.2. Puponga Formation (Member). The Puponga Formation is the uppermost portion of the North Cape Formation. Hence, it is aged back to the Late Cretaceous. As a consequence of its limited lateral extent (Figure 2.4), it was given a member status instead of formation by Thrasher 1992 (King and Thrasher, 1996). The Puponga Formation was interpreted as being accumulated in a lower deltaic to estuarine depositional system. This formation was described as containing ridges of coal (Bierbrauer and Leitner, 2011; Bal and Lewis, 1994). The Puponga Formation represents a potential reservoir, within the Rua Nose at the southeastern part of the study area at which it would be capped by the marine shale regional seal and juxtaposed against the Farwell Formation (Bal and Lewis, 1994). The lithology of the formation can be divided as follows: coarse sandstone at the upper portion alternating with claystone, and the lower part consisting of claystone interbedded with sandstone (Bierbrauer and Leitner, 2011). Moreover, the whole formation experiences numerous coal seams embrace about 3% of the formation thickness (Bal and Lewis, 1994; Anthony et al., 2005; Mills et al., 2007).

2.3.3. Farewell Formation. The Farewell Formation represents the lowest formation of the Kapuni Group. This formation used to be descried as Late Cretaceous fluvial to shallow marine successions. However, it was reassigned to be Paleocene in age. The uppermost section of the North Cape Formation (The Puponga Formation) is superimposed unconformable by the Farewell Formation, which onlaps over many rise areas (King and Thrasher, 1996; Bland and Strogen, 2012). As King and Thrasher (1996)

indicated that the Paleocene strata of the Farewell Formation are unconformably superimposed the uppermost Late Cretaceous succession of the Pakawau Group.

At the Kupe South field, controlled by the Manaia Fault, north-drainage fluvial system signifies the Farewell depositional environment (Figure 2.5). Notwithstanding, marine intrusions were distinguished at Kupe South-2, -4, and -5 to be later designated as shoreline transgression toward the study area (King and Thrasher, 1996). Thus, the strata of the Farewell Formation are commonly coursing upward regressive deposits of terrestrial sandstone cycles with series of transgression fining upward sediments mainly claystone (Schmidt and Robinson, 1990). The Farewell Formation has rare or no coal measures opposite to that in the Puponga Formation (Constantine, 2008). In the area of interest, the top of the Farewell Formation corresponds to the Eocene unconformity underlying the seal rock (Otaraoa Formation).

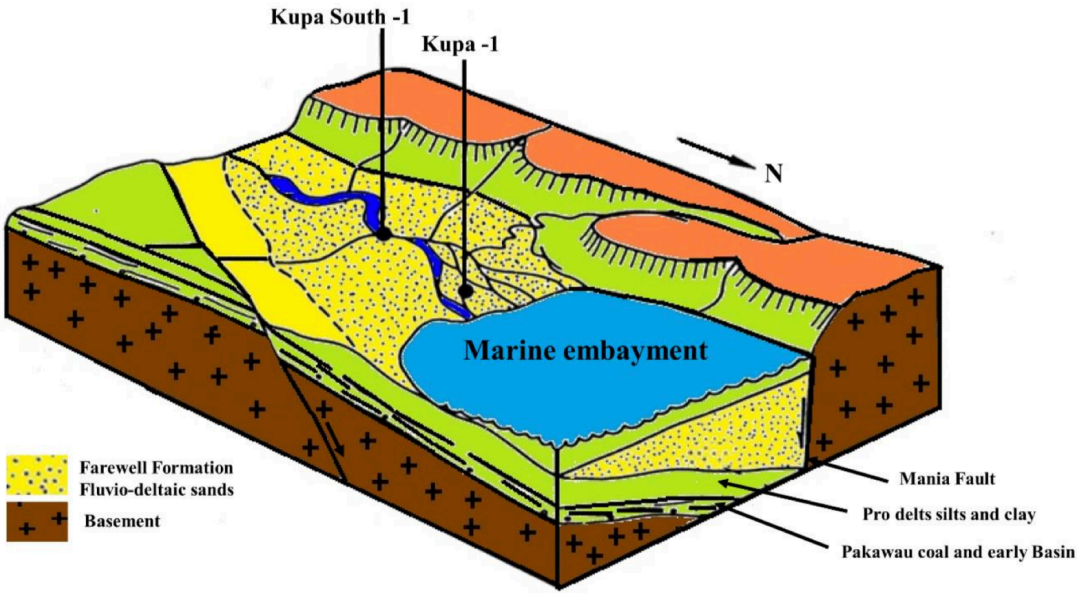

Figure 2.5. Schematic illustration of the Farewell Formation fluvial and shallow marine depositional environment in Kupe Area. Notice, the north-drainage fluvial system (Mathews and Bennett, 1987).

In the Kupe South field, the lower portion of the Farewell Formation represents the source rock (Figure 2.6) whereas the upper part signifies the high-quality hydrocarbon reservoir associated with high net-to-gross value that makes it the key target offshore reservoir (Bierbrauer and Leitner, 2011). The wells of the Kupe South field (e.g., Kupe South-4) have penetrated about 400-500 m of early Paleocene-age strata.

2.3.4. Otaraoa Formation. The Otaraoa Formation is characterized by Oligocene succession of fine-grain calcareous siltstone and mudstone in addition to sub-marine fan sand reach intervals (Tariki sandstone) and Matapo Sandstone Member at the base of the formation. This formation indicates the initiation of major shoreline transgression in the central Taranaki Basin (Palmer, 1985). The sharp change from shallow marine Matapo Sandstone to continental slope mudstone Otaraoa Formation designates the rapid subsidence and marine transgression during the time of deposition (Strogen et al., 2014).

The eastern margin of the Taranaki Peninsula represents the depositional center of the sedimentation (King et al., 2009). The thickest section of Otaraoa Formation measured 1200 m, whereas it thins to reach less than 100 m in the west of the Peninsula region and in other offshore locations, but in the study area the formation was typically 200-600 m thick. The sediments of this formation were derived from uplifted area at the east of the Taranaki Fault and accumulated in the upper bathyal water depths to the outer shelf (King et al., 2009). The marine Otaraoa Formation provides good seal rock as it unconformably overlies the reservoir Farewell and Puponga formations in the Kupe South vicinity (Schmidt, 1989).

2.3.5. Taimana Formation. The Taimana Formation depositional time bonded between very late Oligocene to the beginning of the early Miocene. Its sediments are characterized by fine-grained deposits of calcareous siltstone, sandstone, and mudstone with thin limestone interbeds and was accumulated in environment ranges from the outer shelf to uppermost slope (King et al., 2009; Roncaglia et al., 2008). The elongated eastern border of the Taranaki Basin represents the depocenter of the formation. The general thickness of the formation measures less than 250 m in the western parts of the basin at which the sediments were less than the accommodation space.

2.3.6. Lower and Upper Manganui Formation. The Manganui Formation deposited during the Miocene in shelf, slope, and basin floor water depth. The formation comprised predominately of mudstone and siltstone, but it includes stringers of sandstone and limestone elongated to the basin eastern boundary (King et al., 2009). The formation has a column 1700 m thick in the Peninsula region, but in the Kupe region, it ranges from 700 to 1000 m thick and conformably overlies the Taimana Formation. It was acknowledged that subdividing the formation to Lower Manganui and Upper Manganui formations is convenient (King and Thrasher, 1996; Roncaglia et al., 2008).

In the Kupe South field, fine sediments were accumulated in the initial bathyal foredeep subsidence. Thereafter, the acumination space had infilled aggregately by Mid-Miocene sediments to reach the shelf depth. Near the area of interest, the Manaia Fault had uplifted during the Miocene, causing the central and the northern part of the Manaia Anticline axis to be raised to shelf depths. About 200 m of later Miocene shelf mudstone and siltstone succession was measured in the Kupe-1 well. The strata of Middle to Late Miocene are absent in Kupe and Kapuni fields south of the Manaia Anticline (King and

Thrasher, 1996). The homogeneity of the formation is reflected on the seismic section as low-moderate amplitude with lateral subparallel to wavy continuity (Hansen and Kamp, 2004)

2.3.7. Kiore Formation. The Kiore Formation is identified as strata aged in the late Miocene and is 100-180 m thick in the Kupe region. The lithology of the formation was described as massive to laminated siltstone, sandy siltstone, and sandstone. It is also characterized by a variety of discontinues and nested channels filled with massive sandstone, siltstone, conglomerate, and limestone (King et al., 2009). The environment of the deposition is characterized as outer shelf to upper slope water depths (150-400 m water depth). The shelfal facies preserved at the top portion of the regressive systems tract right below the unconformity (Vonk and Kamp, 2008). In 2007, the Kiore Formation was announced as one of the Late Miocene reservoir targets in the eastern Taranaki Hillcountry (King et al., 2009). The formation is absent within most of the Kupe South field, yet two (Kupe South-1 and Kupe South-2) of the used wells in this study have penetrated the formation.

2.3.8. Matemateaonga Formation. The Matemateaonga Formation is sandstone-dominated succession aged in the uppermost Miocene to Early Pliocene with 1400 m rock column in central area of the Toru Trough. The oldest sediments deposited in this locality are shelf, marginal marine, and terrestrial sediments (King and Thrasher, 1996). The formation lithology was described as muddy sandstone, siltstone, mudstone, limestone/shellbeds, coal, and spots of conglomerate. The conglomerate can be found in areas with formation on-lap with basement such as the southeastern locality of the basin. Unlike the shellbeds in the underlying Kiore Formation, the shellbeds in this formation

are continuous and are comprised of conglomeratic broken fossils or scattered pebbles in coarse sandy matrix (King et al., 2009). The base of the formation represents regional unconformity having Late Miocene tectonic inversion of the southern and eastern section of the Taranaki Basin (Vonk and Kamp, 2008). Afterwards, regional subsidence of the unconformity surface occurred and was followed by marine transgression and deposits onlaping southward over older formations to the west of the Taranaki Fault (Vonk and Kamp, 2008).

2.3.9. Tangahoe Formation. The Tangahoe Formation was deposited during the Early Pliocene subsidence, which was influenced by new activated subduction movement (Taranaki pull-down). This tectonism has affected the southeastern section of the Taranaki Basin and combined it with Wanganui regions to become one contiguous depocenter (King et al., 2009). The formation mainly consists of massive siltstone, approximately 20 m of fine sandstone intervals, and thin shellbeds. The environment of deposition can be described as shelf to bathyal water depths (King et al., 2009). The NW seismic reflection of the Kupe South field corresponded to the Tangahoe Formation as bland amplitude. However, it shows successions of inclined and offlapping reflectors interpreted as progradational shelf foresets toward NE (King and Thrasher, 1996). Based on the seismic progradational pattern, fining upward trends, and shoaling upward trends of the deposits, the shelf-accumulated systems of the Tangahoe Formation are studied to be highstand systems tract (King and Thrasher, 1996).

The lithofacies of the Tangahoe Formation are varied among its vertical succession. The different lithologies within the formation accumulated while recurrent transgressions and regressions cycle over shelf and coastal plains (Naish et al., 2010). All

of the lithofacies were divided into associations named siltstone, sandstone, composed sandstone with siltstone (Heterolithic), and shellbeds. Each of these formation subdivisions represents depth range within intertidal to mid-shelf environments (Naish et al., 2010).

2.3.10. Giant Foresets Formation. The Giant Foresets Formation is identified as mainly fine-grained accumulations of Pliocene to Pleistocene in age. It primarily consists of siltstone and mudstone with interspersed sandstone. The formation interval represents the thickest unit of the western platform up to 2200 m thick (King and Thrasher, 1996). According to Hansen and Kamp (2004), the continuing aggradational-progradational stacking patterns of the Pliocene-Pleistocene time are identified as continental marginal accumulations of the the Giant Foresets Formation. Prograding wedge restricted from the shelf break to deep slope environment was building toward the southeast. Within this formation there is topset aggradation (shelf facies) continuing laterally without disruption into the foreset (slop facies) and into the bottomset (basin floor). This continuity indicates high rate of sediment supplies (King and Thrasher, 1996).

2.4. PETROLEUM SYSTEM

The Taranaki petroleum systems have relative timing of requisite elements, which are demonstrated in Figure 2.6. Kupe South field's hydrocarbon accumulations were originated from the Late Cretaceous to Paleocene, organic-rich, sedimentary source rocks that were thermally cooked in the basin kitchen regions under the affection of the younger overburden rocks and then migrated into shallower sandstone units within the structural traps.

2.4.1. Source Rock. The geochemical type of the hydrocarbon accumulations in most of New Zealand traps is backed to coaly facies of Late Cretaceous to Paleogene in age, yet the coal-bearing strata of New Zealand basins cover the majority of the periods from the Jurassic to Miocene (Figure 2.6). This wide age range of the coal-rich units indicates that the vital factors are maturation history and facies, not the age of the organic matter (NZP&M, 2014). As a result, the coal-rich units within the Late Cretaceous Pakawau Group succession and the Paleogene Kapuni Group strata are considered to be potential source rocks in the Taranaki Basin. This result was reached based on the analysis of the organic content, hydrogen richness, and maturity constraints of the units, which were obtained from the majority of the wells in the basin (King and Thrasher, 1996). The distributions of the coal seams within the Paleogene layers suggest the overall extent of marine transgressive cycles, with mainly terrestrial sediments being accumulated towards the ESE. The Paleogene Farewell Formation shows less coal measures to the south of Kapuni Field with variation in marine impact. However, in the Kupe South field, the source rock is suggested to be the Farewell Formation kitchen area to the northeast or the lower portion of the formation that is comprised of a significant amount of organic matter, which have very good hydrocarbon generative potential. Underlying the Farewell Formation, the older Late Cretaceous marginal marine deposits of the North Cope Formation exhibit low potential to generate hydrocarbon (King and Thrasher, 1996). However, the upper portion of the formation at which the coaly Puponga Member/formation is situated has good potential to expel hydrocarbons as the formation is rich in organic matter.

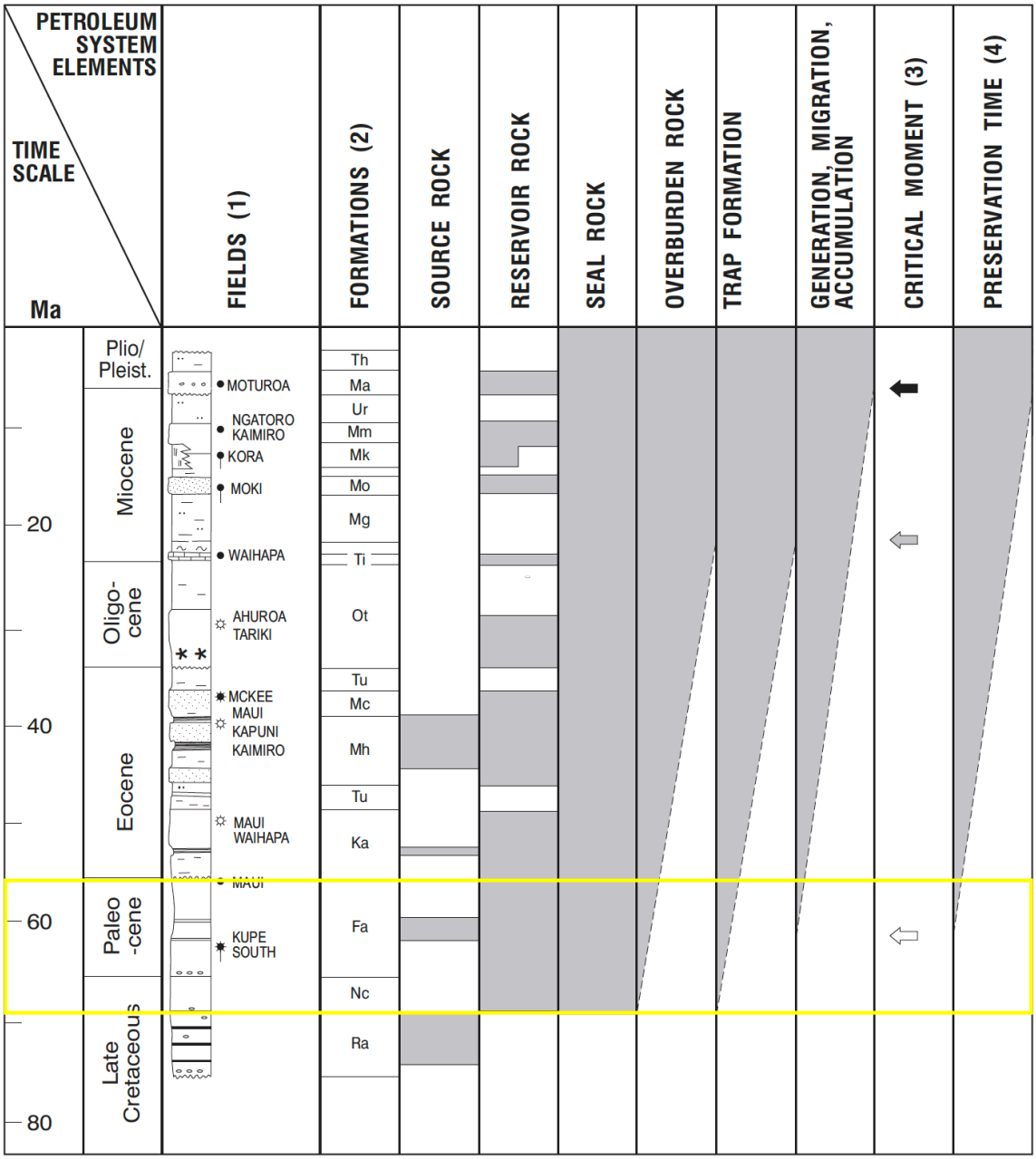

Figure 2.6. Event chart of Taranaki petroleum systemsillustrating the timing of requisite elements (gray colored). Note that the marked yellow area demonstrates the relative timing of requisite elements for the Kupe South field (Late Cretaceous-Paleocene), and the Generation, Migration, and Accumulation of this period hydrocarbons are at initial stages (Modified from King and Thrasher, 1996).

2.4.2. Maturity and Migration. The source rocks need to be overburdened to variable depth ranges to generate and expel hydrocarbons. This is generally related to the properties of the source rock and the history of the heat flow to which the source rock was subjected. Nowadays, over most New Zealand basins, thermal studies took place to suggest that the burial depth required for the source rocks to have hydrocarbon generative potential ranges from 4000 m to 4500 m (NZP&M, 2014). However, locations such as the Great South Basin at which the source rocks subjected to longer burial time, require burial depth of approximately 3000 m to have hydrocarbon generative potential. After the coal seams are considered to be the source rock of the majority of Taranaki hydrocarbons, recent studies suggest that leaf cuticles form much kerogen that converts to oil are the potential organic matter. Thus, the large accumulation of oil in Taranaki reservoirs (e.g., Tui and Maari- Manaia fields) may be generated and expelled from cuticle-rich coals (NZP&M, 2014).

2.4.3. Reservoir. The Kupe South field reservoir sequence is primarily the Paleocene Farewell Formation. However, the swampy lower deltaic fluvial to upper estuarine Puponga Formation is considered another reservoir section in the Momoho area. The Farewell sandstone unit of fluvial braid and coastal plains has good porosity exceeding 20% (Schmidt and Robinson, 1990). This sandstone reservoir is described primarily as medium-to-coarse grained with good permeability ranging up to several hundred mD (NZP&M, 2014). In the Momoho-1 well area, the reservoir is divided into a lower unit (Puponga Formation) and upper unit (Farewell Formation), with total thickness achieving 400 m. The Oligocene Otaraoa Formation provides good seal rock for the underneath reservoir sequence (Constantine, 2008).

The reservoir quality in three Kupe South wells (Figure 1.3) shows slight differences from one well to another. The first well is the Momoho-1 well. This well intersects 24.4 mMD of gross thickness that contains 7.2 mMD of net gas pay in the Farewell Formation (29.5% N: G). The average porosity of the formation is 24.0% with 55.8% average gas saturation. The second is the Kupe South-4 well, which is located 2.4 km to the north of the Momoho-1. It was drilled and encountered 35.4 m gross gas column (12 m net). Puponga and the underneath North Cape Formation at this well are dry. The gas column at the upper portion of the Farewell Formation was tested to show flowed gas rate 10.3 MMCFD and condensate at a maximum rate of 610 BBLD (Constantine, 2008).

The formation pressure testes in the Kupe South wells indicated that the reservoir is not in communication with other reservoirs in the Kupe field; it represents a separate pool. The final well is the Kupe South-5, which was drilled at 1.2 km SSE of the Momoho-1 well. The well penetrated a 37.8 m gross oil column (15.8 m net) accumulated at the top of the Puponga Formation and is sealed by marine shale of the Otaraoa Formation (Constantine, 2008). The Farewell Formation was eroded, and base marine shale represents the Oligocene unconformity. Two evaluation tests were run separately. The first was run over the lower half of the oil column to show no flow to surface, probably due to tight formation. The second test was run over the upper half of the oil column and succeeded to flow oil (39.5o API) and gas to the surface at a stabilized rate of 1310 BOPD and 3.7 MMSCFD, respectively (Constantine, 2008).

2.4.4. Seal. In general, the mudstone layers in the Taranaki Basin are widespread and provide top or internal seals to the reservoirs. Most of the reservoir formations

beneath the seal rock in the Eastern Mobile Platform are over-pressurized, indicating that the overlying seal rocks are regionally effective (King and Thrasher, 1996). In Kupe South field, the Late Eocene to Oligocene marine shale of the lower Otaraoa Formation is overtop all the reservoir formations and provides good seal rock (Constantine, 2008). Faulting affects the distribution of the hydrocarbons in the Momoho-1 area and provides different scenario of sealing. The most likely scenario is the Denby D Fault plane not sealing but the KS4 Fault plane is sealing. This must extend the gas pool eastwards into the Momoho East compartment (Constantine, 2008).

2.4.5. Diageneses. Generally, the diageneses history in the Taranaki Basin has its effects on reservoir quality and on the generation and migration of the hydrocarbons. In Kupe South for example, during the burial of the sandstone of the Farewell Formation, the composition of the pore water has experienced a major shift, causing the formation to contain a diagenetic mineral accumulation (Figure 2.7) (King and Thrasher, 1996). Early calcite was crystalized from meteoric pore water trapped during deposition of the Farewell Formation. Thereafter, marine pore water seeps from overlying Otaraoa marine mudstone, causing chlorite/smectite to be formed before the late Miocene compaction was completed (King and Thrasher, 1996). Late calcite and carbonates probably have formed from connate meteoric waters that were expelled from Cretaceous underlying deposits to the reservoir formation.

Later kaolinite and secondary porosity were formed along Miocene-Pliocene unconformity as a result of local meteoric invasion. The dissolution of silicate and mainly carbonates has caused a development in sandstone secondary porosity, which implies the presence of a high amount of solvents and a means of migration from source rocks to

reservoirs. According to King and Thrasher (1996), the chemicals expelled from maturing kerogen, such as carbon dioxide and organic acids, might be the potential solvents. The hydrocarbons migration pathways from the source rock to the up-dip reservoir are probably a combination of original primary porosity, rock fractures, and secondary porosity that generated earlier (King and Thrasher, 1996).

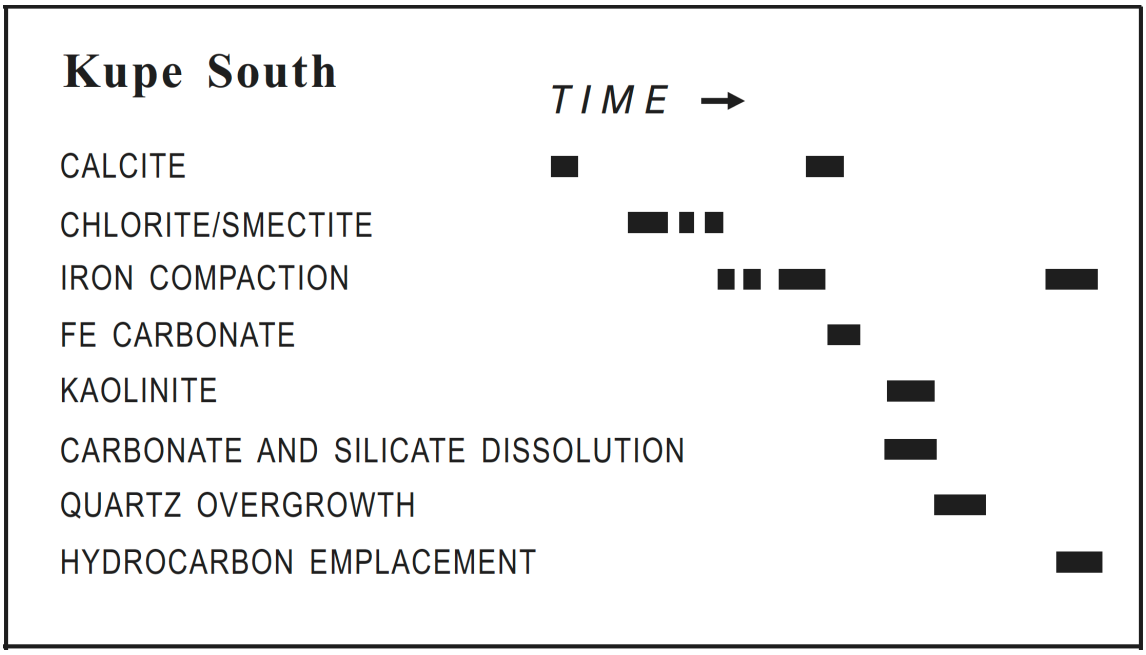

Figure 2.7. Generalized diagenetic sequences in the Kupe South Field, Taranaki Basin, New Zealand (Modified from King and Thrasher, 1996).

2.4.6. Traps. All significant petroleum accumulations presently known in the Taranaki Basin are structural trapped. All of these traps were formed in the Neogene age within the Eastern Mobile platform. However, the Kupe South field has an extra component of stratigraphic trapping that was interpreted as an unconformity trap (Figure 2.8) below the base marine shale (King and Thrasher, 1996; NZP&M, 2014). The structural traps in the Kupe South are anticlines of positive structural inversion controlled from the west by one major bounding fault (Manaia Fault). Any element of stratigraphic

trapping in the Taranaki Basin appears to be ancillary. The reservoir distributions in the Kupe South field may be partly controlled by lithology-dependent diagenetic effects (King and Thrasher, 1996).

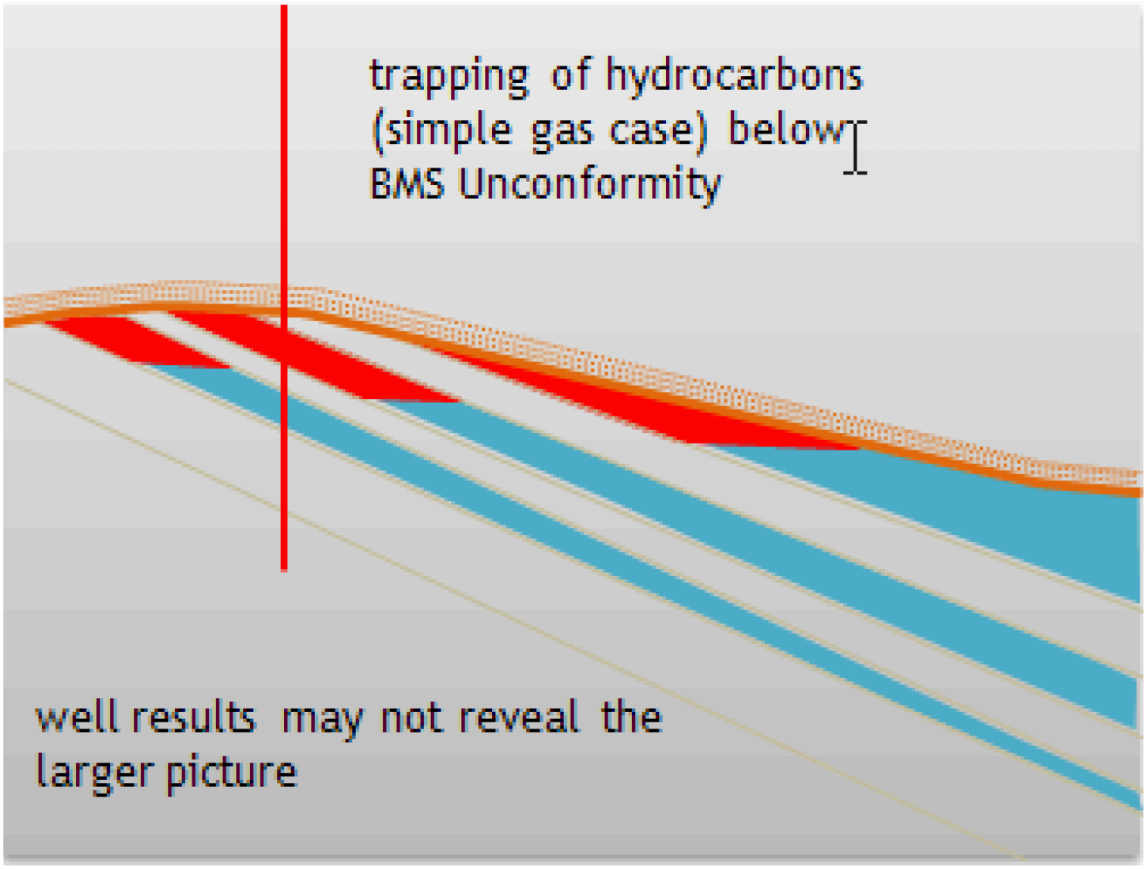

Figure 2.8. Theoretical unconformity trap in the lower Farewell Formation (Bierbrauer and Leitner, 2011).

2.4.7. Timing. The development timing of fundamental geological parameters in any petroleum system is obligatory for hydrocarbons to then be expelled, migrated, and trapped commercially in reservoir rocks. In Kupe South, the reservoir sandstone diageneses influenced migration of the hydrocarbons, which were then trapped in the Pliocene to present (King and Thrasher, 1996).

2.5. SEISMIC STRATIGRAPHY

The seismic reflectivity is influenced by several factors related to the distribution of the physical properties and the consistency of the geological parameters within the lithology. As an example, the mineral distributions within a rock layer vary laterally, which will accordingly lead to density variation. Additionally, well locations might not be situated accurately on a vertical seismic plane and the formation top projection might be superimposed incorrectly onto the seismic section. Hence, superimposing the lithostratigraphic units with its corresponding seismic reflectors may be not possible. In this study, each seismic reflector is chosen as near as possible to its equivalent log-based lithostratigraphy, but variation in accuracy must be anticipated.

3. DATA AND METHODOLOGY

3.1. KUPE_3D SEISMIC DATA

The 3D offshore seismic survey data utilized in the study were obtained from New Zealand Petroleum and Minerals (NZP&M). The Kupe 3D seismic data was acquired in 1989, license PPL 38116, and then was merged with 1987 exploration 3D data to cover the southern half of the PML 38146. The areal extent of the 3D seismic data used in this study is approximately 135 km^2 (Figure 3.1), which was covered by total of 345 inlines and 1609 crosslines with grid spacing of 13.33m x 25m to generate the final data volume with 5 s TWT (Singh, 1989).

3.1.1. Data Acquisition Parameters. In total, the reconnaissance 3D data of 1987 and 1989 were acquired through 757 kilometers of sail line. The two seismic data sets were acquired in the offshore Taranaki Basin by Western Geophysical with LRS 16 recording system and DFS-V NO. 357 system, respectively. Then seismic survey data were processed and merged as Kupe South 1987/1989_3D Seismic Survey by Tensor Pacific Pty. Ltd. for TCPL Resources Ltd. The survey acquisition parameters are displayed in Tables 3.1 and 3.2.

3.1.2. Polarity Check. Normal European polarity (- SEG polarity) was preserved through the data set. If there is an increase in the acoustic impedance, the reflection is registered on the displayed tape as negative number and is shown as white trough (Schmidt, 1989).

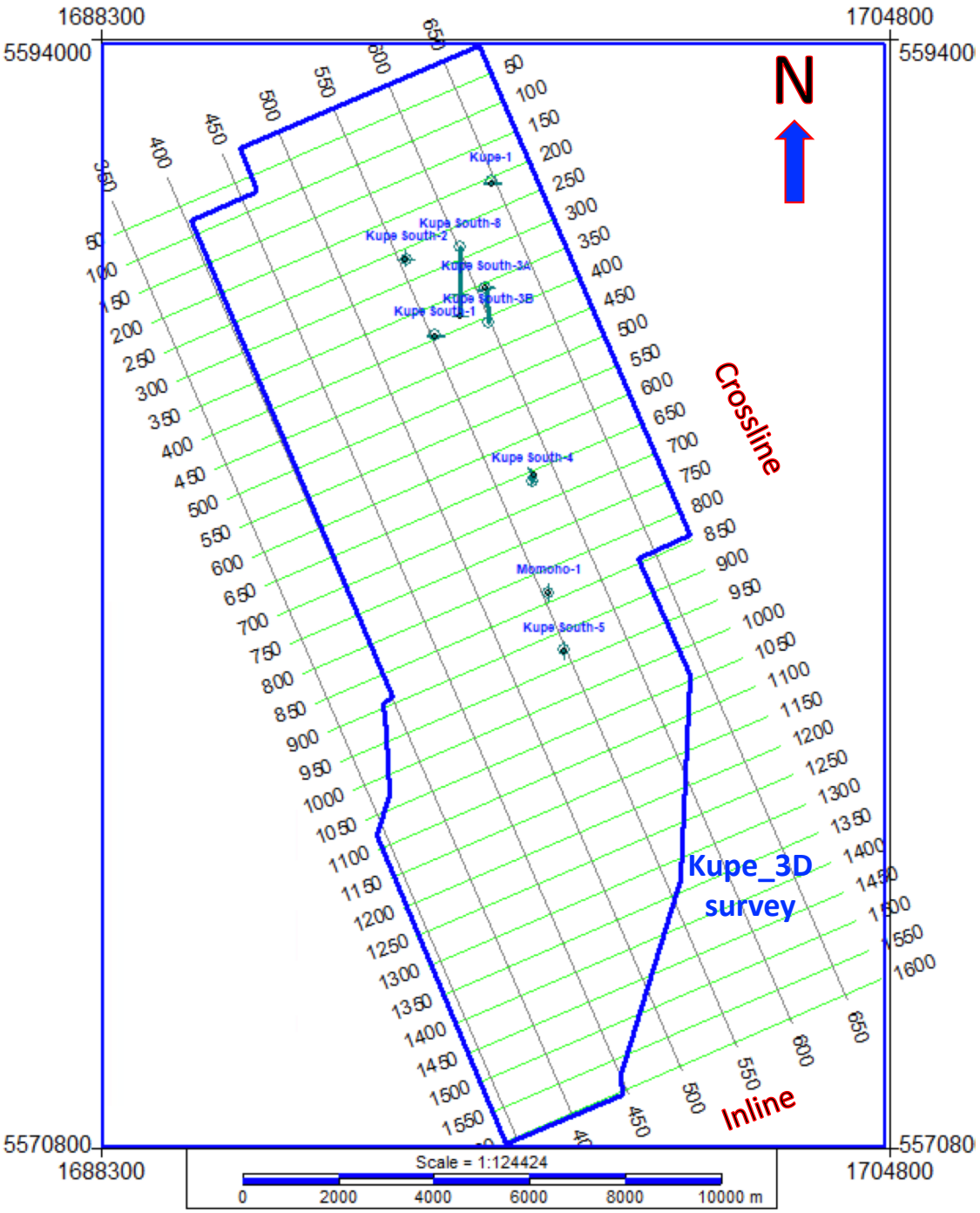

Figure 3.1. Kupe_3D survey with the well locations. Inline and crossline interval displayed is 50.

Table 3.1. 1987 acquisition parameters for the Kupe_3D survey (Singh, 1989).

PARAMETERS	**VALUE**
Recording system	LRS 16
Recording format	SEGD 6250 B.P.I.
Recording length	6 seconds
Sample rate	2 milliseconds
Gain mode	I.F.P.
Source	Airgun
Array volume	1565 in^3
Array pressure	4500 P.S.I.
Gun depth	6 meters
Shot interval	26.66 meters
Recording channels	240 array formed to 120
Group interval	13.33m array formed to 26.66m
Hydrophones/group	6
Streamer depth	8.5 meters
Near offset	231 meters
Far offset	3403 meters

Table 3.2. 1989 acquisition parameters for the Kupe_3D survey (Singh, 1989).

PARAMETERS	**VALUE**
Recording system	DFS-V NO. 357
Recording format	SEGB 6250 B.P.I.
Recording length	6 seconds
Sample rate	2 milliseconds
Gain mode	I.F.P.
Source	Airgun
Array volume	1040 in^3
Array pressure	4500 P.S.I.
Gun depth	6 meters
Shot interval	25 meters
Recording channels	120
Group interval	25
Hydrophones/group	20
Streamer depth	6 meters
Near offset	170.8 meters
Far offset	3145.8 meters

3.2. WELL DATA

The kupe_3D dataset includes 12 wells. The first well drilled within the study area was the Kupe-1 in 1975. Then, series of wells were drilled between 1987 and 1991, and others from 2007 to 2008. Some of these wells were exploratory and appraisal, while others were developmental (Table 3.3). Figure 3.1 shows the location of each well drilled within the study area. Most of the wells have a variety of wireline logs such as gamma ray, resistivity, spontaneous potential, density, caliper, and sonic logs, except the well Kupe South-3A (Table 3.4).

Table 3.3. Previous drilling history within the study area.

WELL	SPUD	TYPE	TOTAL DEPTH (meter)		RESULT (Discovery)	RESULT
			mMDRT	mTVDSS		
Kupe-1	1975	Exploration	3681.7	3672.6	oil shows	Plug & Abandon
Kupe South-1	1986	Exploration	3502.7	3469.7	oil & wet gas	P&S
Kupe South-2	1987	Exploration	3249.7	3216.2	oil & wet gas	P&S
Kupe South-3	1987	Appraisal	3447.0	3187.7	oil & wet gas	P&S
Kupe South-4	1989	Appraisal	3800.0	3755.9	wet gas	Plug & Abandon
Kupe South-5	1990	Appraisal	3200.0	3168.9	oil discovery	P&S
Kupe South-6	2008	Development	3385.0	3319.7	oil & wet gas	Gas-condensate producer
Kupe South-7	2008	Development	3454.0	3191.5	oil & wet gas	Plug & Abandon
Kupe South-7ST1	2008	Development	3503.0	3277.5	oil & wet gas	Gas-condensate producer
Kupe South-8	2008	Development	3834.0	3317.9	oil & wet gas	
Momoho-1	2008	Exploration	3145	3105.4	Gas-condensate	Plug & Abandon

Table 3.4. Log chart for each well drilled within the study area.

Well Name	Well logs														
Kupe South-1	BS	CALI	DENS	DRHO	DTC	GR	NEUT	PEF	RESD	RESM	RESS	SP	TEMP	TENS	
Kupe South-2	BS	CALI	DENS	DRHO	DTC	GR	NEUT	PEF	RESD	RESM	RESS	SP	TEMP	TENS	
Kupe South-3A	No wireline logging was performed														
Kupe South-3B	BS	CALI	DENS	DRHO	DTC	GR	NEUT	PEF	RESD		RESS	SP	TEMP	TENS	
Kupe South-4	BS	CALI	DENS	DRHO	DTC	GR	NEUT	PEF	RESD	RESM	RESS	SP	TEMP	TENS	
Kupe South-5	BS	CALI	DENS	DRHO	DTC	GR	NEUT	PEF	RESD	RESM	RESS	SP	TEMP	TENS	
Kupe South-6	BS	CALI	DENS	DRHO	DTC	GR	NEUT	PEF	RESD	RESM	RESS	SP	TEMP	TENS	DTS
Kupe South-7	BS	CALI	DENS	DRHO	DTC	GR	NEUT	PEF	RESD	RESM	RESS				
Kupe South-7ST1	BS	CALI	DENS	DRHO	DTC	GR	NEUT	PEF	RESD	RESM	RESS	SP		TENS	DTS
Kupe South-8	BS	CALI	DENS	DRHO	DTC	GR	NEUT	PEF	RESD	RESM	RESS				
Kupe-1	BS	CALI	DENS	DRHO	DTC	GR	NEUT		RESD		RESS	SP	TEMP		
Momoho-1	BS	CALI	DENS		DTC	GR	NEUT	PEF	RESD	RESM	RESS		TEMP	TENS	DTS

BS-Bit size; CALI-Caliper; DENS-Density; DRHO-Bulk density correction; DTC-Delta- T Compressional; DTS-Delta-T Shear; GR-Gamma Ray; NEUT-Neutron; PEF- Photoelectric factor; RESD-Deep Resistivity; RESM-Medium Resistivity; RESS- Shallow Resistivity; SP-Spontaneous Potential; TEMP-Cartridge Temperature; TENS- Cable Tension.

3.3. METHODOLOGY

The 3D seismic dataset of the study area was first imported to the Kingdom Suite software 2017 in its SEGY form using NZGD2000 as survey datum. After that, the well logs, formation tops, and the check shot data (TD charts) were also imported. Then, these datasets were utilized in generating and displaying the synthetic seismograms on the vertical sections of the seismic cube (well to seismic tie), which helped signify and interpret the target horizon after all of the major faults within the target interval were manually picked.

The Petrel software was used to enhance and condition the data to reduce noise that was recorded during data acquisition to increase reflection continuity. A number of attributes were generated, including edge detection (variance and chaos), and frequency decomposition attributes. RGB (red, green and blue) and CMY (cyan, magenta, and yellow) color blending were applied utilizing Box Probe to reveal more edge continuity for fault and channel detection.

Finally, both the Petrel and the Kingdom Suite software were used simultaneously to detect and interpret the target horizons and faults. Fault polygon, time structure map, average velocity map, and depth structure map were generated to create fault and horizon model. Figure 3.2 provides general visualization of the workflow.

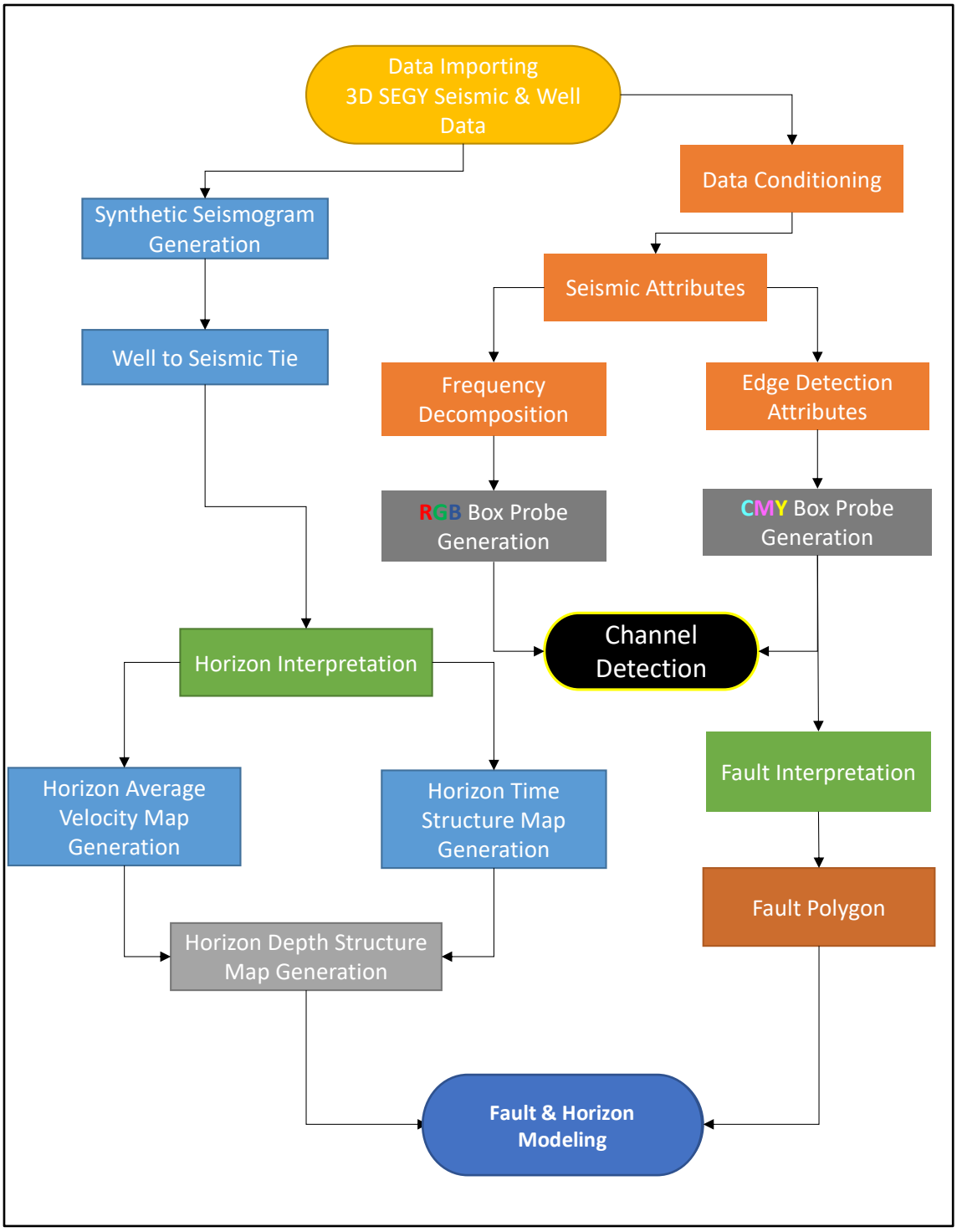

Figure 3.2. Interpretation workflow.

4. SEISMIC ATTRIBUTES AND BOX PROBES GENERATION

Seismic attributes are used in structural and stratigraphic interpretations as they boost the geological and geophysical features by justifying them and enhancing their manifestation. In addition to the seismic attributes, one of Geobody Probe tools used in this study can be defined as a recent method to do opacity-controlled visualization of voxels along predefined boundaries (box probe). The Box Probe is three-dimensional body of voxels that can be resized to an area of interest. Figure 4.1 demonstrates five seconds of vertical section with Tangahoe and Farewell formation intervals highlighted in yellow.

4.1. ATTRIBUTE VOLUME DERIVATION

For the seismic attribute generation, Petrel 2017 was used to produce the seismic volume attributes, such as amplitude gain control (AGC), frequency filtering, structural smoothing, variance, chaos, envelop, iso-frequency, and instantaneous phase. The amplitude gain control (AGC), frequency filtering, and structural smoothing were used as post-stack processing attributes. Variance, chaos, and envelop were mostly utilized as structural attributes. Iso-frequency and instantaneous phase were used generally for stratigraphic purposes. All of the attribute volumes were built with the Petrel using the volume attribute dialog. However, the input parameters were varied based on the quality of the visualization and the objective of the attribute outputs. Each of the attribute volumes was created after several experimentations were applied to visually determine the best parameters. Initially, virtual attribute was generated at which the input parameters were adjustable. Thus, the right parameters for the best output were

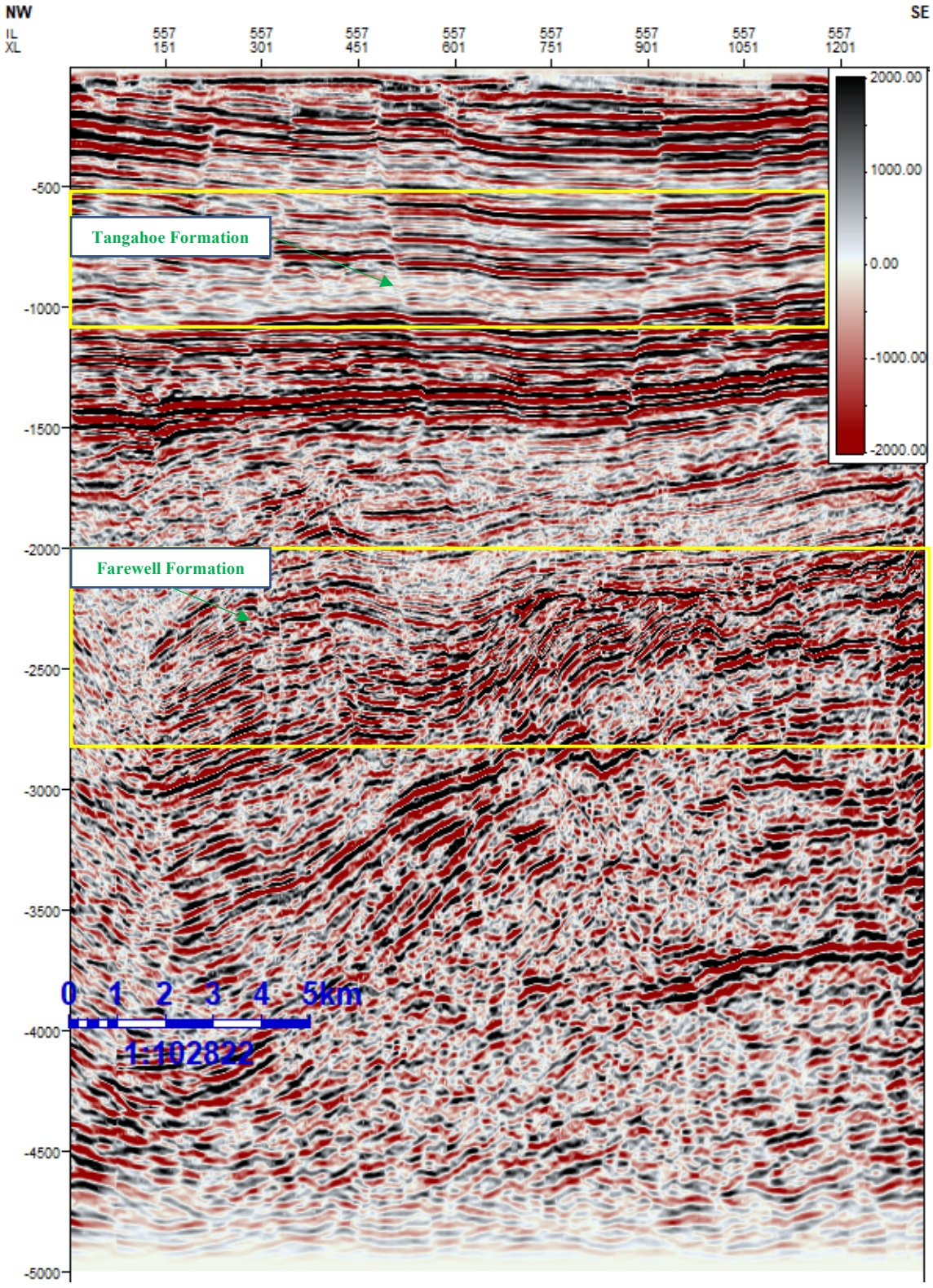

Figure 4.1. Inline 557 vertical section (5 second TWT) with highlighted intervals of study (yellow boxes).

were determined. At this point, the virtual attribute volumes were realized to their permanent ZGY files.

4.1.1. Post-Stack Attributes. The amplitude gain control (AGC), frequency filtering, and structural smoothing attributes were used as post-stack processing for filtering and conditioning the original amplitude volume to better prepare it for structural attribute generation and interpretation.

4.1.1.1 Amplitude Gain Control (AGC). AGC is a post-stack processing procedure used in this study to intensify low amplitudes among the original amplitude cube and moderate very high amplitudes in the intension of increasing the structural interpretability. To generate this attribute, an RMS window of 1000 was applied. A noticeable difference was observed from the original amplitude volume (Figure 4.2B).

4.1.1.2 Frequency filter. Frequency filter is the next step in enhancing the seismic data after the AGC volume is produced. The frequency filter attribute was utilized on the previously created AGC volume to aid in reducing noise from the seismic signal and enhancing particular seismic events. Its creation is very similar to the AGC attribute. However, its effect on the inputs is different; the frequency filter holds back a large portion of the seismic energy. Consequently, modification of the color table was required as the input parameters of the filter have been changed. To create this attribute, an Omsby filter and a Hamming taper were chosen as input parameters because they showed the best noise reduction without losing much seismic energy (Figure 4.2C).

4.1.1.3 Structural smoothing. The attribute of structural smoothing was utilized to smooth the input seismic energy of the frequency filtered volume and improve the continuity of its seismic reflectors (Figure 4.2D). This attribute has principal component

of dip and azimuth calculation preformed to define the local structure. Then, structurally guided gaussian filter with edge enhancement parameters were chosen to smooth the seismic data corresponding to the dominated structural direction, and to enhance the detected edges, respectively.

4.1.2. Structural and Stratigraphic Attributes. Variance, chaos, envelop, iso-frequency, and instantaneous phase attributes used to identify structural and stratigraphic characteristics such as faults, channels, and formation tops within the early Pliocene Tangahoe Formation and Paleocene Farewell Formation. Variance and iso-frequency volume attributes were also used in the Geobody Probe (Box Probe) generation.

4.1.2.1 Chaos. The chaos attribute is a type of variance attribute. It calculates the lack of organization in dip and azimuth directions. However, it differs from variance in terms of the orientation of the calculation window: while variance uses a vertically oriented window, chaos uses a horizontally oriented one.

In this study, Petrel was used to measure the level of chaos between traces within the previously conditioned seismic data. Values of directional sigmas (X=2.5, Y=2.5, and Z=2.5) were inserted to specify the dimensions of the calculation window. The chaos attribute volume which was generated utilizing these values showed superior unchaotic visualization of the faults. However, small faults are unobservable as in the variance attribute (Figure 4.3C). The high chaotic patterns refer to the existence of faults. The chaos color bar is scaled from 0 to 1, where 1 is the most chaotic.

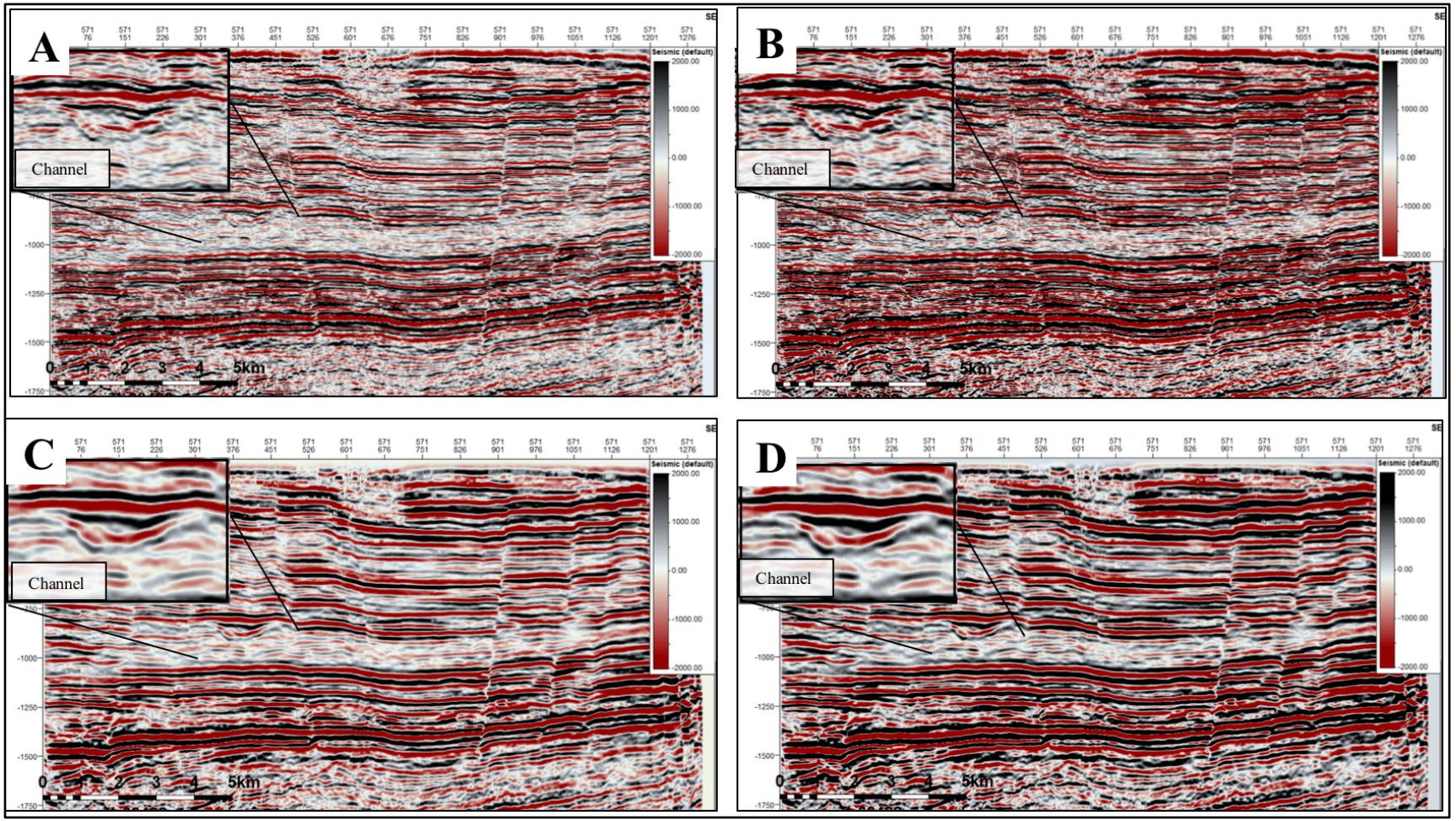

Figure 4.2. Uninterpreted Inline 571 illustrating seismic amplitude throughout data conditioning. A) Original seismic vertical section, notice channel, before data conditioning. B) After applying Amplitude Gain Control (AGC). C) After adding Frequency Filtering. D) After the structural smoothing. Notice channels are clearly visible after data conditioning.

4.1.2.2 Variance (Coherence). The variance attribute measures the similarity in waveform shape between seismic traces using a vertically oriented window. This attribute was used in this study to isolate edges from the input seismic data at both intervals for the Tangahoe and Farewell formations. High variance events indicate the existence of faults, which causes discontinuities in the horizontal continuity of the amplitude. Variance is also applicable to reveal stratigraphic features such as reefs and channels if it is applied with a short window. Therefore, three different variance volumes (1, 2, and 3) were created using variable parameters (Table 4.1).

Variance Volume 1 was realized after the virtual mode showed the best vertical display of processed high-angle major and minor faults. These faults are located within the upper portion of the dataset at which the Giant Foresets, the Tangahoe, and the Matemateaonga formations were deposited (Figures 4.3B and 4.4). Variance Volume 2 provides high clarity, resolution, and detection of the same faults mentioned above in addition to minor faults, but in horizontal display instead of the vertical display used in Volume 1 (Figure 4.5). Parameters of Variance Volume 3 demonstrated in Table 4.1 were established based on the capability of identifying deeper situated faults that had affected the lateral and vertical distribution of the Farewell Formation (Figure 4.6).

Table 4.1. The parameters used to produce variance volume.

Parameters name	Variance Volume 1	Variance Volume 2	Variance Volume 3
Inline range	1	1	4
Crossline range	7	7	7
Vertical smoothing	27	47	60
Dip correction	Not applied	Not applied	On

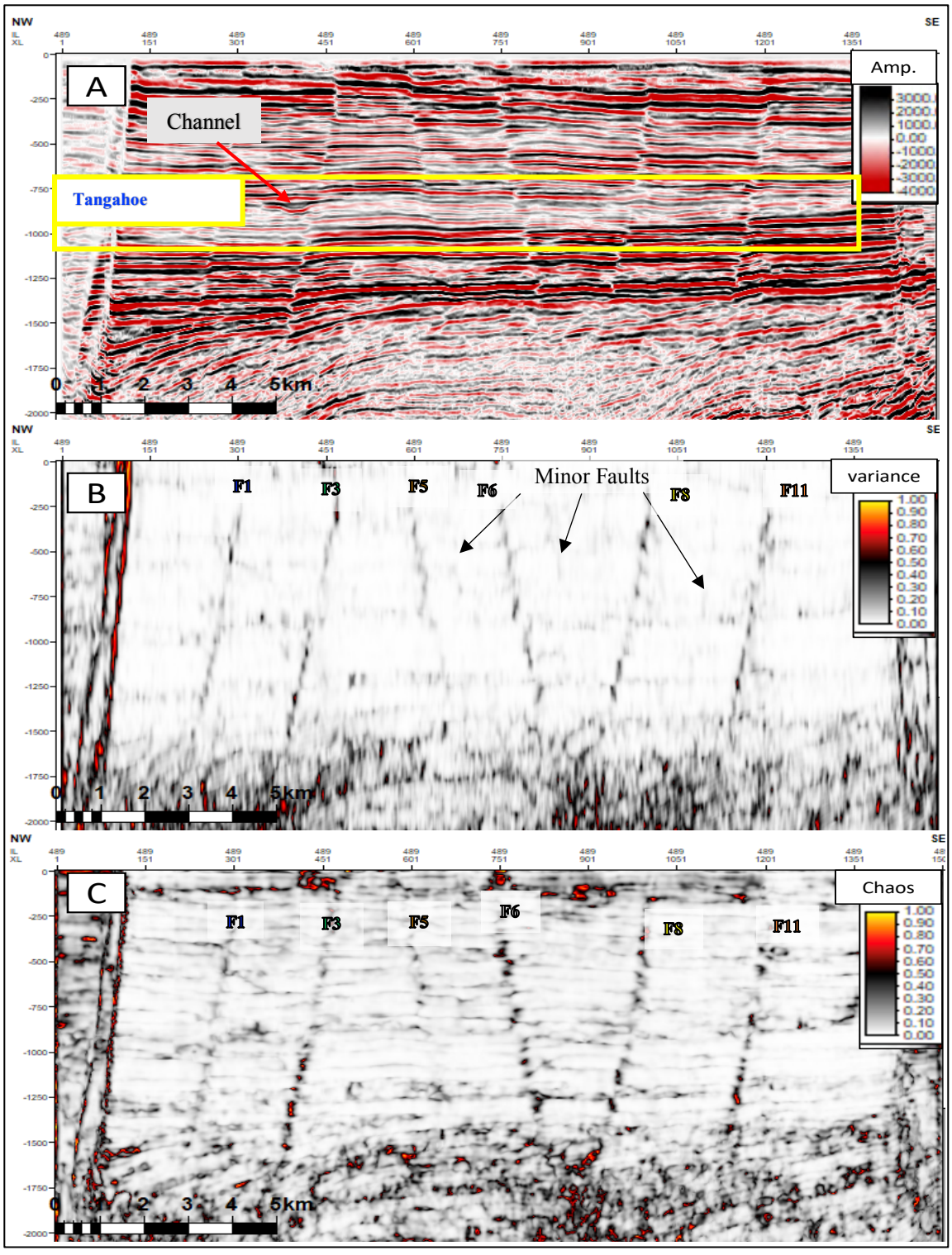

Figure 4.3. Inline 489 vertical seismic sections. A) Conditioned amplitude vertical display. B) Variance attribute seismic section. C) Chaos attribute vertical section. The Variance attribute is preferred as it can reveal small faults (Notice the arrows). Chaos will not only enhance faults but also allows too much chaotic texture within this seismic data.

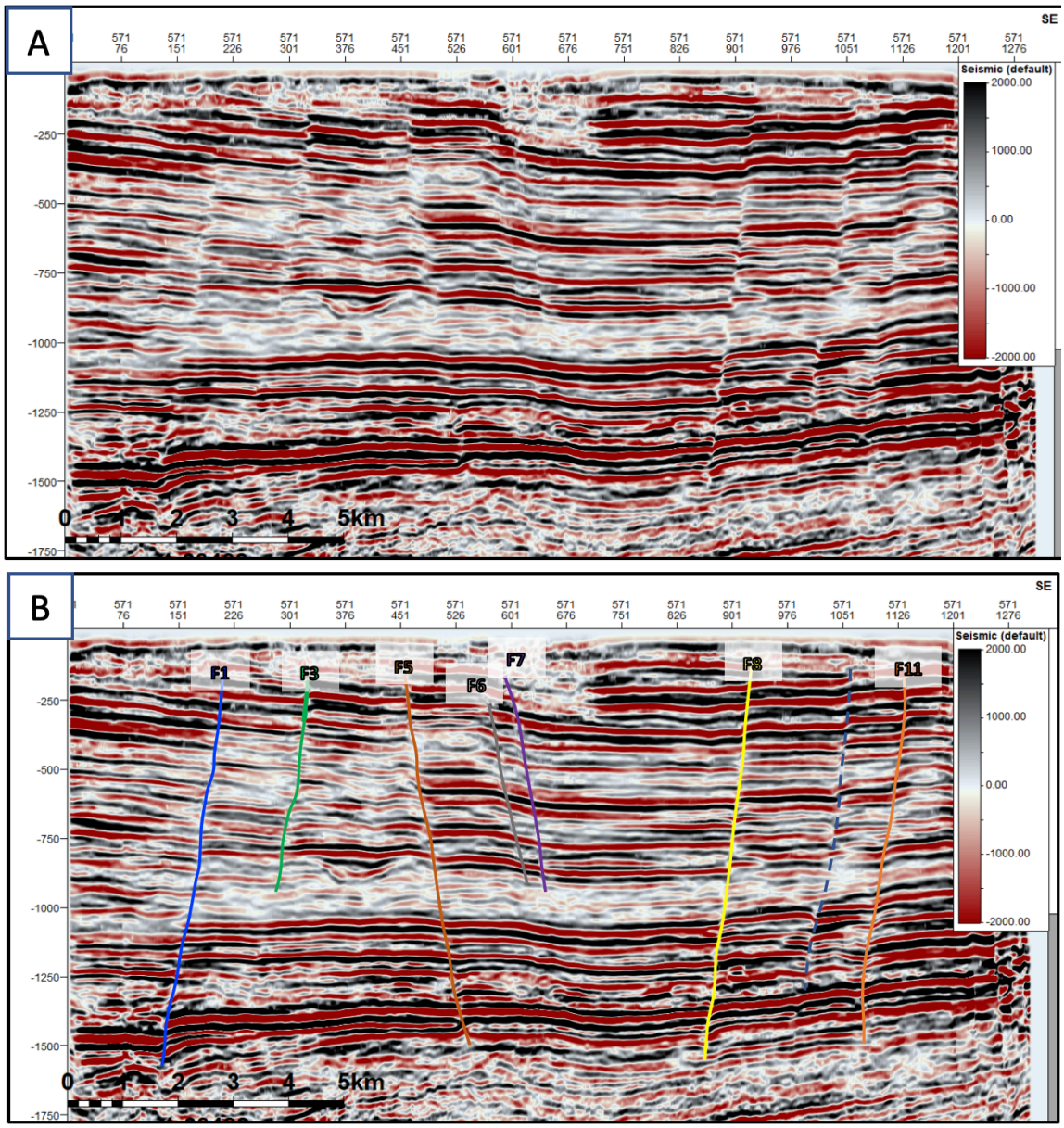

Figure 4.4. Inline 571 illustrating post-filtering fault interpretation.A) Uninterpreted seismic section. B) Fault interpreted vertical section. The color bar shows the amplitude values. The target horizon (Top Tangahoe Formation) is between 0.7 to 0.9 milliseconds (17.8 km long section).

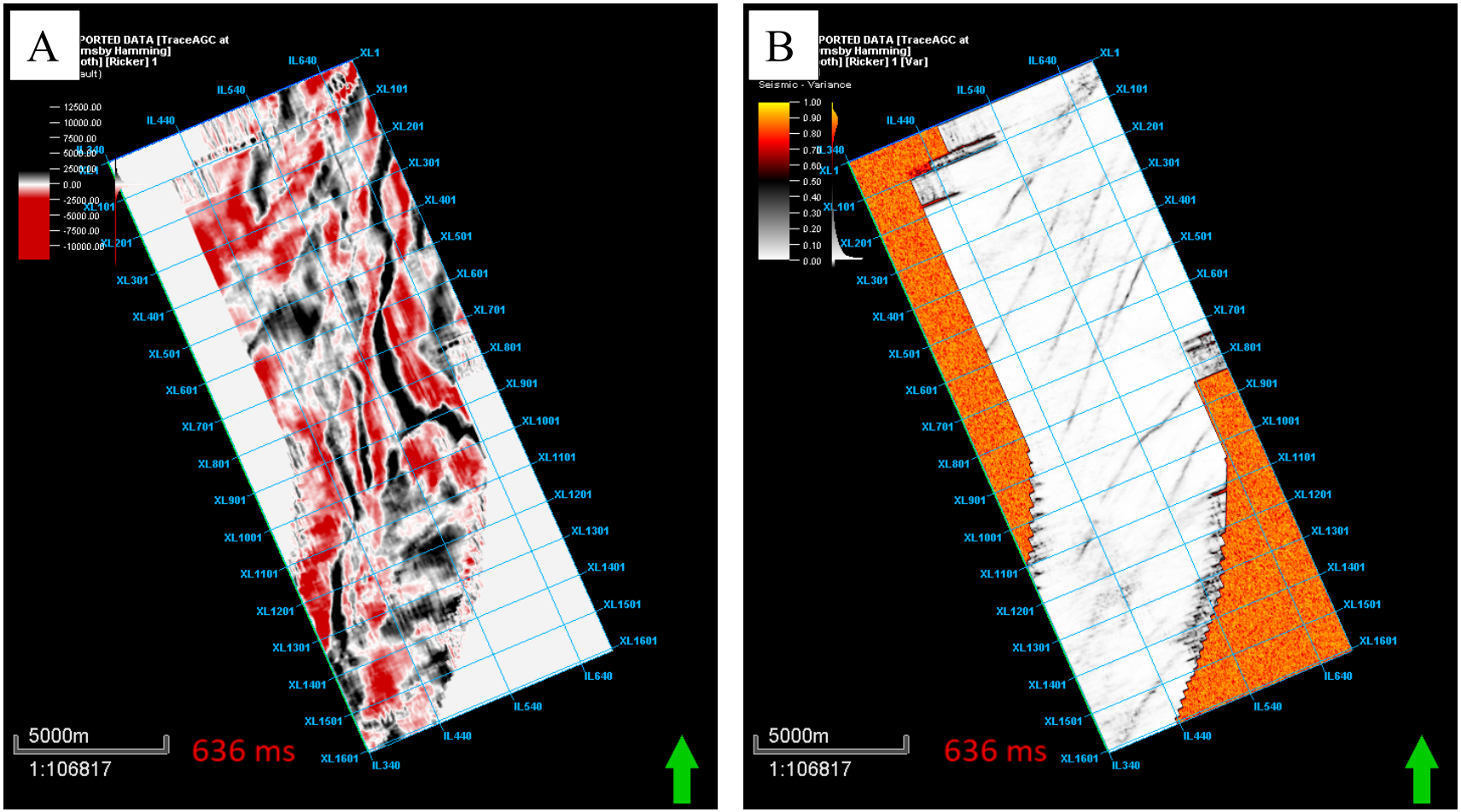

Figure 4.5. Time slices at 636 ms illustrating general view of faults trending NE-SW above the Tangahoe Formation. A) An amplitude time slice. Notice faults are barely seen. B) A Variance Volume 2 time slice clearly reveals the faults after edge detection Variance attribute was applied. These faults are displayed in Figure 4.2 which illustrates the vertical extent of faults penetrating the Tangahoe Formation.

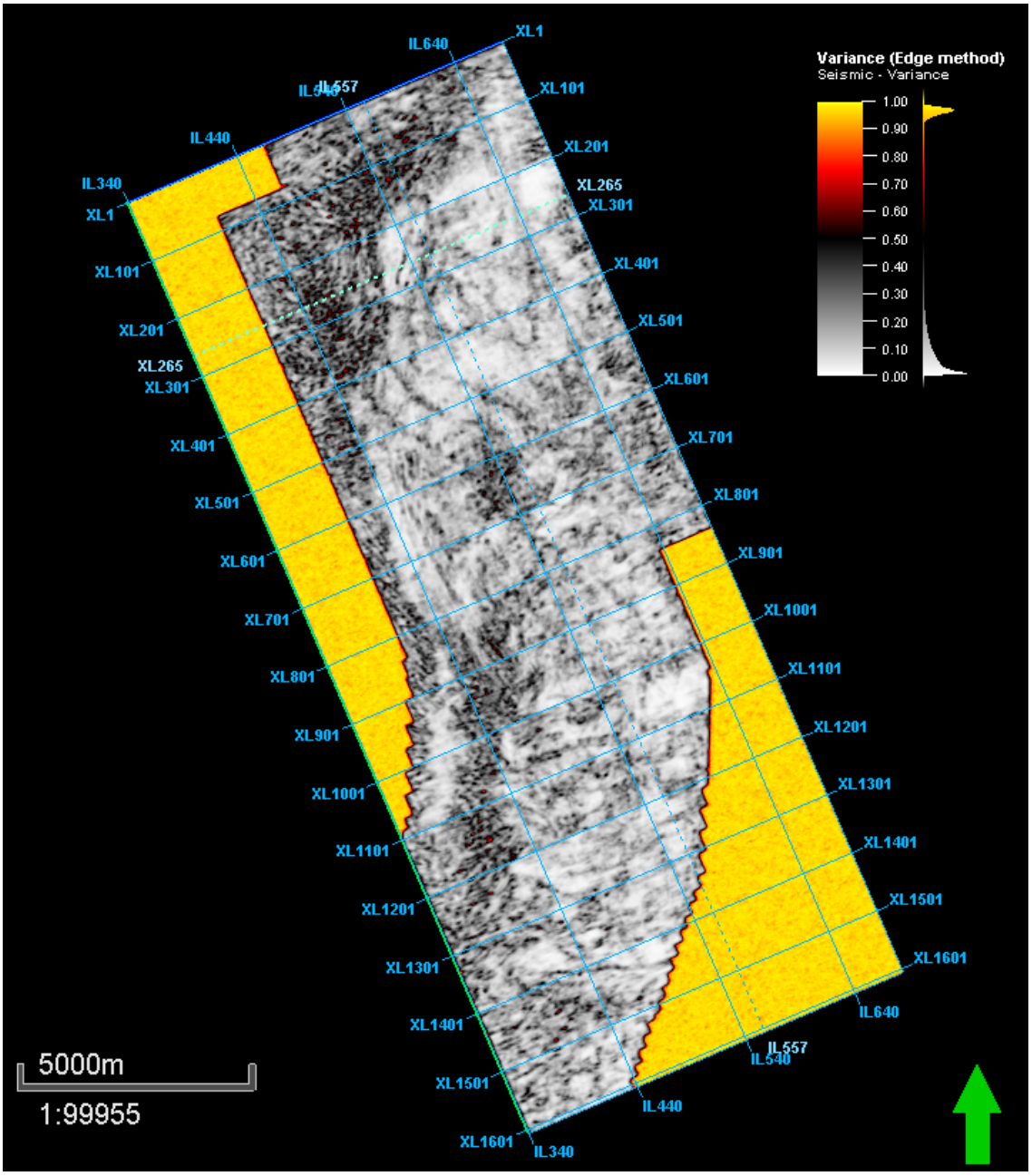

Figure 4.6. Uninterpreted time slice at 2228 ms through Variance Volume 3 (Edge detection) attribute. It clearly reveals major and minor faults that might have caused the Farewell Formation to be found deeper in well KS-1.

A 2228 ms time slice of Volume 3 provides the best lateral extent of the faults that might have affected the Farewell Formation to be found 100-meter deeper than pre-drilling predicted depth in the Kupe South-1. Further usage of the three variance volumes (1, 2, and 3) will be discussed more later in the Geobody Probe section.

4.1.2.3 Envelope. The envelope attribute is known as the total instantaneous amplitude of the analytic trace despite the phase might be associated directly with the variability of other trace attributes. This amplitude varies roughly from 0 to the highest absolute magnitude value within an individual seismic trace. The envelope of the seismic signal can be derived from single interface contrast or from several interfaces depending on the bandwidth of the seismic. The envelope of seismic trace is calculated using the following formula:

$$E(t) = \sqrt{(R\ (t))^2\ + (Q\ (t))^2}\ , \qquad (1)$$

where R(t) is the real seismic trace and Q(t) is the quadrature trace, which is computed by taking Hilbert transform of the real seismic trace R(t). The envelope attribute can be used as an effective discriminator for bright spots caused by gas accumulations, major lithological changes that are caused by strong energy reflections, sequence boundaries, and lateral changes indicating faulting.

Calculating envelope for the Kupe survey was conducted in the Petrel utilizing a Hilbert filter window of 3. This short window provided high resolution of fault visualization on the vertical display of the Otaraoa (cap rock), the Farewell (reservoir), and the underlying Puponga formations. This attribute helped determine the general distribution of faults and fractures within the target area and examine the cause of finding

the top of the Farewell Formation 100 m deeper than the predrilling predicted depth of the Kupe South-1 well. The revealed information from the envelope attributes indicated that a normal fault has shifted down the Farewell Formation at the borehole area (Figure 4.7).

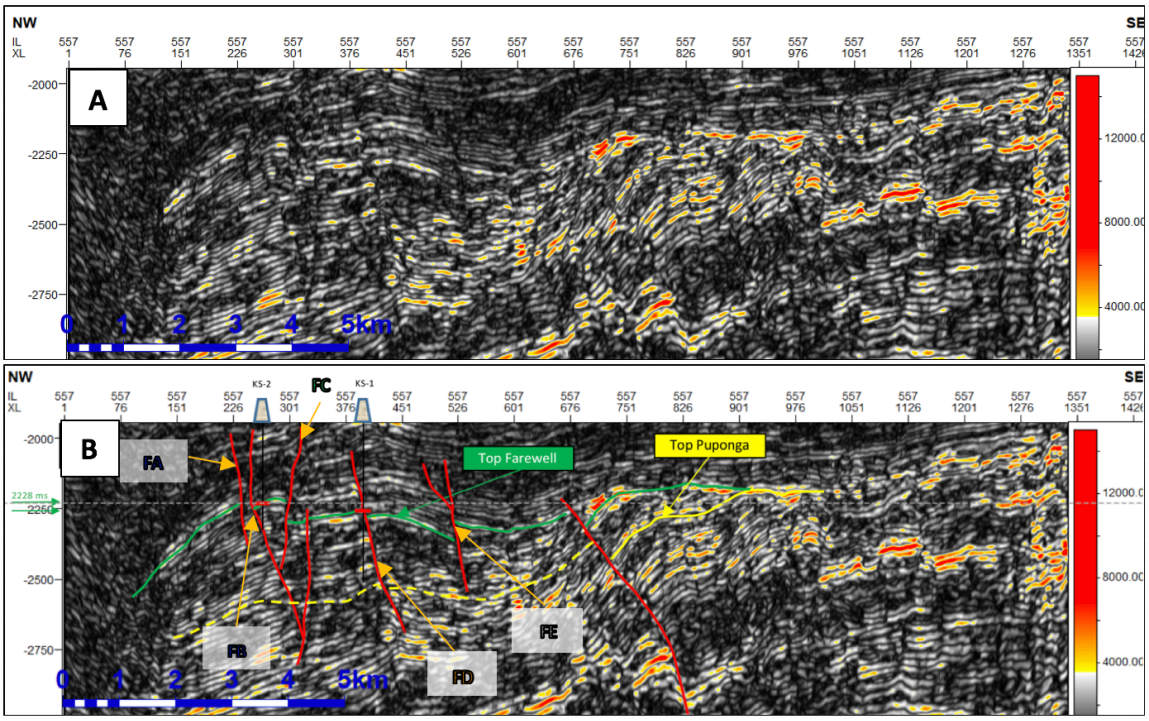

Figure 4.7. Vertical inline section 557 through the envelope attribute volume. A) Uninterpreted envelope section revealed the distributions of major, and minor faults besides huge number of fractions. B) Interpreted vertical section show major and minor faults highlighted in red lines.

4.1.2.4 Instantaneous phase. The instantaneous phase attribute is a decent indicator of reflector continuities and discontinuities. Thus, it aids in determination of faults, sequence boundaries, bed interfaces, pinch outs, and regions of onlap patterns. Regardless the waveform, the instantaneous phase attribute is calculated sample by sample using the following equation:

$$\text{Phase} = \arctan\left[\frac{(Q(t))}{(R(T))}\right], \qquad (2)$$

where R(t) is the real seismic trace and Q(t) is the quadrature trace, which is computed by taking Hilbert transform of the real seismic trace R(t). To create the instantaneous phase attribute for the Kupe survey, a Hilbert filter window of 3 was used. This attribute helped in distinguishing the faults that controlled the depth differences at the top of the Farewell Formation. Additionally, the attribute provides an amplitude independent display that is particularly beneficial for revealing continuity of reflectors that diverge greatly in their amplitude. Figure 4.8 displays an inline of the 3D data after it is transformed into the instantaneous phase attribute.

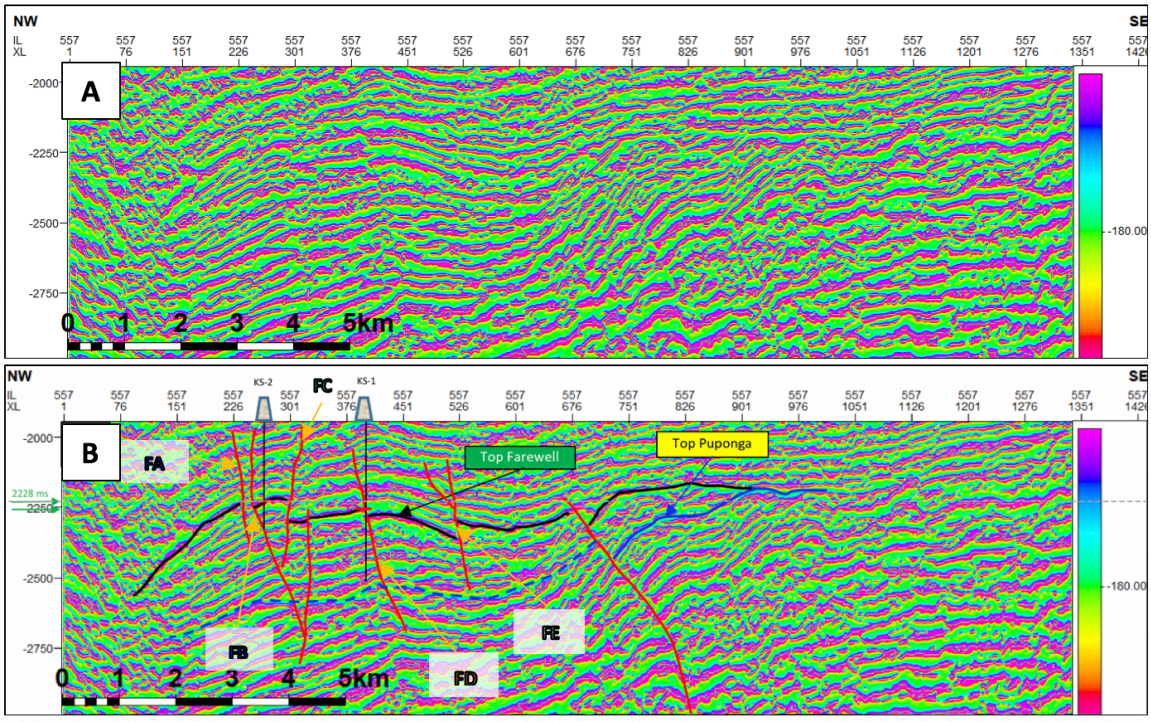

Figure 4.8. Instantaneous phase vertical inline section 557 showing discontinuities due to fault throws. A) Uninterpreted section revealed on discontinuities. B) Interpreted section. Formation tops are highlighted. The distributions of the faults that control the reflector continuities of top Farewell Formation are marked in red lines.

The structural and stratigraphic visualization revealed by previously stated attribute volumes alongside the information found in KS-1 and KS-2 wells aided in understanding and highlighting the vertical and adjacent distribution of the top Farewell Formation (reservoir) across the inline 557, which intersects the KS-1 and KS-2 wells. The seismic interpretation indicates that two major faults are the main cause that the top Farewell Formation is deeper than predicted in the KS-1 borehole. The first fault, named FD fault, is a north-west trending normal fault with throw of about 20 m, and fault plane dipping 70° to the southwest. Second, the FC fault was interpreted as reverse fault with throw of approximately 90 m. This fault trended NNE with dipping around 75° toward WWN. The final interpretation is demonstrated in Figures 4.7, 4.8, 4.9, and 4.10.

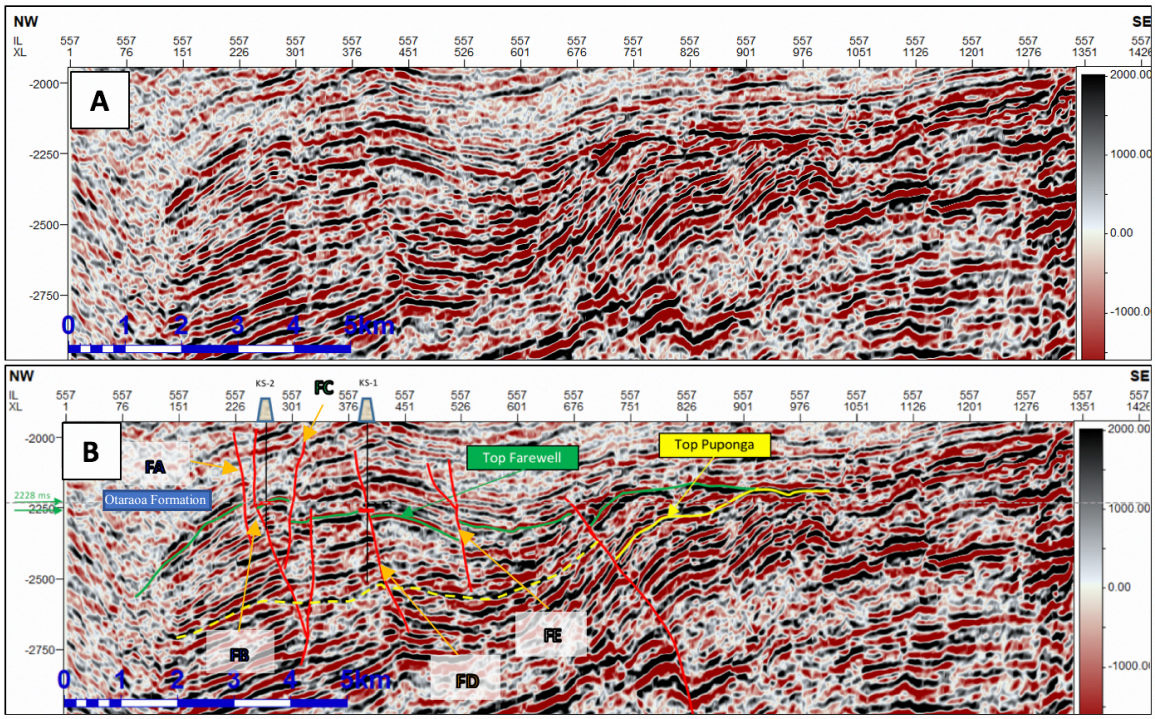

Figure 4.9. Amplitude vertical inline section 557 at the Farewell Formation. A) Uninterpreted seismic section. B) Interpreted section. Formation tops are highlighted. The distributions of the faults that controls the reflector continuities of top Farewell Formation are marked in red.

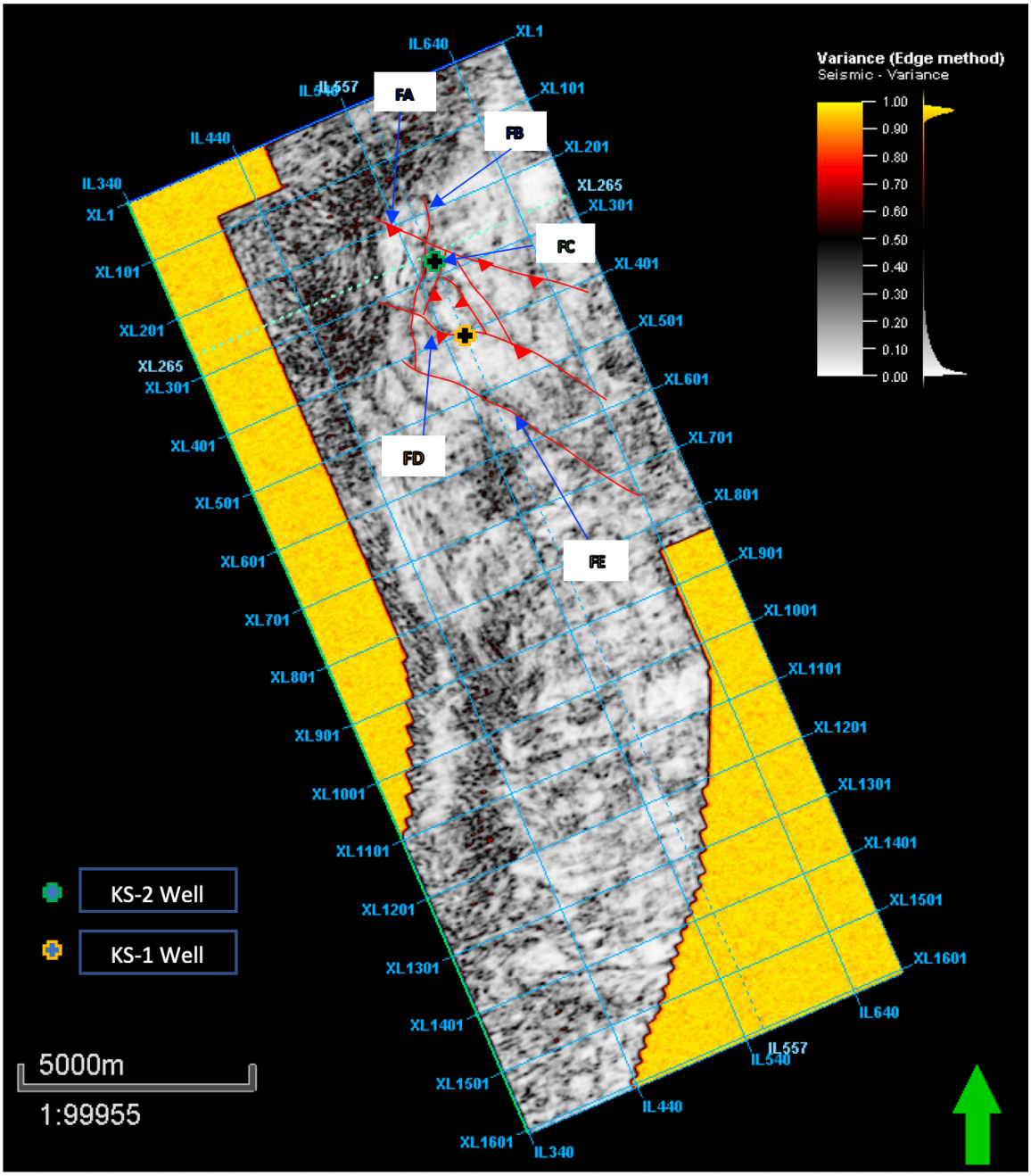

Figure 4.10. A time slice at 2228 ms through variance (edge detection) volume 3 attribute demonstrating fault distributions. The major faults (FC and FD indicated in red) caused the Farewell Formation to be found deeper in the well KS-1.

4.1.2.5 Iso-frequency component. The iso-frequency attribute was developed because the make-up of the input seismic signal is a contribution of individual

frequencies. This attribute works on isolating frequency-dependent changes in the input signal, such as fluid effects and stratigraphic thinning. The produced volume is the local contribution of the selected frequency at each sample position. Three volumes of iso-frequency attribute were generated in this study to reveal stratigraphic features (channel) (Figure 4.11). The lengths of the analysis windows 1.2, 1.8, and 2.7 were used to extract the contribution of the frequencies 10 Hz, 12 Hz, and 15 Hz, respectively. These parameters were determined based on direct visualization during the virtual mode.

4.2. PROBE CREATION AND COLOR BLENDING

Probes are objects used for visualizing 3D seismic data and to blend multiple volumes. Moreover, they allow the extraction of a three-dimensional portion of any seismic volume along predefined geometry, such as box, surface, and well probes. The probe object to be used in this study is the Box Probe.

4.2.1. Box Probe. The Box Probe can contain up to three seismic volumes. These seismic volumes can be combined into one data volume that can be reshaped, resized, and tilted. Thus, the interlaced volume can be colored to generate blended color models (RGB model and CMY model). RGB stands for red, green, and blue, whereas CMY stands for cyan, magenta, and yellow. In this study, the Box Probe method was applied using the Petrel 2017 software for structural highlighting and to define stratigraphic thinning features that can be found at channel edges.

4.2.1.1 RGB blend. RGB color blending models were utilized as a technique to combine information of three different inputs for visual analysis. Three iso-frequency

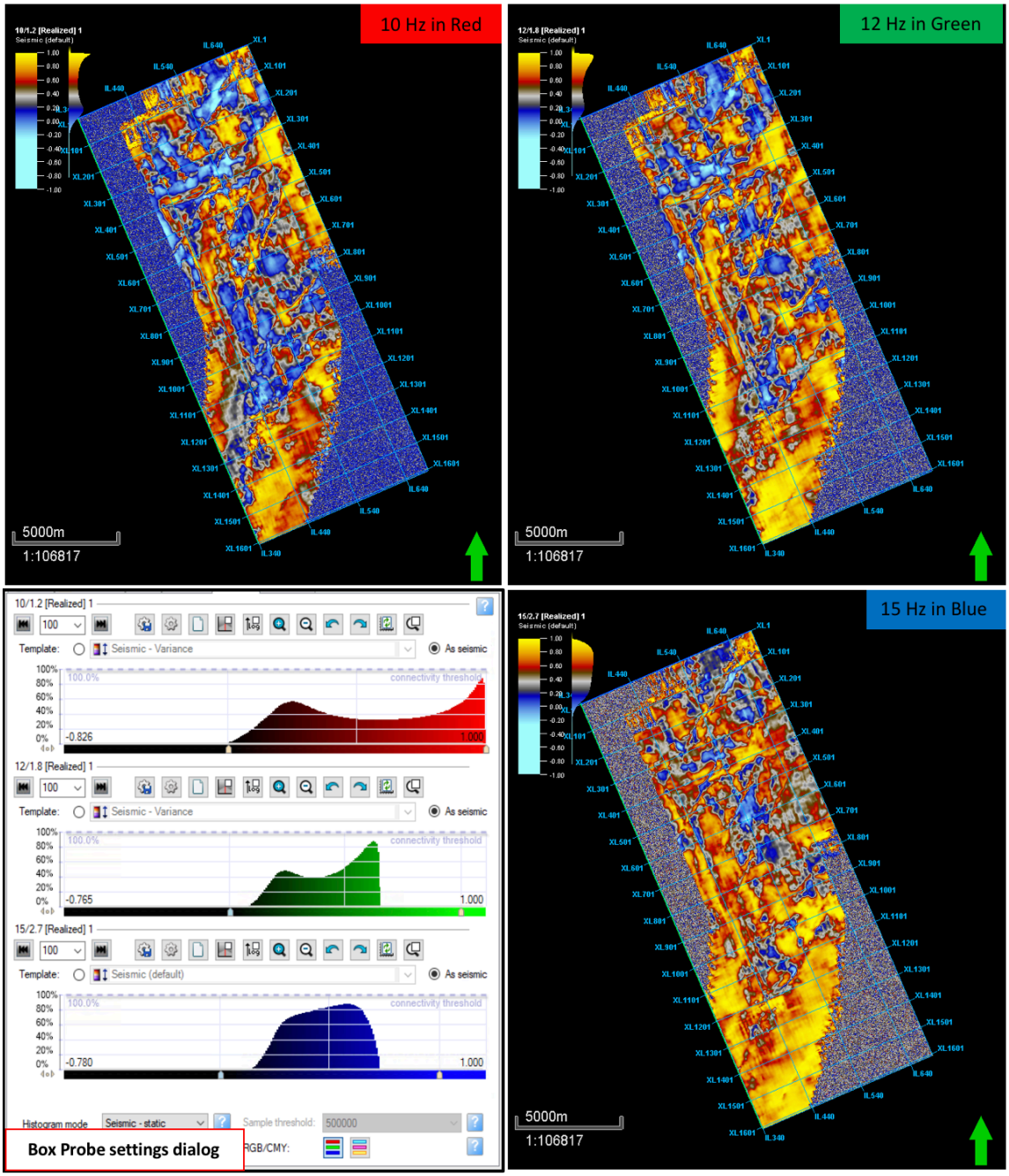

Figure 4.11. RGB color model in the probe setting dialog window illustrating three time slices of isolated frequency volumes (10 Hz, 12 Hz, and 15 Hz).

seismic attributes (10 Hz, 12 Hz, and 15 Hz) were used to characterize the stratigraphic feature of interest (channel) that was noticed at the top of the Tangahoe Formation. Each of these decomposed frequencies was entered into colored channel in the box probe (Figure 4.11). 10 Hz frequency volume was inserted in the red channel, 12 Hz frequency volume was inserted in the green channel, and 15 Hz frequency volume was inserted in the blue channel. Consequently, each of the inputs was mapped individually to the red, green, and blue monochromatic components of the RGB space. The information from three different volumes were then combined (Figure 4.12). Figure 4.13 shows a comparison between the combined frequencies before and after the RGB blending technique was applied. The channel is clearly revealed and highlighted in yellow.

4.2.1.2 CMY blend. CMY color blending is based on the same principle of the RGB color blending. However, the CMY color blending visualizes the entered seismic attributes in another visual scheme (Figures 4.14). In this study, the target is to visualize small faults and fractures at the Tangahoe interval utilizing the three variance attributes previously mentioned (Table 4.1). The CMY box probe model was created to see subtle information that is not readily visible from each attribute in isolation (Figures 4.15 and 4.16). The final result showed that the major faults were emphasized, and some minor faults were revealed. Series of normal faults were noticed using the rectangular display of the produced box probe (Figure 4.17). Additionally, the channel edges were detected at diverse time slices where they were highlighted, and faults were annotated (Figure 4.18).

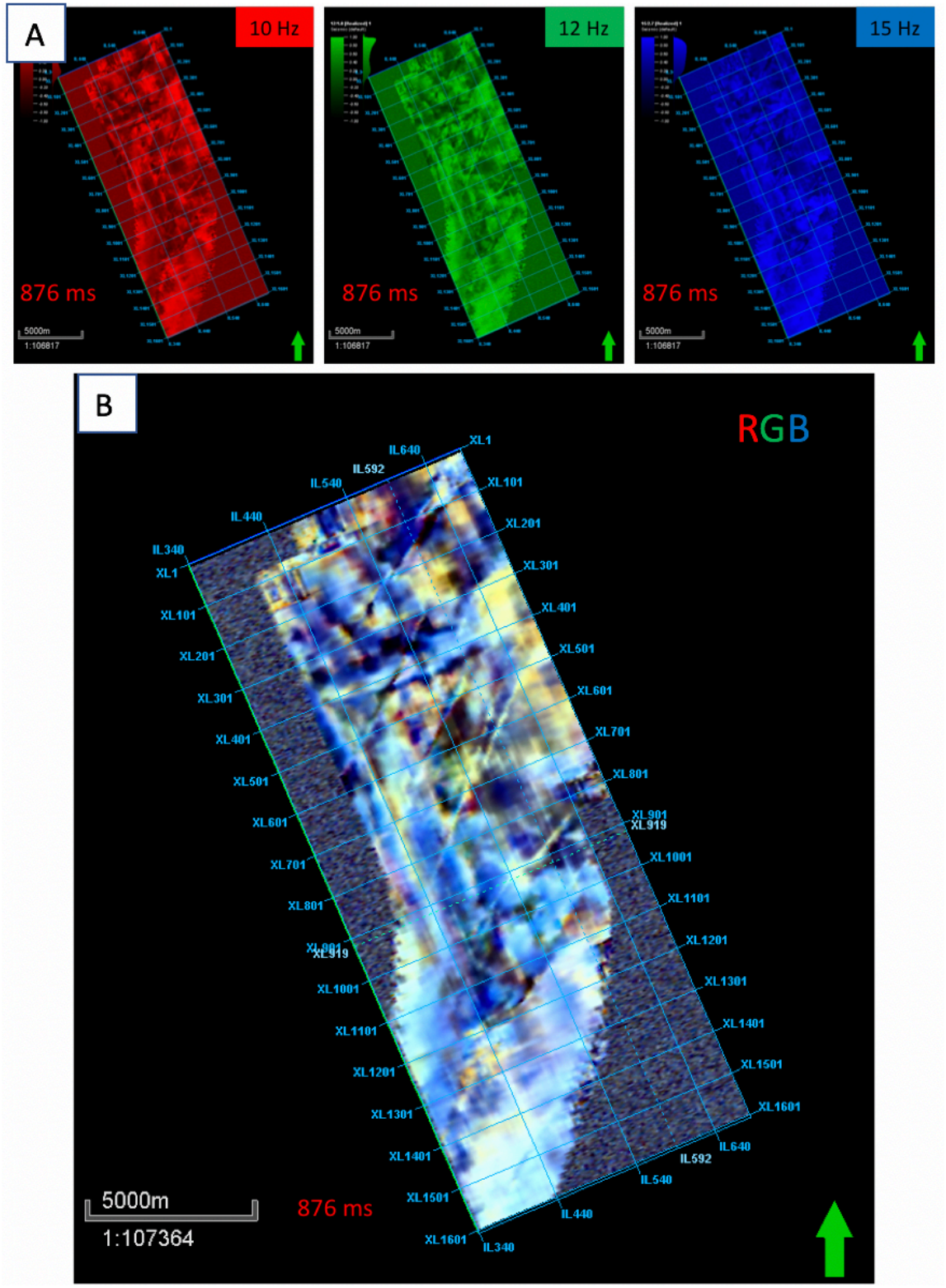

Figure 4.12. Box Probe color blending outputs of isolated and combined RGB time slices at 876 ms. A) Three frequency time slices in their specified colors. B) Combined frequency RGB time slice at 876 ms.

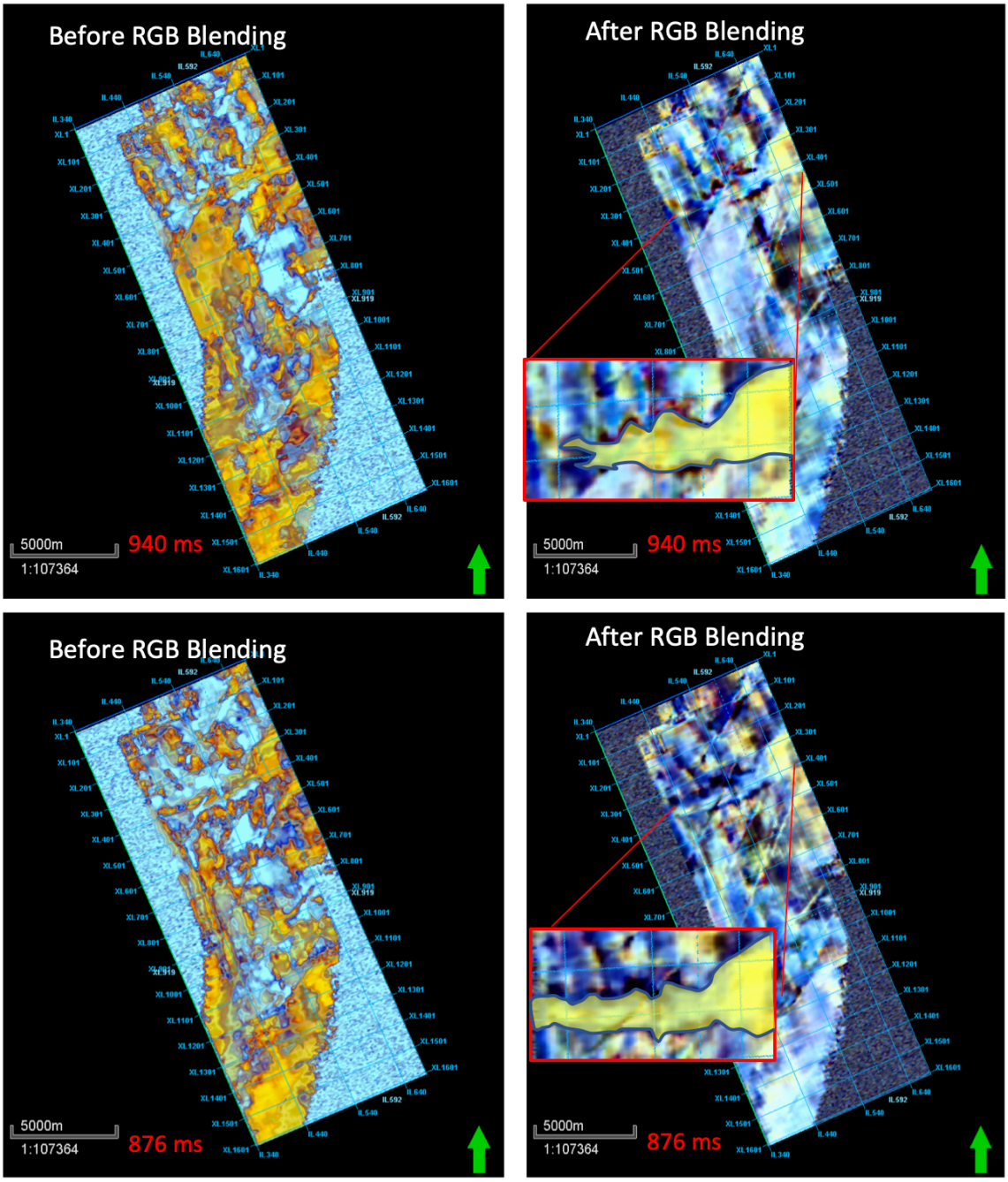

Figure 4.13. Combined frequency time slices before and after RGB color blending. On the left side are 876 ms and 940 ms time slices of combined frequencies (10 Hz, 12 Hz, and 15 Hz). On the right side are the RGB model of the same slices. Notice channel before and after RGB color blending. Channel is highlighted in yellow.

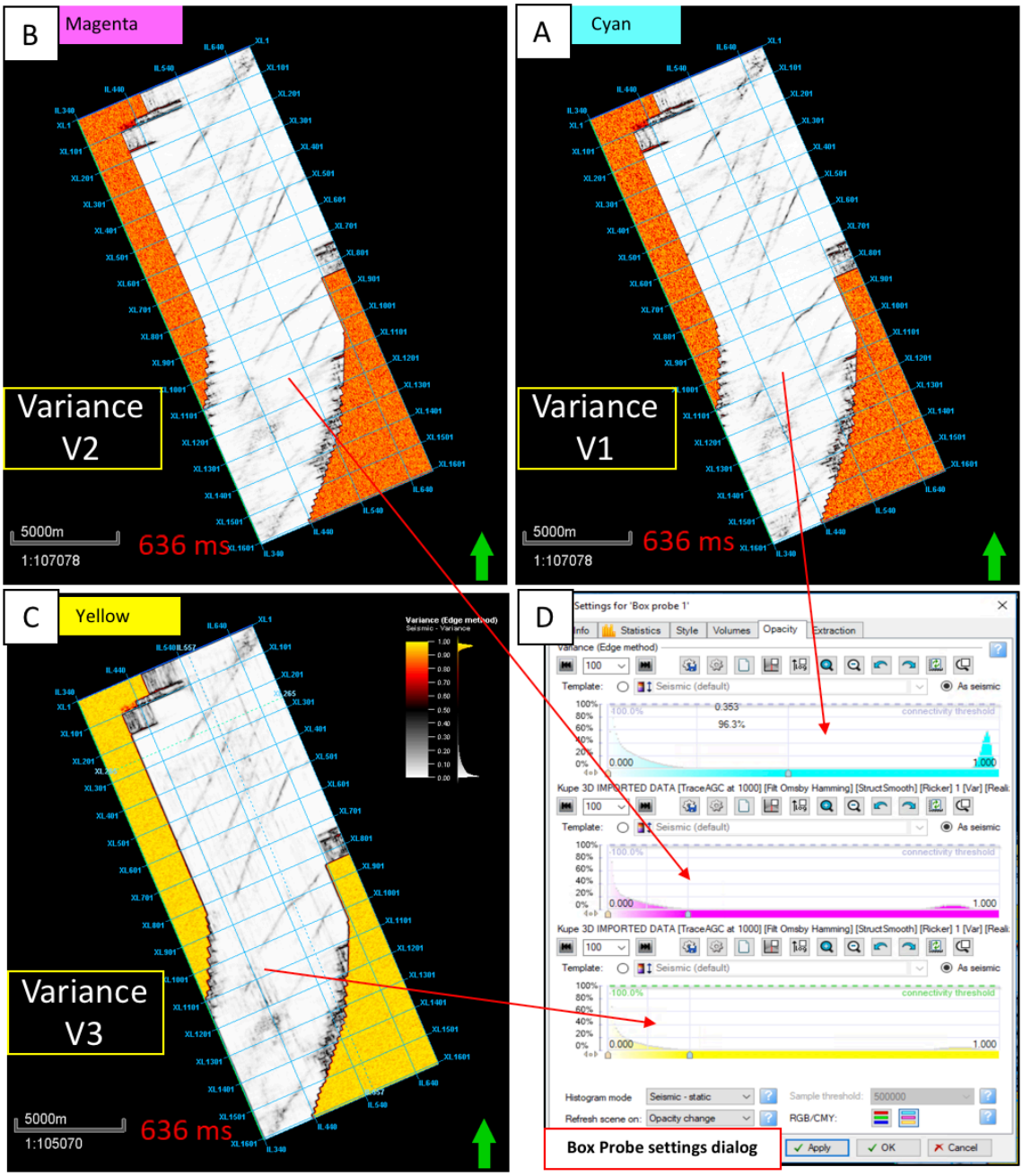

Figure 4.14. CMY Box Probe dialog window with different variance time slices through the used volumes. A) Time slice at 636 ms through the variance volume 1. B) Time slice at 636 ms through the variance volume 2. C) Time slice at 636 ms through the variance volume 3.

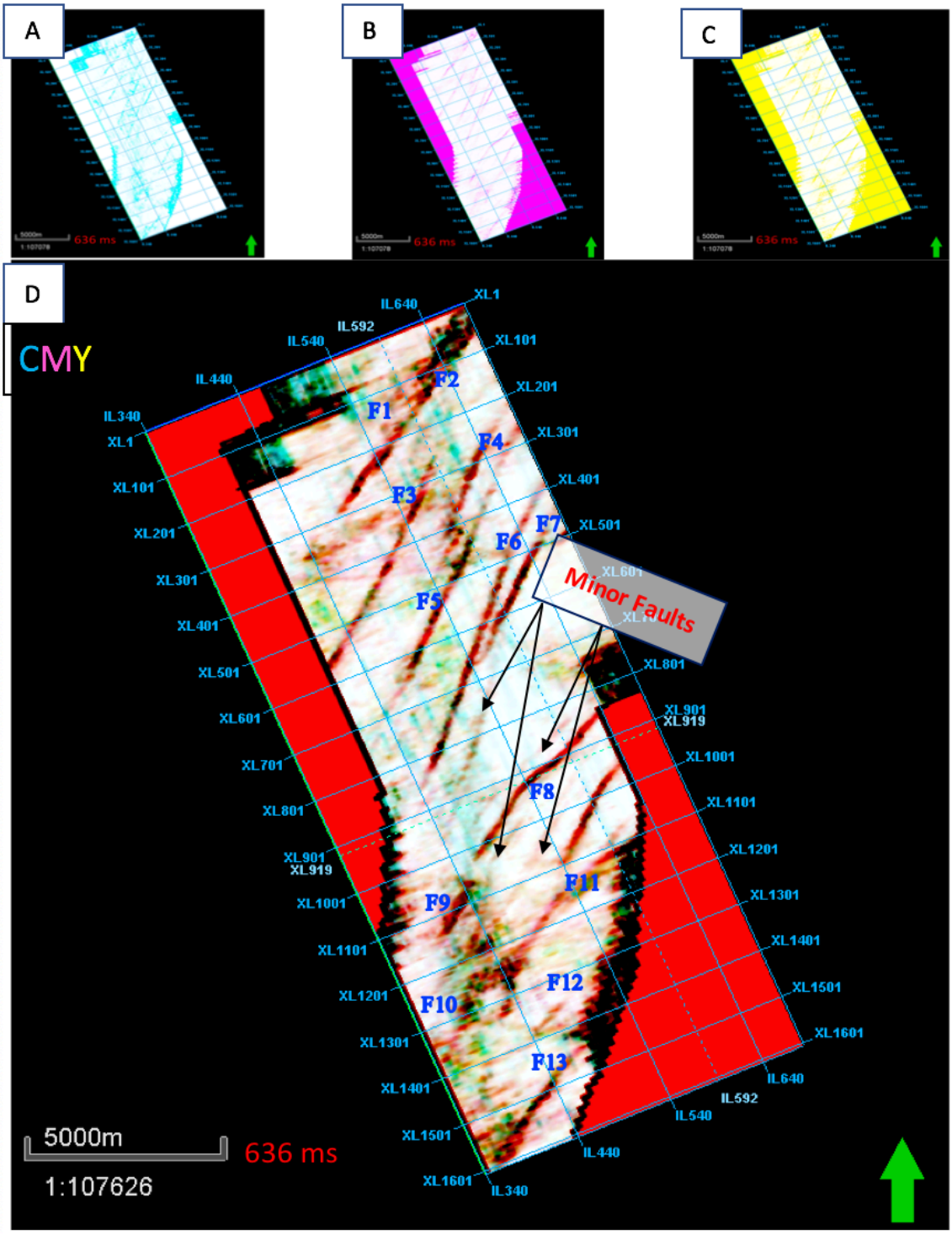

Figure 4.15. Time slices at 636 ms of variance CMY model. The three time slices above are through the used variance volume attributes (A, B, and C) before being combined into one box probe. D) CMY time slice at 636 ms through the combined variance volumes after the CMY color blending was finalized. Notice the major faults are annotated in blue and minor faults are indicated in black arrows. The faults are oriented along the northeast-southwest direction, and approximately parallel to each other.

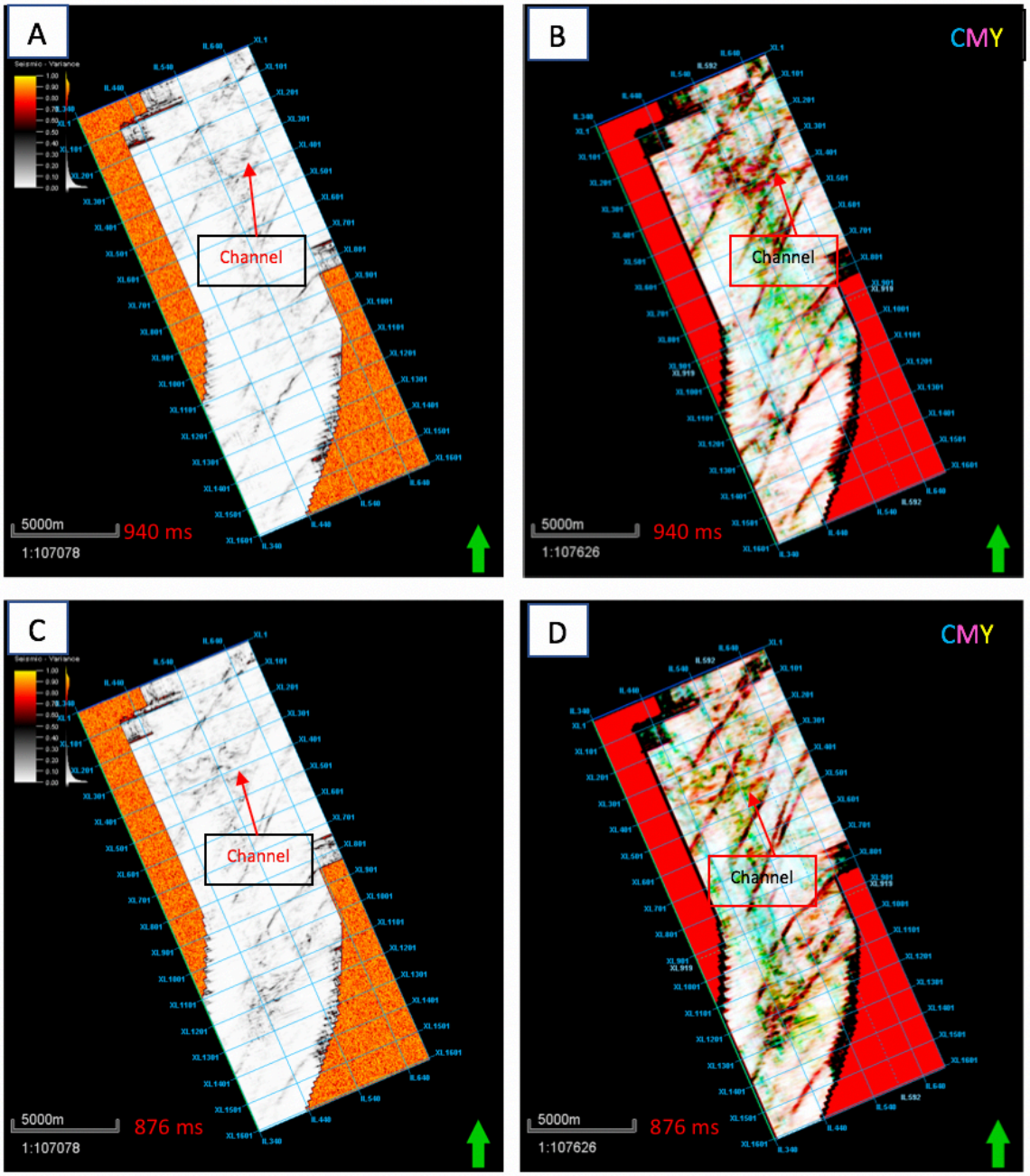

Figure 4.16. Time slices of CMY variance Box Probe in the Tangahoe Formation. (A) and (C) combined variance time slices at 876 ms and 940 ms before CMY color blending was applied. (B) and (D) variance box probe after CMY color blending was applied. Notice the faults and channel are easily detectable in the CMY model

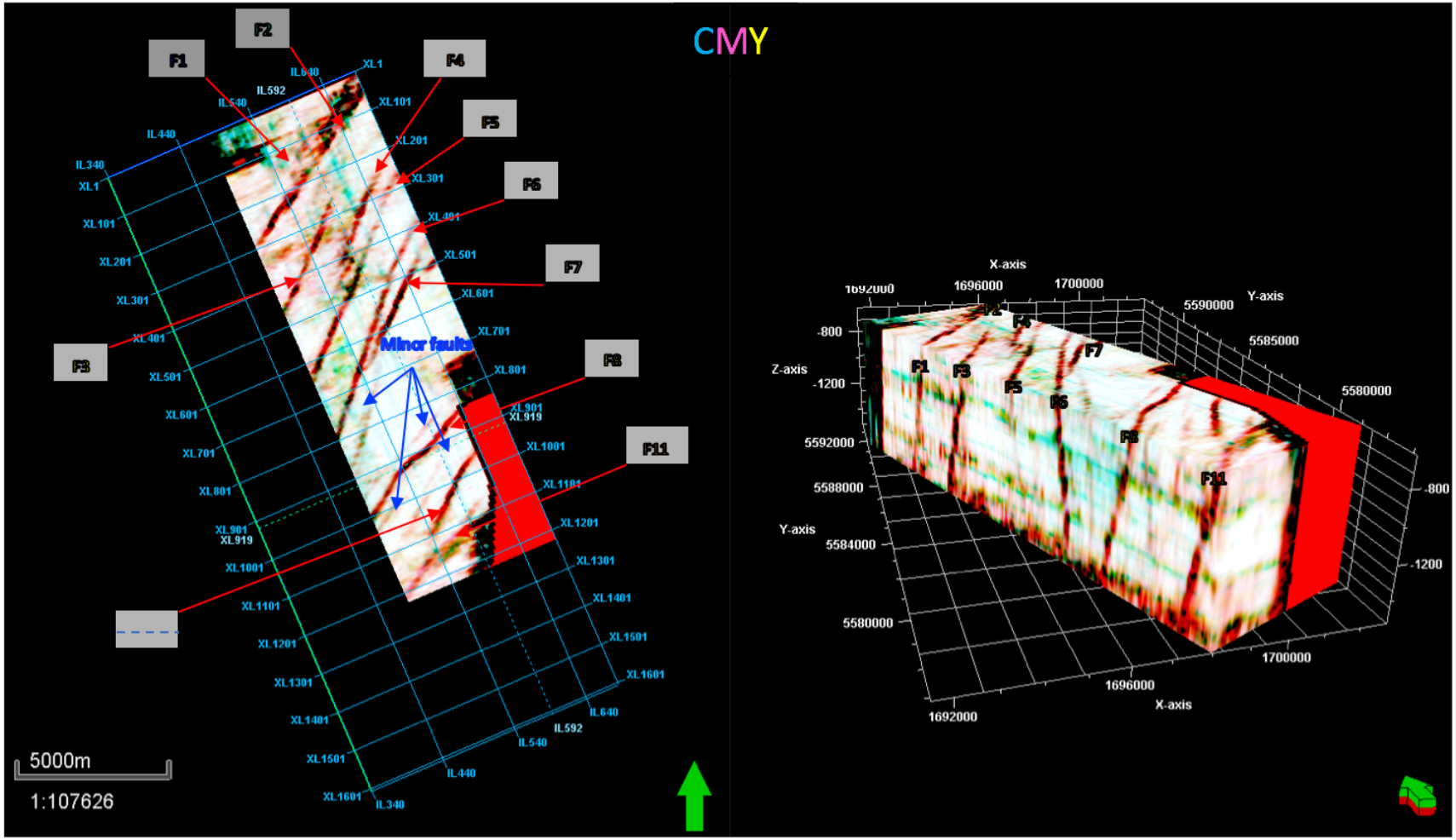

Figure 4.17. CMY Box Probe of variance volumes illustrating faults in 3D view. The left side demonstrating map of the major and minor faults which are indicated by Red and Blue arrows, respectively. The right-side shows the Box Probe from the south.

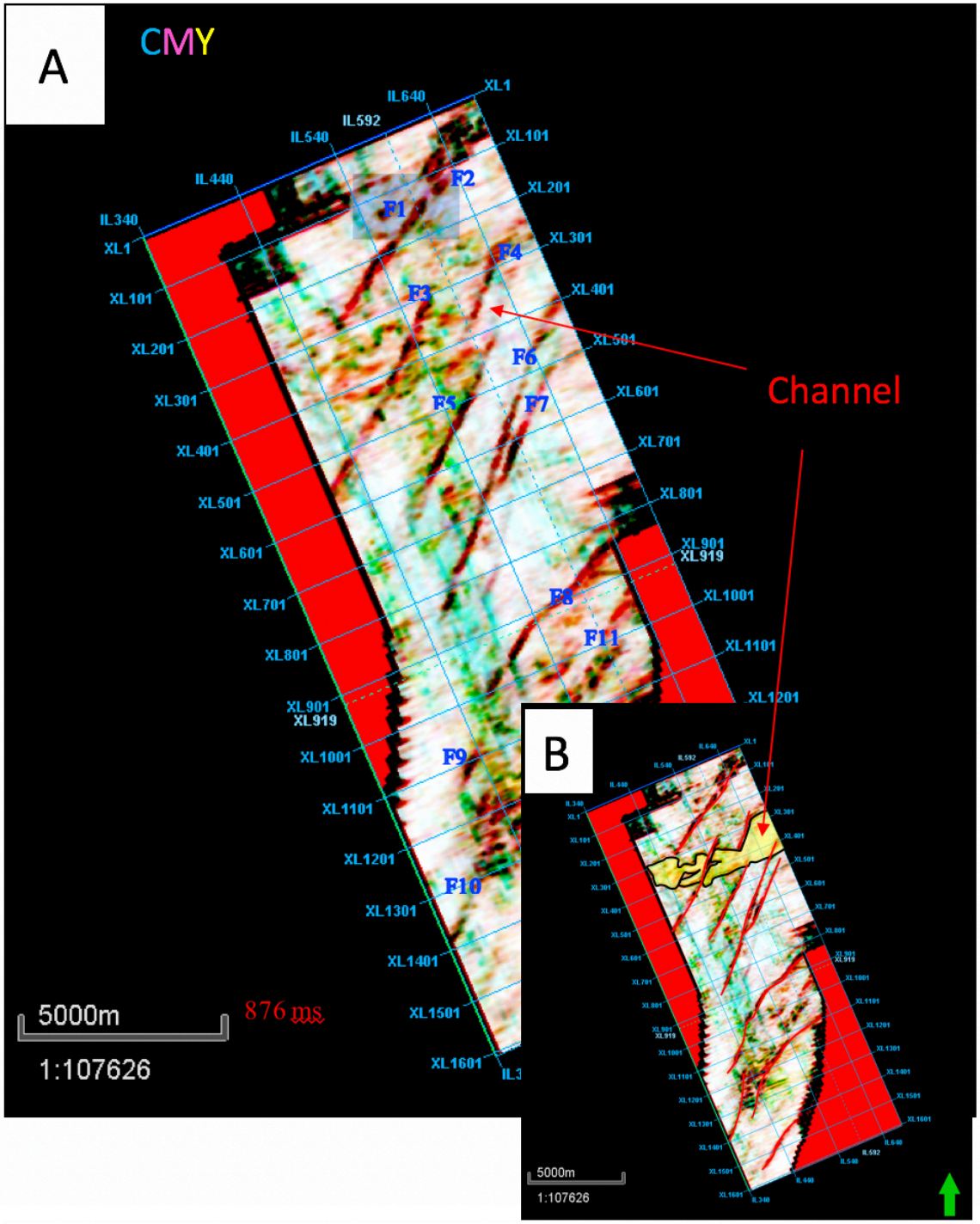

Figure 4.18. CMY Box Probe time slice at 876 ms showing faults and channel in the Tangahoe Formation. A) CMY time slice at 876 ms shows channel and faults annotated. B) Channel and main faults are highlighted in yellow and red, respectively.

5. STRUCTURAL AND STRATIGRAPHIC INTERPRETATION

This chapter presents the results of seismic interpretation of Kupe-3D data. It focuses primarily on the Tangahoe Formation and its faults that have been developed during the Miocene to Pliocene including Late Pliocene channel. Kingdom Suite 2017 and Petrel 2017 were utilized in this study for geological and geophysical interpretation. Seismic to well tie, structural interpretation, and stratigraphic interpretation were finalized based on the previously (Chapter 4) discussed seismic attributes and the data obtained from the Kupe wells.

5.1. SYNTHETIC SEISMOGRAM AND WELL TIE

The synthetic seismograms were generated to tie the well data and formation tops to the seismic reflections. To create a synthetic seismogram, several data parameters are needed in the synthetic generator. In this study, Kingdom Suite 2017 was used to generate the synthetic seismograms utilizing parameters, such as time-depth chart (TD chart), DTC log as sonic log, density logs, gamma ray log alongside resistivity log as reference, seismic wavelet, and extracted seismic traces. The TD charts were primarily generated using the TDC (sonic) logs, which use the English unit unlike other well logs that use metric unit. Thus, these charts required unit transformations before doing any further importation of the parameters into the synthetic generator. After the unit correction was done, seismic wavelet and real trace were extracted from a 75 m radius around the borehole. Then all parameters were inserted into the synthetic generator and all the synthetics were created to then be manually shifted, squeezed, and stretched to achieve the highest cross correlation (r) value possible.

The synthetic seismograms were generated for Kupe South-1, Kupe South-2, Kupe South-4, Kupe South-5, and Momoho-1 to have better illustration of the overall distribution of specific formation tops (Tangahoe and Farewell formations) within the study area. All of the produced synthetics showed a good cross correlation (r) values of more than 0.7 except that in the wells Kupe South-1 and Kupe South-4, which barely reached 0.652 and 0.648, respectively. The Kupe South-5 synthetic seismogram and all associated parameters mentioned above were chosen to be an illustration of the final result (Figure 5.1).

5.2. FAULT INTERPRETATION

The most effective seismic attribute that aided in fault interpretation in this study is the variance attribute. This attribute enhanced the reflector discontinuities that occur due to fault angular throws. Moreover, the CMY model emphasized the faults in a three-dimensional visualization utilizing three different parameterized variance volumes (Figures 4.15 and 4.17).

Major and minor faults were identified using the seismic attributes and then were interpreted within the Kupe-3D survey. However, only thirteen normal faults that remarkably deformed the top Tangahoe Formation were taken in consideration. These faults are located in the upper portion of the vertical seismic section at which the Tangahoe Formation was deposited (Figure 4.1). All thirteen faults were picked each five inline intervals to provide decent resolution and models.

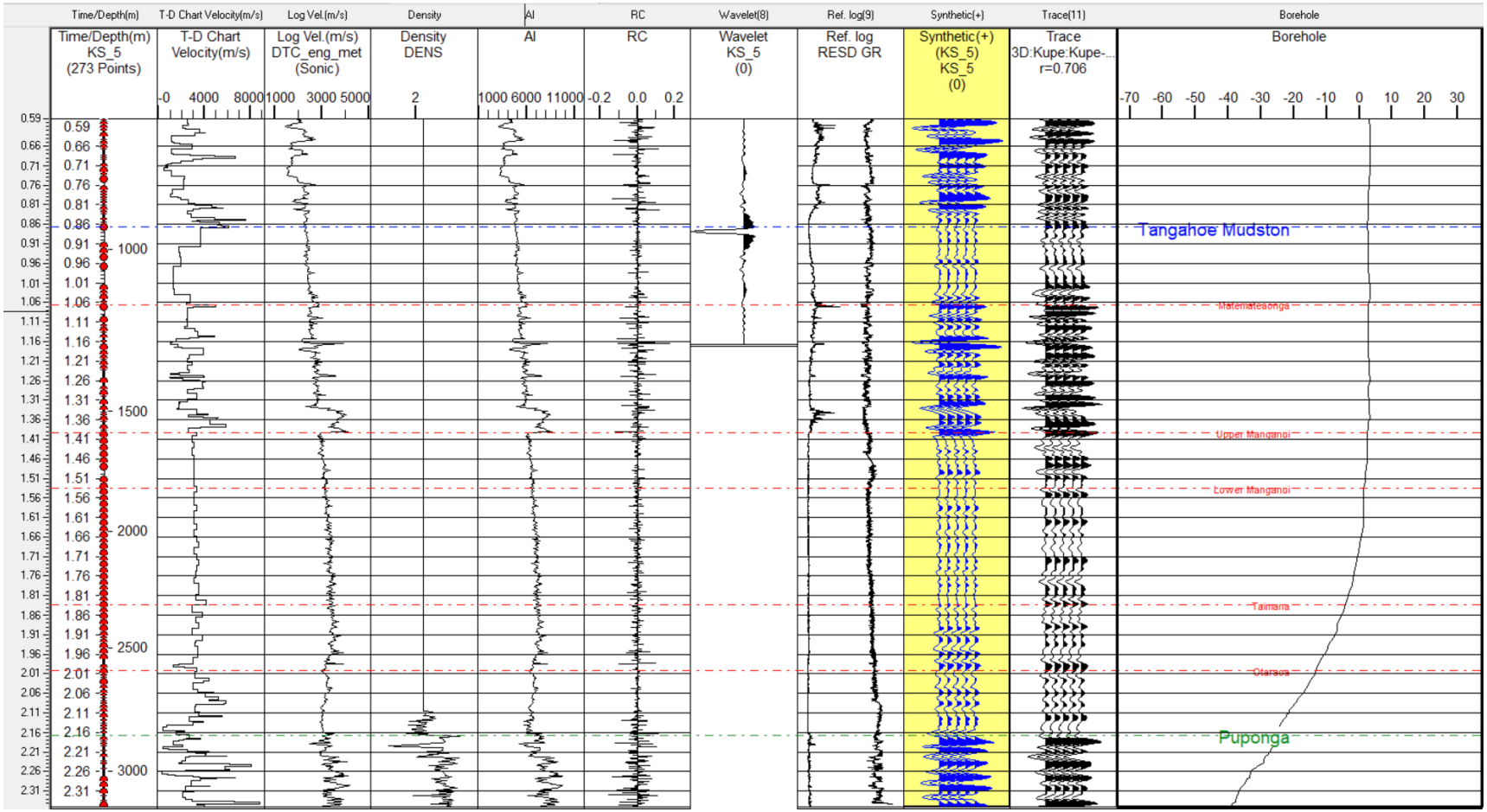

Figure 5.1. Synthetic seismogram of the Kupe South-5 well showing good well to seismic tie along with all the inserted parameters.

After accomplishing fault picking, fault polygons were generated and subsequently superimposed with the top Tangahoe maps. The faults were assigned as F1 to F13 (Figure 5.2) starting from north to south. All of these faults are normal faults, indicating that they were developed under tensional stress. Overall fault orientations after examination were found to be NE-SW trending with two opposite fault plane dipping directions; Fault F1, F3, F8, F11, F12, and F13 have fault planes dipping toward the northwest, whereas F2, F4, F5, F6, F7, F9, and F10 are dipping toward the southeast direction. These faults construct a local rift system that contains developing grabens due to extensional stress affecting the area. The main graben is positioned at the central portion of the study location and is bounded by F7 and F8 normal faults. Another graben is noticed at the northern part of the study area and bounded from the south by F1 fault. The development of fault and fracture patterns in the study could be due to the reversal movement of the Manaia Fault and its accompanying Manaia Anticline. The location of these structures is illustrated in Figure 1.2 which shows that the Manaia Fault is located out of the study area limit. The Manaia anticline axial plane is approximately parallel to the inline seismic section. Thus, the anticline is invisible in the inline display used in this study while it is observable in the crossline. A compaction drape over the Manaia Anticline may be associated, causing tensional stress in the overlaying strata which in turn caused the interpreted normal faults of the upper interval. Additionally, it could be deduced that the Manaia Fault is still under compactional force. However, based on the noticed horst and graben patterns (sagging) in Figure 5.2, the source of the extensional force may be derived from post compactional relaxation in the area. In this case, normal throw among the Manaia thrusting fault should have occurred.

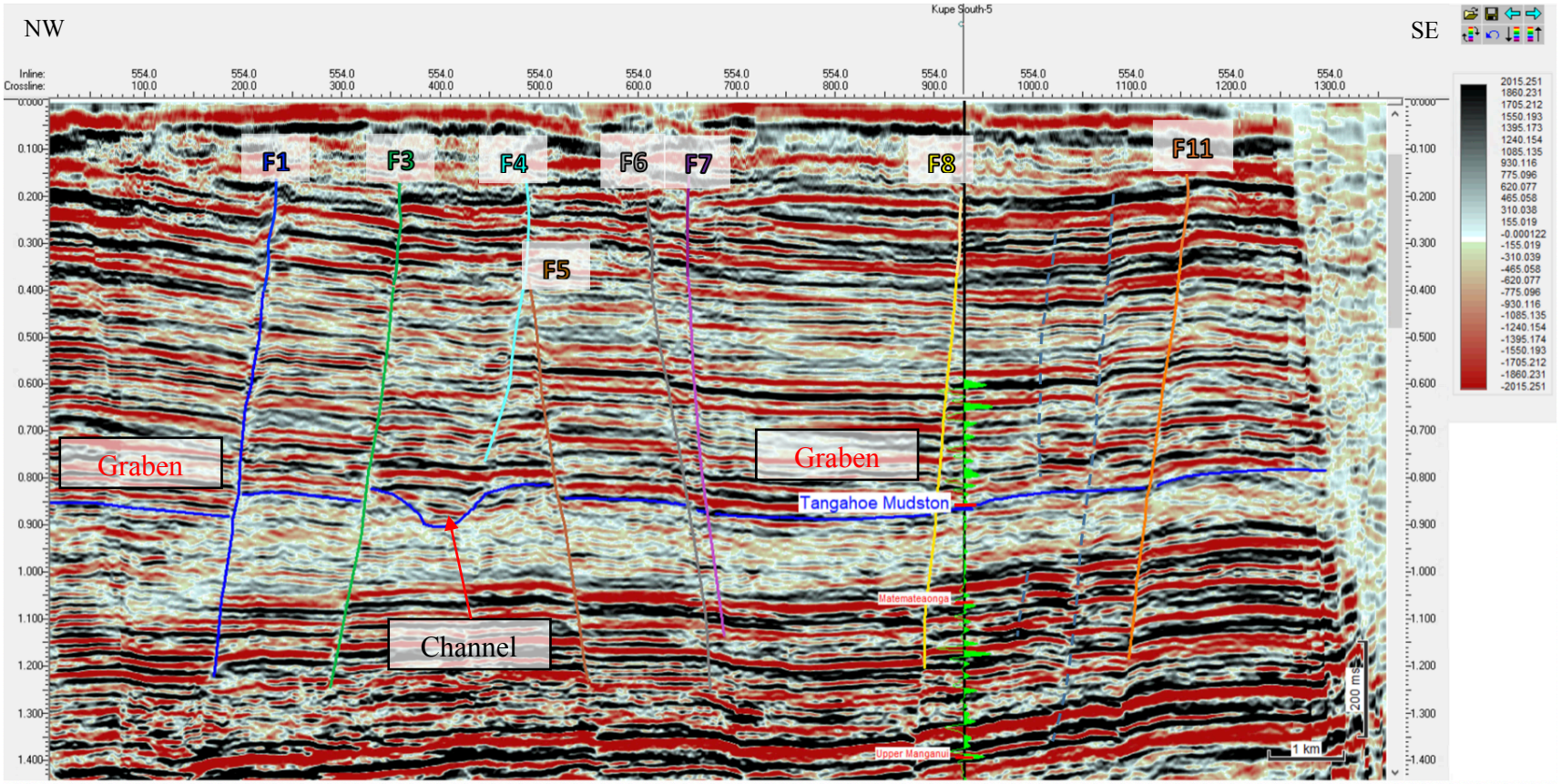

Figure 5.2. Interpreted Inline 554 seismic section. The synthetic seismogram tied to the seismic data. The colored lines represent interpreted faults and the blue horizon is the top Tangahoe Formation (17.8 km long section).

5.3. HORIZON INTERPRETATION

After performing the fault interpretation, top Tangahoe horizon was tracked from the Kupe_3D seismic data. This horizon was picked after the associated reflector was define based on the knowledge obtained from the seismic to well tie (Figure 5.2). The horizon was then picked manually with five inline intervals within the study survey. The next step was to create time structural map, average velocity map, and depth structural map to visualize the structural and the stratigraphic features and present them in time and depth domain 3D models.

5.3.1. Time Structural Map. When the whole horizon was picked, data points were recorded as X, Y, and Z, where X and Y define the location of the picked point, and Z represents the two-way travel time (TWT) of that points. Then, the Kingdome interpolated the value of these data points using an inverse distance to power gridding method. To finalize the time structure map, a time contour map was generated after the fault polygons had been contributed with the time horizon map (Figure 5.3).

In this study, the objective of the time structure map is to provide sufficient information about the dipping of the concerned top Tangahoe Horizon and to reveal the channel geometry besides the effect of the interpreted faults on the horizon.

Generally, the top Tangahoe Horizon is dipping in the northeast direction toward which the intensity of the interpreted faults is increased. This may indicate that the local normal fault rift system was not evolving under the compaction drape of the Mania Anticline but under post compactional relaxation movement of the Manaia Fault that bounded the study area from the west. As introduced in Section 2, the Tangahoe Formation was deposited during the Early Pliocene subsidence, which was

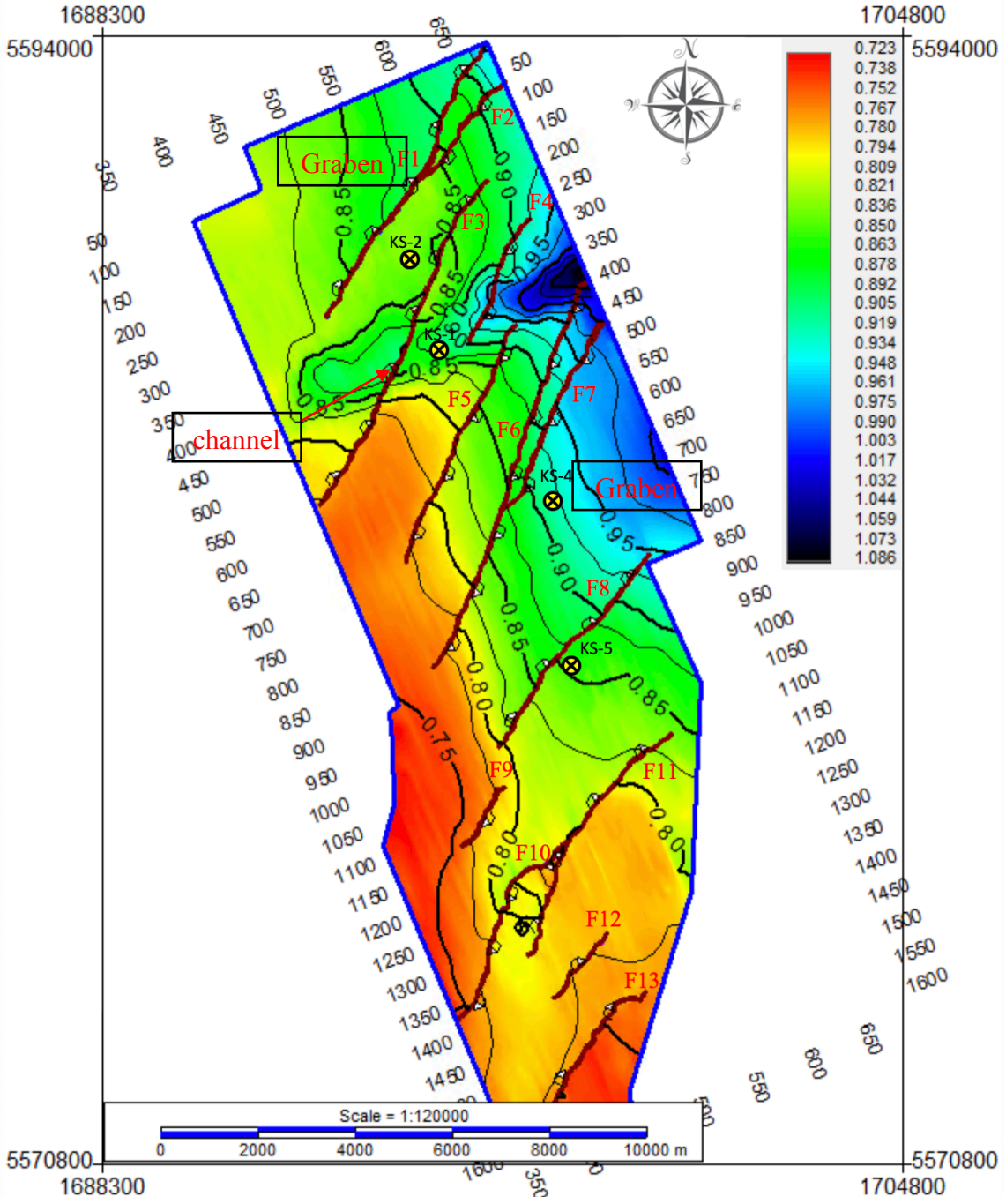

Figure 5.3. Time structure map of the top Tangahoe Horizon. The map illustrates 13 identified normal faults (F1 to F13, dipping direction indicated by white triangles). The color bar shows the time values in seconds. The structure map displays a dipping toward the northeast. A northeast dipping channel was observed in the northern part of the map.

influenced by new activated subduction movement. Hence, these faults can be aged between Pliocene to Pleistocene. The target paleochannel is also dipping and deepening toward the northeast. Furthermore, this paleochannel is affected by the fault system. This indicates that the area was dipping toward the northeast before the fault system even existed. Thus, the early Pliocene subsidence must be the cause of the general dipping noticed in the time structural map. However, local subsidence among the local rift system within the study area was observed in the northeastern portion of study area. This pull-down could be due to the post compactional relaxation of the Manaia Fault. Figure 5.4 illustrates a 3D visualization of interpreted top Tangahoe Horizon, thirteen faults, and paleochannel along with their dipping directions.

5.3.2. Average Velocity Map. The average velocity map was generated in order to create the depth structure map. The Kingdome software created this map using the formation top data from chosen wells, the acquired velocity points, and the inverse distance to power gridding.

The average velocity map indicates that the average velocity of the top Tangahoe Horizon generally increases toward the southeast direction. Velocities vary from 1900 m/s to 2113 m/s. The lowest velocity is observed around Kupe South-1, and the highest velocity is detected around Kupe South-4 (Figure 5.5).

5.3.3. Depth Structural Map. A depth structural map is vital to represent the geometry of horizon in its depth instead of time. Thus, the depth map for top Tangahoe Formation was constructed utilizing the formerly created time and average velocity maps by multiplying the value of the average velocity to its corresponding two-way travel time.

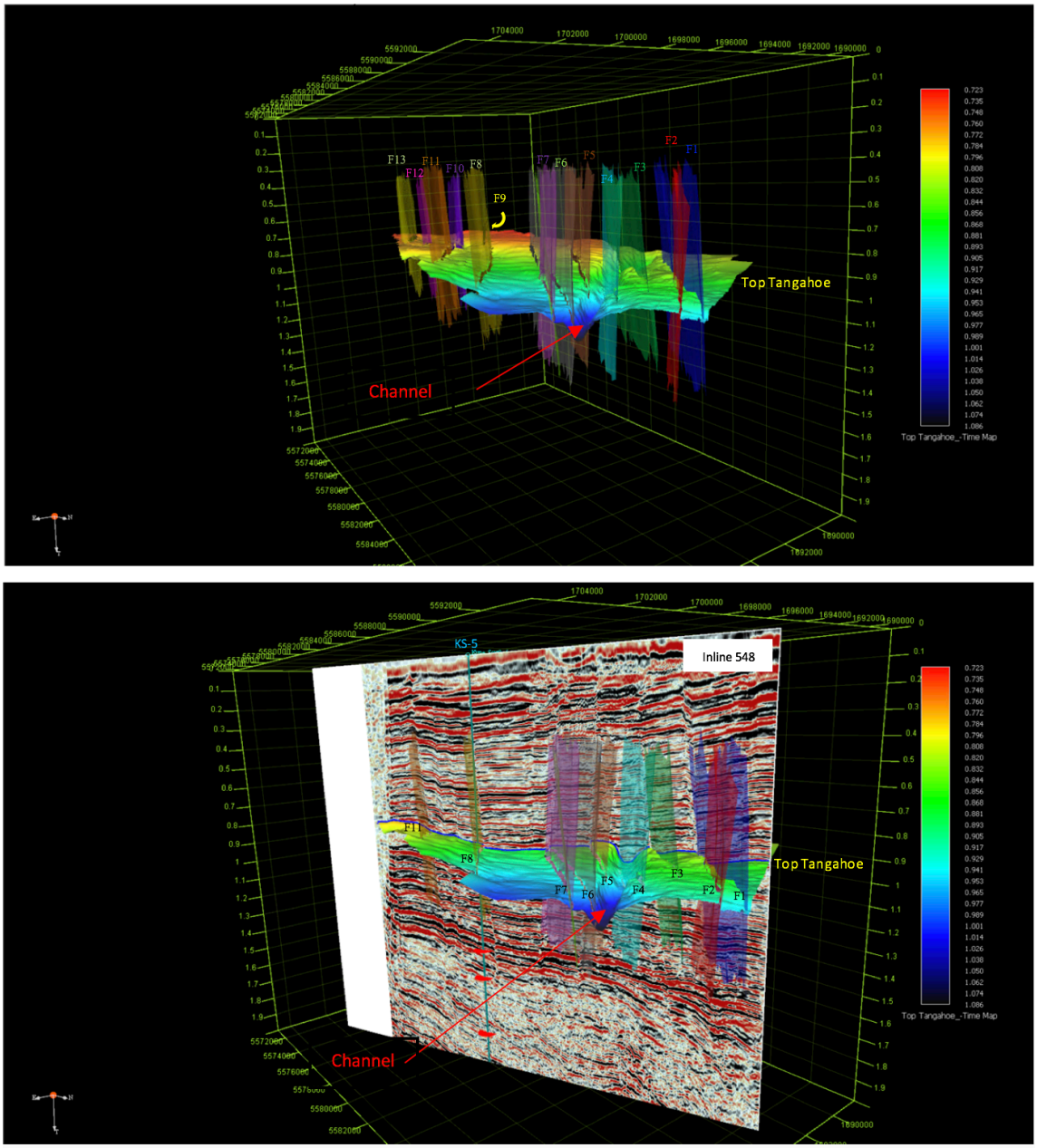

Figure 5.4. 3D display of the top Tangahoe Formation. The model illustrates thirteen interpreted faults, the top Tangahoe Horizon, and paleochannel. The color bar represents the TWT in seconds. The colorful vertical surfaces illustrate major faults. Inline 548 is displayed along with the projection of well Kupe South-5.

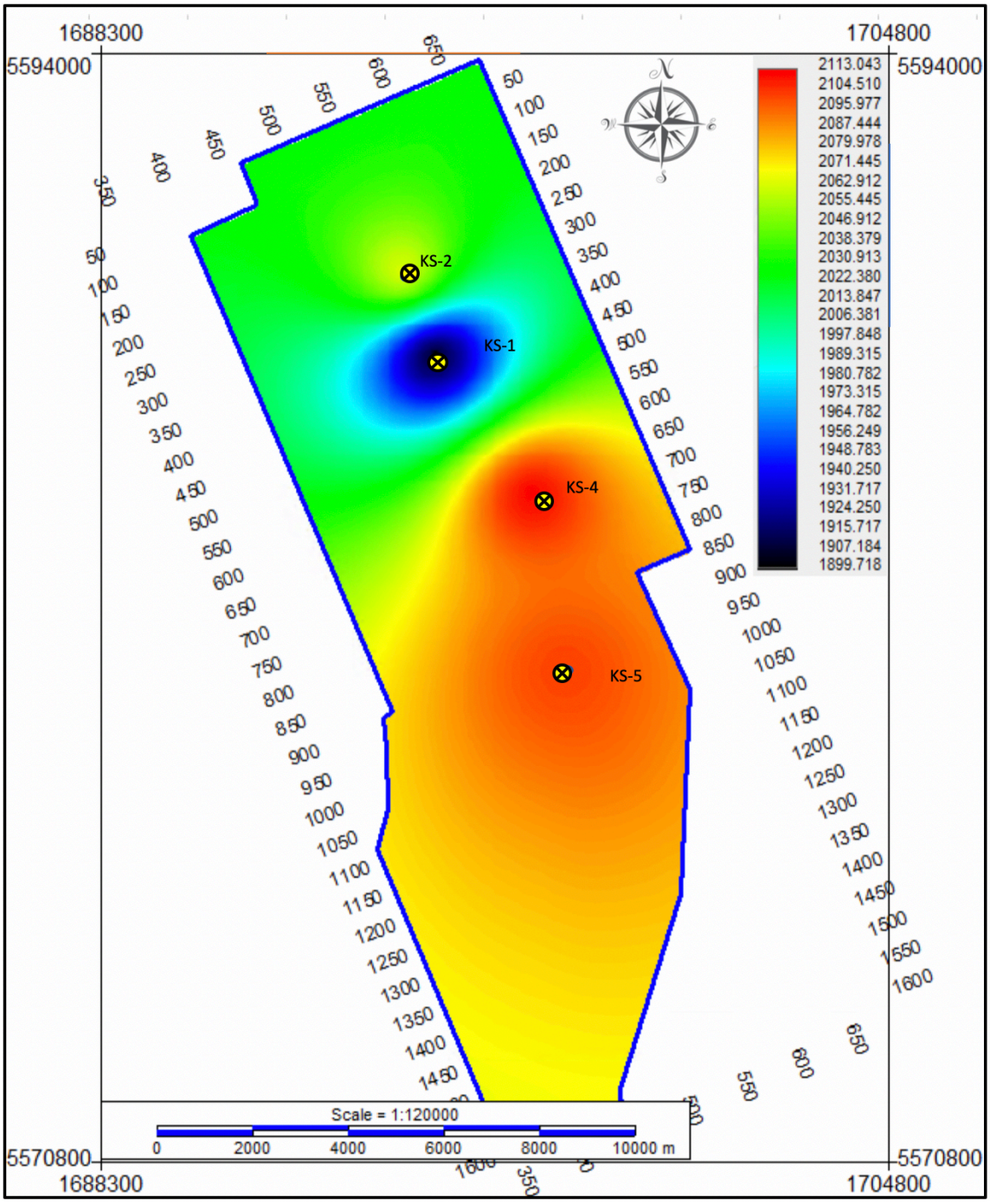

Figure 5.5. Average velocity map of the top Tangahoe Horizon. The color bar displays the velocity in meter per second. Velocities range from 1900 m/s to 2113 m/s. The lowest velocity is around well Kupe South-1, and the highest velocity is around well Kupe South-4. The average velocity decreases toward the northwest.

Figure 5.6 demonstrates the depth structural map with all interpreted faults annotated from F1 to F13.

The top Tangahoe depth map provides sufficient visualization of the horizon dipping value and reveals the paleochannel geometry in meters. The depth map indicates that the depth to the top Tangahoe Formation generally increases toward the northeast direction. The depth varies approximately from 750 m to 1090 m. The deepest point was observed at the northeastern end of the channel, whereas shallowest location was detected along the southwest side of the map (Figure 5.6). The depth map was displayed in 3D window to diagnose the approximate thickness of the paleochannel. With the help of the color bar, the thickest part of the channel was found to be around 130 m at the northeast portion of the study area. Additionally, the fault scarps of the thirteen interpreted faults are clearly visual. The northeastern sagging among the developing local rift system and its main graben are identified (Figure 5.7).

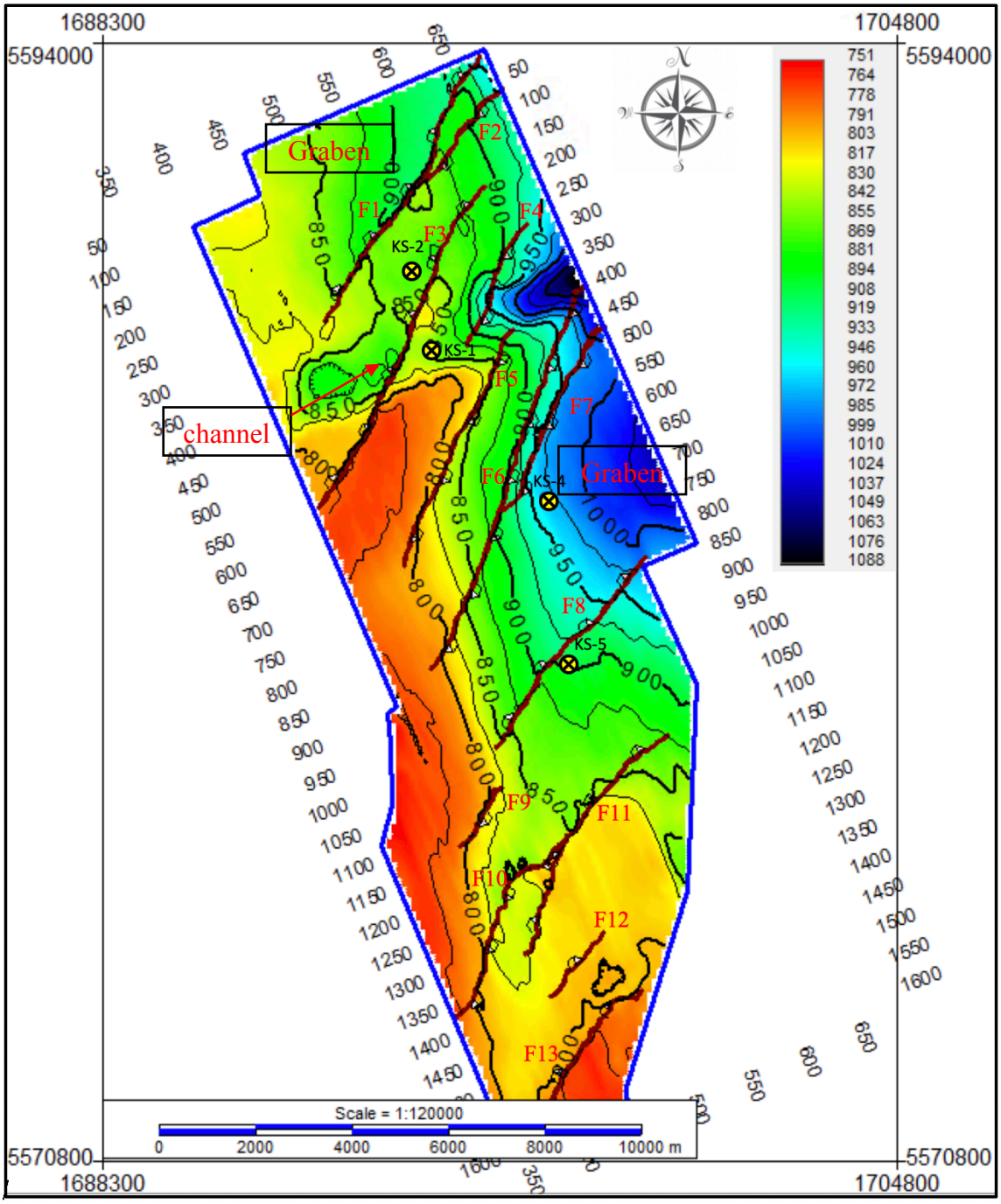

Figure 5.6. Depth structural map of the top Tangahoe Horizon. The map demonstrates the interpreted major faults. The color bar displays the depth values in meter. The map shows a general dipping toward the northeast. A northeast dipping channel was observed in the northern part of the map.

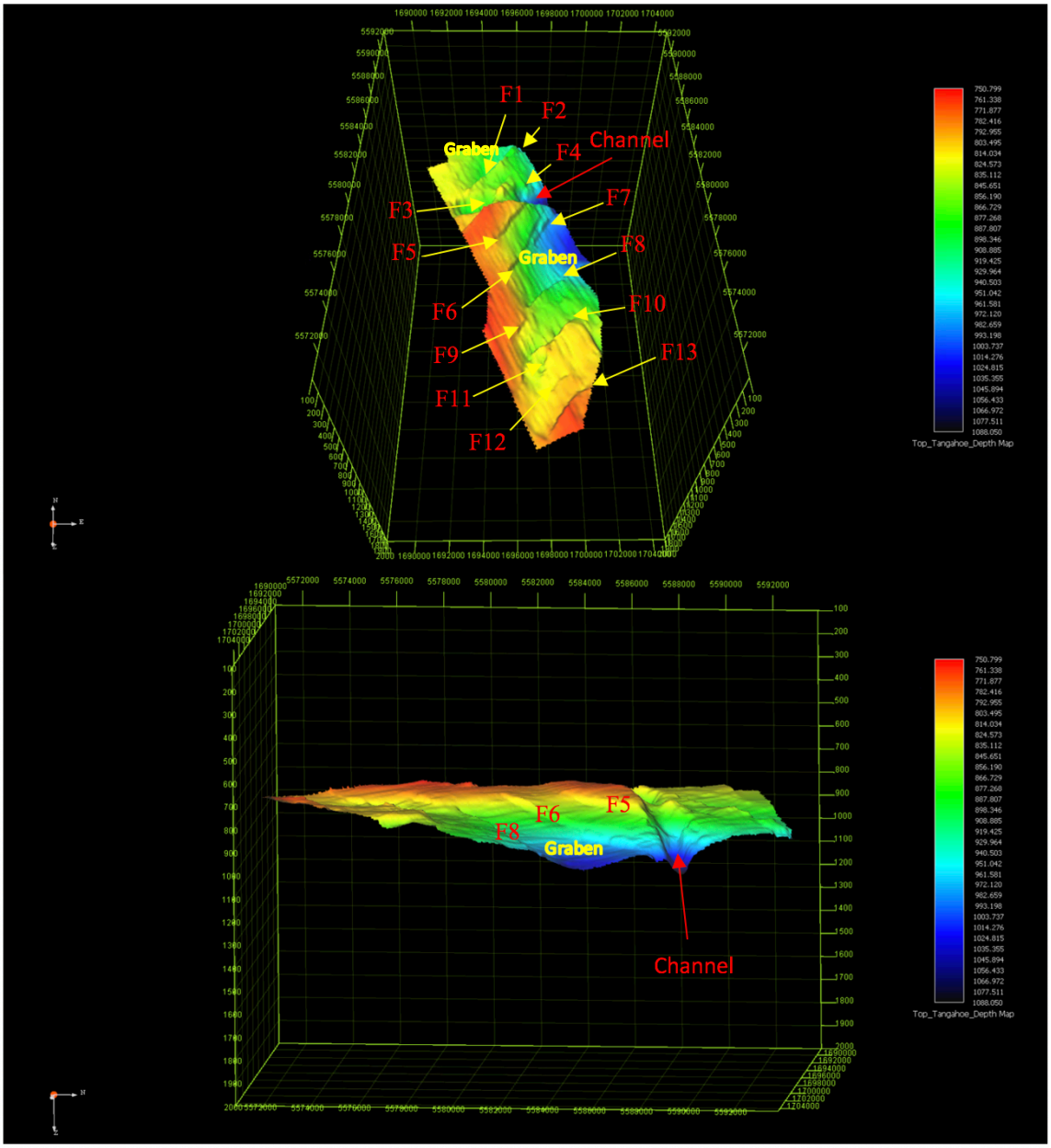

Figure 5.7. 3D depth view of the top Tangahoe Horizon from deferent angles. The 3D cube displays dipping direction of the horizon which generally dipping toward the northeast. The color bar represents the depth values in meter. The paleochannel indicated in red was observed at the northern part of the study area. Fault scarps and the developing graben are visible.

6. CONCLUSIONS

Kupe_3D seismic survey was examined in this research along with its accompanied well data. Various seismic attribute volumes were generated to help preforming structural and stratigraphic interpretation of the target formations (Farewell and Tangahoe formations).

6.1. STRUCTURAL INTERPRETATION

Thirteen normal faults were interpreted as contributing to the top Tangahoe Formation. These faults were taken into consideration to analyze and identify their geometry and initiation force. Overall orientations of these faults are trending NE-SW with two opposite fault plane dipping directions (northwest and southeast). These faults construct a rift fault system that contains developing grabens due to extensional movement affecting the area. It was found that these faults are a group of normal faults constructing a local rift system. These types of faults indicate that the area is developing under tensional stress. The reversal movement of the Manaia Fault and the Manaia Anticline compaction drape are potential causes of this rifting. However, the post compactional relaxation movement of the Manaia Fault that bounded the area from the west gave a more logical conclusion to the initiation force of this fault system.

Within the Paleocene Farewell Formation, several faults were identified utilizing attributes such as variance, envelope, and instantaneous phase. The structural and stratigraphic visualization provided by these volume attributes together with the information found in KS-1 and KS-2 wells aided in understanding and interpreting the distribution of the top Farewell Formation (reservoir) across the inline 557, which

intersects both KS-1 and KS-2 wells. The two major faults are the main causes that the top Farewell Formation is deeper than predicted depth in KS-1 borehole. The first fault, named the FD fault, is a northwest trending normal fault with throw of about 20 m and fault plane dipping 70° to the southwest. Second, the FC fault was interpreted as reverse fault with throw of approximately 90m. This fault is trending NNE with dipping around 75° toward WWN.

6.2. STRATIGRAPHIC INTERPRETATION

Seismic reflection geometries for paleochannel at the top of Tangahoe mudstone were recognized and interpreted in this study. Additionally, the top Farewell Formation was identified and interpreted across the inline 557.

Generally, the top Tangahoe Formation is dipping toward the northeast direction toward, where the intensity of the interpreted faults is increased. The target paleochannel was found to be dipping and deepening toward the northeast direction. The deepening increment suggested that the paleo-river was running toward the northeast direction. Furthermore, this paleochannel is affected by the fault system, which indicates that the area was dipping toward the northeast before the fault system even existed. The depth map displayed in a 3D window demonstrates the approximate thickness of the paleochannel. The thickest part of the channel was found to be approximately 130 m at the northeast portion of the study area, whereas it was shallowing up-dip direction to record about 60 m. Variance and iso-frequency attributes were constructed in addition to RGB color blending technique to better reveal paleochannel stratigraphic features.

6.3. RECOMMENDATIONS

The computer utilized in this study has low features relative to that recommended by the Petrel's software developer. For example, the graphic card and RAM should be upgraded. Hence, the RGB and CMY color blending visualization will be improved significantly. This will allow the interpreter to sufficiently indicate the stratigraphic and structural features at deeper depths (lower frequencies). Therefore, more faults that might have deformed the Farewell Formation will be diagnosed.

REFERENCES

Anthony, D.P., C.E. Gilbert, G.F. Sutherland, B.A. Pidgeon, K.L. Mills, and G.P. Pass, / Origin Energy Resources New Zealand Ltd (2005), Kupe Central Field Area (CFA) Subsurface Development Plan, Offshore Taranaki Basin, New Zealand, Unpublished Report, OF0401-PLN-00-A-0008.

Bal, A., D.W. Lewis (1994a), A Cretaceous-early Tertiary macrotidal estuarine-fluvial succession: Puponga Coal Measures in Whanganui Inlet, onshore Pakawau sub-basin, northwest Nelson, New Zealand. New Zealand journal of Geology and Geophysics 37, P. 287–307.

Bierbrauer K. and B. Leitner / Origin Energy NZ Pty Ltd (2011), 2010 Kerry 3D Seismic Interpretation Report, Offshore Taranaki Basin, New Zealand, Ministry of Economic Development, New Zealand, Unpublished Petroleum Report, PR 4333.

Bland, K.J., and D.P. Strogen (2012), Regional seismic transects of selected lines from Taranaki Basin, New Zealand, Lower Hutt: Institute of Geological and Nuclear Sciences Ltd, GNS Data Series 7a.

Constantine, A. / Origin Energy Resources New Zealand Ltd (2008), Momoho-1 Well Completion Report, Ministry of Economic Development, New Zealand, Unpublished Petroleum Report, PR 4022.

Fohrmann, M., E. Reid, M.G. Hill, P.R. King, H. Zhu, K.J. Bland, D.P. Strogen, L. Roncaglia and G.P.L. Scott (2012), Seismic reflection character, mapping and tectono-stratigraphic history of the Kupe area (4D Taranaki Project), south-eastern Taranaki Basin, GNS Science Report 2012/36.

Hansen, R.J., and P.J.J. Kamp (2004), Late Miocene to early Pliocene stratigraphic record in northern Taranaki Basin: Condensed sedimentation ahead of Northern Graben extension and progradation of the modern continental margin, *New Zealand Journal of Geology and Geophysics*, 47(4): p. 645-662.

Higgs, K.E., P.R. King, J.I. Raine, R. Sykes, G.H. Browne, E.M. Crouch, J.R. Baur (2012), Sequence stratigraphy and controls on reservoir sandstone distribution in an Eocene marginal marine–coastal plain fairway, Taranaki Basin, New Zealand, *Marine and Petroleum Geology*, 32(1): p.110–137.

King, P.R., and G.P. Thrasher (1996), Cretaceous-Cenozoic Geology and Petroleum Systems of the Taranaki Basin, New Zealand., Lower Hutt: Institute of Geological and Nuclear Sciences, *Institute of Geological and Nuclear Sciences*, Monograph 13.

King, P.R., K.J. Bland, R.H. Funnell, R. Archer, L. Lever (2009), Opportunities for underground geological storage of CO2 in New Zealand - Report CCS-08/5 - Onshore Taranaki Basin overview, GNS Science Report 2009/58.

Knox, G.J., (1982), Taranaki Basin, structural style and tectonic setting, *New Zealand Journal of Geology Geophysics* 25, p. 125–140.

Mathews, E.R., and. D.J. Bennett / New Zealand Oil & Gas Ltd (1987), Kupe South-1 Well Completion Report PPL 38116, Ministry of Economic Development, New Zealand, Unpublished Petroleum Report, PR 1284.

Mills, K., G. Sutherland, C. Gilbert, and A. Rek (2007), Momoho-1 Well Proposal, Offshore Taranaki Basin, New Zealand, PML 38146.

Naish, T.R., F. Wehland, G.S. Wilson, G.H. Browne, R.A. Cook, H.E.G. Morgans, M. Rosenberg, P.R. King, D. Smale, C.S. Nelson, P.J.J. Kamp, B. Ricketts (2005), An integrated sequence stratigraphic, palaeoenvironmental, and chronostratigraphic analysis of the Tangahoe Formation, southern Taranaki coast, with implications for mid-Pliocene (c. 3.4–3.0 Ma) glacio-eustatic sea-level changes, *Journal of the Royal Society of New Zealand*, 35(1-2): p. 151-196.

NZP&M (New Zealand Petroleum & Minerals) (2014), New Zealand Petroleum Basins., New Zealand, Wellington: Ministry of Business, Innovation and Employment.

Roncaglia, L., H.E.G.Morgans, M.J. Arnot, J. Baur, H. Bushe, C.M. Jones, P.R. King, M. Milner, H. Zhu (2008), Stratigraphy, well correlation and seismic-to- well tie in the Upper Cretaceous to Pliocene interval in the Kupe region, Taranaki Basin, New Zealand. Interdiction to stratigraphic database in PETREL, GNS Science Report 2008/07.

Schmidt, D.L. / TCPL Resources Ltd (1989), Kupe South field Taranaki Basin 1987 reconnaissance 3D seismic survey Processing and interpretation report, Ministry of Economic Development, New Zealand, Unpublished Petroleum Report, PR 1670.

Schmidt, D.S., P.H. Robinson (1990), The structural setting and depositional history for the Kupe South Field, Taranaki Basin, Ministry of Commerce, Wellington (1990), 1989 *New Zealand Oil Exploration Conference proceedings*, P. 151–172.

Singh, R. / TCPL Resources Ltd (1989), Seismic processing report, Kupe South 1987/89, Ministry of Economic Development, New Zealand, Unpublished Petroleum Report, PR 1533.

Strogen, D.P., K.J. Bland, A. Nicol, P.R. King (2014), Paleogeography of the Taranaki Basin region during the latest Eocene–Early Miocene and implications for the 'total drowning' of Zealandia, *New Zealand Journal of Geology and Geophysics*, 57(2): p. 110-127.

Thrasher, G.P., P.R. King, R.A. Cook (1995), Taranaki Basin petroleum atlas., New Zealand, Lower Hutt: Institute of Geological and Nuclear Sciences Ltd, 50 maps plus booklet.

Palmer, J., (1985) Pre-Miocene lithostratigraphy of Taranaki Basin, New Zealand, *New Zealand Journal of Geology and Geophysics*, 28(2): p. 197-216.

Vonk, A.J., P.J.J. Kamp (2008), The Late Miocene Southern and Central Taranaki Inversion Phase (SCTIP) and related sequence stratigraphy and paleogeography, New Zealand, Auckland: *In Proceedings of the 2008 New Zealand Petroleum Conference*.

VITA

Housam Hussein Grabeel was born in Al Zawia, Libya. In August 2008, he graduated from the University of Zawia with a bachelor's degree in Geology. In 2010, he joined the oil industry in Libya where he worked with an Italian company "GEOLOG" as a mud-logger and geologist assistant. In 2012, he moved to the French company "Schlumberger," which gave him coursework in well logging interpretation and well parameters monitoring at its center in Paris. He built a good career at this company then he decided to leave in 2014 to pursue his studies abroad. The Libyan Ministry of Higher Education provided him a master's scholarship. Consequently, Housam moved on to begin his Master of Science in Geophysics at Missouri University of Science and Technology, to which he received in December, 2018.